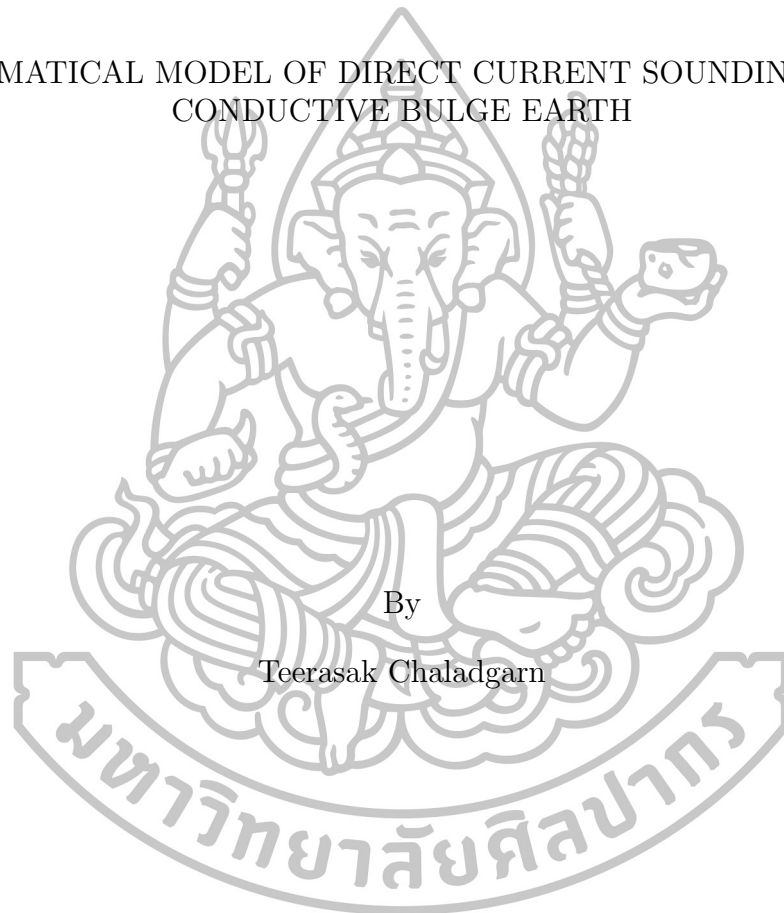




MATHEMATICAL MODEL OF DIRECT CURRENT SOUNDING FOR A
CONDUCTIVE BULGE EARTH



By

Teerasak Chaladgarn

A Thesis Submitted in Partial Fulfillment of the Requirements for the Degree of
Doctor of Philosophy Program in Mathematics
Department of Mathematics
Graduate School, Silpakorn University
Academic Year 2015
Copyright of Graduate School, Silpakorn University

MATHEMATICAL MODEL OF DIRECT CURRENT SOUNDING FOR A
CONDUCTIVE BULGE EARTH



A Thesis Submitted in Partial Fulfillment of the Requirements for the Degree of
Doctor of Philosophy Program in Mathematics
Department of Mathematics
Graduate School, Silpakorn University
Academic Year 2015
Copyright of Graduate School, Silpakorn University

แบบจำลองทางคณิตศาสตร์ของการใช้ไฟฟ้ากระแสตรงสำรวจพื้นดินที่มีสภาพนำไฟฟ้าแบบนูน



วิทยานิพนธ์นี้เป็นส่วนหนึ่งของการศึกษาตามหลักสูตรปริญญาตรีบัณฑิต

สาขาวิชาคณิตศาสตร์ (หลักสูตรนานาชาติ)

ภาควิชาคณิตศาสตร์

บัณฑิตวิทยาลัย มหาวิทยาลัยศิลปากร

ปีการศึกษา 2558

ลิขสิทธิ์ของบัณฑิตวิทยาลัย มหาวิทยาลัยศิลปากร

The Graduate School, Silpakorn University has approved and accredited the Thesis title of "Mathematical Model of Direct Current Sounding for a Conductive Bulge Earth" submitted by Mr. Teerasak Chaladgarn as a partial fulfillment of the requirements for the degree of Doctor of Philosophy in Mathematics

.....
(Associate Professor Panjai Tantatsanawong, Ph.D.)

Dean of Graduate School

...../...../.....

The Thesis Advisor

Associate Professor Suabsagun Yooyuanyong, Ph.D.

The Thesis Examination Committee

..... Chairman

(Dr. Nairat Kanyamee, Ph.D.)

...../...../.....

..... Member

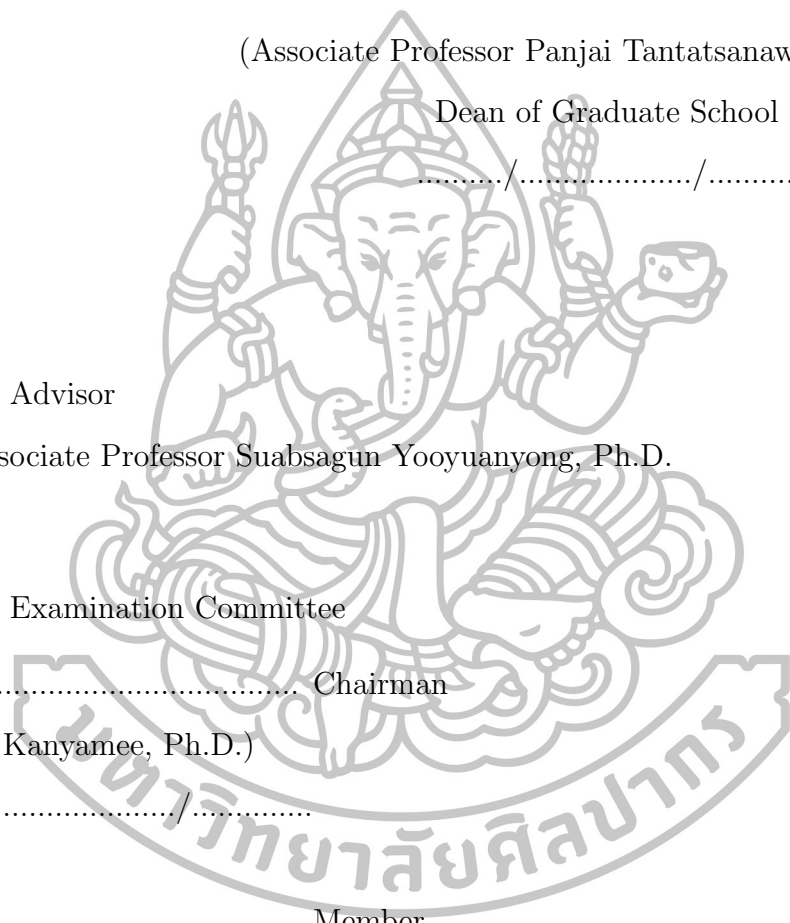
(Dr. Warin Sripanya, Ph.D.)

...../...../.....

..... Member

(Associate Professor Suabsagun Yooyuanyong, Ph.D.)

...../...../.....



53305801 : MAJOR : MATHEMATICS
 KEY WORDS : HANKEL TRANSFORMS/ NORMALIZED APPARENT
 RESISTIVITY/ MAGNETOMETRIC RESISTIVITY/ BULGE
 TEERASAK CHALADGARN : MATHEMATICAL MODEL OF DIRECT
 CURRENT SOUNDING FOR A CONDUCTIVE BULGE EARTH. THESIS
 ADVISOR : ASSOC. PROF. SUABSAGUN YOOYUANYONG, Ph.D. 97 pp.

Mathematical models are presented in this thesis. The main objective of our study is to explore conductivity of the ground structure. The first mathematical model of Resistivity Method is conducted via numerical technique of Finite Element Method to show the scalar potential under the ground. The results of scalar potential are plotted to show behavior of them. The geometric model used is one layer having an exponentially conductivity profile defined by $\sigma_{over}(z) = \sigma_0 e^{-b(z-l)^2/2}$ where b and l are positive constants and l is used to located the peak of the bulge, z is the variable of the depth and σ_0 is a positive constant. Four probes are located on the ground surface. Two of them are direct current source and the another two probes for voltage measurements. The boundary conditions are denoted and the scalar potential are computed and plotted under MathLAB platform. For the second mathematical model, normalized apparent resistivity resulting from the injection of electric current into the ground is considered and can be used to explore the earth's structures. The analytical solution of normalized apparent resistivity from DC source located on a two-layered earth model is formulated. The conductivity of overburden is denoted by $\sigma_{over}(z) = \sigma_0 e^{-b(z-l)^2/2}$, $0 \leq z \leq d$, where d is the thickness of overburden. The conductivity of host medium, $z > d$, is denoted by a constant and is given by $\sigma_{host}(z) = \sigma_0$. The Hankel transforms and the power series method are used to solve the partial differential equation to get the potential functions. The expression for the Wenner configuration is introduced to formulate the normalized apparent resistivity. In order to determine the normalized apparent resistivity, numerical solutions are computed to show the behavior of the curves by using Chave's algorithm while some parameters are given. The computation results of normalized apparent resistivity are plotted against electrode spacing. An inverse problem via the use of the Newton-Raphson in optimization technique is introduced for finding a conductivity parameter of the ground. The method is very successful and leads to very good results with the high speed of convergence. For the same source, different technique, analytical solution of magnetic field response from DC source located on a two-layered uniform conductive host medium, similar to the previous conductivity model, is formulated to be our third mathematical model. The Hankel transforms are introduced to solve the magnetic fields which are expressed in the form of integral expression. In order to determine the magnetic fields, numerical solutions are computed to show the behavior of the field while some parameters are given. The inversion process, using the Newton-Raphson method, is conducted to estimate the true conductivity variation parameter of the ground.

Department of Mathematics Graduate School, Silpakorn University
 Student's signature Academic Year 2015
 Thesis Advisor's signature

53305801 : สาขาวิชาคณิตศาสตร์

คำสำคัญ : การแปลงฮันเกิล/ สภาพต้านทานปรากฏที่ถูกล้อมรั้ว/ สภาพต้านทานแบบแม็กนีโทเมตริก/ บูน

ธีรศักดิ์ ฉลาดการณ์ : แบบจำลองทางคณิตศาสตร์ของการใช้ไฟฟ้ากระแสตรงสำรวจพื้นดินที่สภาพนำไฟฟ้าแบบบูน อาจารย์ที่ปรึกษาวิทยานิพนธ์ : รศ.ดร.สืบสกุล อยู่ยืนยง. 97 หน้า.

วิทยานิพนธ์ฉบับนี้ได้นำเสนอแบบจำลองทางคณิตศาสตร์ โดยวัตถุประสงค์หลักของการศึกษาคือ การสำรวจสภาพนำไฟฟ้าของโครงสร้างพื้นดิน ซึ่งแบบจำลองแรกที่ศึกษาเป็นแบบจำลองทางคณิตศาสตร์ของวิธีการต้านทานซึ่งถูกดำเนินการด้วยระเบียบวิธีเชิงตัวเลขไฟฟ้าในดอ์เอลิเมนต์เพื่อแสดงศักย์ไฟฟ้าใต้พื้นดิน ผลของศักย์ไฟฟ้าที่ได้ถูกนำไปวาดเป็นเส้นกราฟแสดงพฤติกรรมของค่าศักย์ไฟฟ้าที่หาได้ รูปแบบโครงสร้างพื้นดินที่ศึกษาเป็นพื้นดินหนึ่งชั้นที่มีรูปแบบของสภาพนำไฟฟ้าเป็นแบบเอกซ์โพเนนเชียล ซึ่งกำหนดโดย $\sigma_{over}(z) = \sigma_0 e^{-b(z-l)^2/2}$ เมื่อ b และ l เป็นค่าคงตัวบวก และ l ใช้แทนตำแหน่งที่สภาพนำไฟฟ้ามีค่าสูงสุด, z แทนความลึกของพื้นดิน และ σ_0 เป็นค่าคงตัวบวก กำหนดจุดตั้งจุดเป็นจุดสำรวจบนพื้นดิน สองในสี่จุดนั้นเป็นจุดที่ปล่อยไฟฟ้ากระแสตรงลงสู่พื้นดินและอีกสองจุดที่เหลือซึ่งอยู่ระหว่างสองจุดแรกใช้สำหรับตรวจวัดแรงดันไฟฟ้า เงื่อนไขขอบเขตถูกกำหนดขึ้นเพื่อนำไปสู่การคำนวณหาศักย์ไฟฟ้าและนำค่าที่ได้มาเขียนกราฟโดยใช้โปรแกรม MATLAB สำหรับแบบจำลองทางคณิตศาสตร์แบบที่สองเป็นการพิจารณาผลของสภาพต้านทานปรากฏที่ถูกล้อมรั้วไลซ์จากการปล่อยไฟฟ้ากระแสตรงลงไปในพื้นดิน ซึ่งสามารถนำมาใช้ในการสำรวจโครงสร้างพื้นดินของโลกได้ การวิเคราะห์หาค่าตอบของสภาพต้านทานปรากฏที่ถูกล้อมรั้วไลซ์คำนวณจากการปล่อยไฟฟ้ากระแสตรงลงบนพื้นดินที่มีโครงสร้างพื้นดินที่มีรูปแบบโครงสร้างพื้นดินเป็นสองชั้น โดยกำหนดสภาพนำไฟฟ้าชั้นบนเป็น $\sigma_{over}(z) = \sigma_0 e^{-b(z-l)^2/2}$, $0 \leq z \leq d$, เมื่อ d แทนความลึกของพื้นดินชั้นบน และสภาพนำไฟฟ้าของชั้นถัดลงไปถูกกำหนดโดยค่าคงตัวให้เป็น $\sigma_{host}(z) = \sigma_0$, $z > d$ การแปลงฮันเกิลและวิธีการอนุกรมกำลังสองถูกใช้ในการแก้สมการเชิงอนุพันธ์ย่อย ซึ่งจะได้คำตอบอยู่ในรูปฟังก์ชันของศักย์ไฟฟ้า โดยการคำนวณหาสภาพต้านทานปรากฏที่ถูกล้อมรั้วไลซ์ใช้วิธีการหาค่าตามวิธีการของ Wenner โดยใช้อัลกอริทึมของ Chave คำนวณหาค่าตอบเชิงตัวเลขของสภาพต้านทานปรากฏที่ถูกล้อมรั้วไลซ์เมื่อกำหนดค่าของพารามิเตอร์บางค่าในสมการ แล้วนำคำตอบที่คำนวณได้มาเขียนกราฟเพื่ออธิบายพฤติกรรมของสภาพต้านทานปรากฏที่ถูกล้อมรั้วไลซ์ที่ได้ สภาพต้านทานปรากฏที่ถูกล้อมรั้วไลซ์ที่มาจากคำนวณจะถูกนำมาเขียนกราฟเปรียบเทียบกับระยะห่างระหว่างจุดสองจุดที่ปล่อยไฟฟ้ากระแสตรง ซึ่งเราใช้วิธีการของนิวตัน-ราฟสัน ในปัญหาย้อนกลับเพื่อหาค่าของพารามิเตอร์ของสภาพนำไฟฟ้าในพื้นดิน ซึ่งเป็นวิธีการที่ประสบความสำเร็จมากและนำไปสู่ผลลัพธ์ของการเข้าสู่ของคำตอบอย่างรวดเร็ว สำหรับแบบจำลองทางคณิตศาสตร์แบบที่สาม เป็นการวิเคราะห์หาค่าตอบของการตอบสนองของสนามแม่เหล็กจากการปล่อยไฟฟ้ากระแสตรงลงสู่พื้นดินที่มีโครงสร้างและสภาพนำไฟฟ้าเช่นเดียวกับแบบจำลองที่สอง โดยใช้การแปลงฮันเกิลในการแก้ปัญหาสนามแม่เหล็ก ซึ่งคำตอบที่ได้จะอยู่ในรูปของอินทิกรัลของฟังก์ชันของสนามแม่เหล็กโดยสามารถคำนวณหาค่าตอบเชิงตัวเลขเพื่อนำไปสู่การอธิบายพฤติกรรมของสนามแม่เหล็กเมื่อกำหนดค่าของพารามิเตอร์บางค่าได้ ในขั้นตอนกระบวนการย้อนกลับเราใช้วิธีการของนิวตัน-ราฟสัน ในการนำไปสู่การประมาณค่าพารามิเตอร์ของสภาพนำไฟฟ้าของพื้นดิน

ภาควิชาคณิตศาสตร์

ลายมือชื่อนักศึกษา.....

ลายมือชื่ออาจารย์ที่ปรึกษาวิทยานิพนธ์

บัณฑิตวิทยาลัย มหาวิทยาลัยศิลปากร

ปีการศึกษา 2558

Acknowledgements

This thesis has been completed by the involvement of people whom I would like to mention here. First of all, I would like to express my sincere gratitude to Associate Professor Dr. Suabsagun Yooyuanyong, my thesis advisor, for his helpful suggestions, valuable comments and consistent encouragement throughout the preparing and writing this thesis. Without his constructive suggestions and knowledgeable guidance in this study, this research would never have successfully been completed.

Sincere thanks and deep appreciation are also extended to Dr.Nairat Kanyamee, the committee chairman and Dr.Warin Sripanya, the committee members, for their comments and suggestions and I would like to express my thankfulness to Dr.Nairat Kanyamee, for her expertise, understanding, patience and kindly guiding me in the Finite Element Method.

In addition, I also wish to take this opportunity to thank Dr. Warin Sripanya and Assistant Professor Dr. Pisuttawan Sripirom Sirininlakul, for their suggestions and knowledgeable guidance in the Fortran Programming Language.

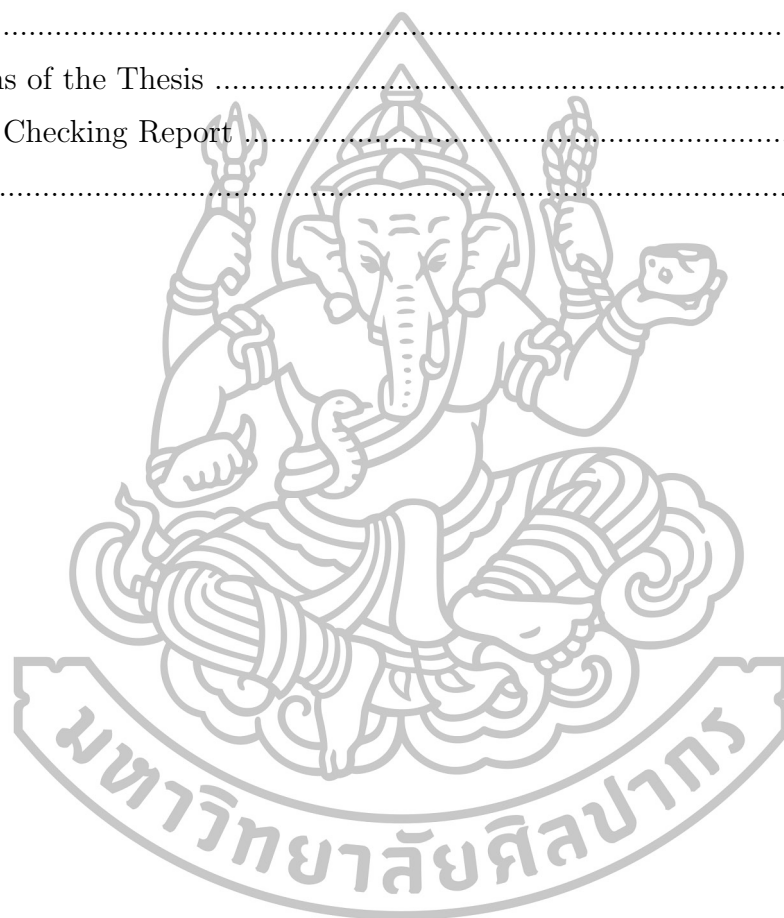
Also, I am grateful to the Centre of Excellence in Mathematics (CEM) and Srinakharinwirot University, for support me in the scholarship throughout my graduate study.

Finally, I would like to express my greatly gratitude to my wife, my family for their love and encouragement during my study.

Table of Contents

	Page
Abstract in English	d
Abstract in Thai	e
Acknowledgements	f
List of Figures	i
List of Tables	k
Chapter	
1 Introduction	1
DC Resistivity Methods and Their Applications	1
Outline of the Thesis	3
2 Finite Element Method for the Scalar Potential Over an Exponential Conductive Earth	5
Introduction	5
Galerkin's Method of Weighted Residuals	6
Method of Weighted Residuals	6
Elliptic Boundary Value Problems	8
Mathematical Modeling	10
Formulation of the Problem	10
Numerical Experiments	32
Conclusions and Discussion	47
3 Inversion of Direct Current for a Conductive Host with a Bulge Overburden	49
Introduction	49
Formulation of the Problem	49
Apparent Resistivity of Two-Layered Earth	54
Normalized Apparent Resistivity	56
Sounding Curves and Discussions	57
Inversion Process	58
Sample Tests	59
Synthesis Data	59
Discussions	60
Summary and Conclusions	61
4 Mathematical Model of Magnetometric Resistivity Sounding for a Conductive Host with a Bulge Overburden	62
Introduction	62
Formulation of the Problem	63
A Geometric 2-Layered Earth Model	68
Solution of Magnetic Field for a 2-Layered Earth Model	68
Numerical Experiments	71
Inversion Process	72

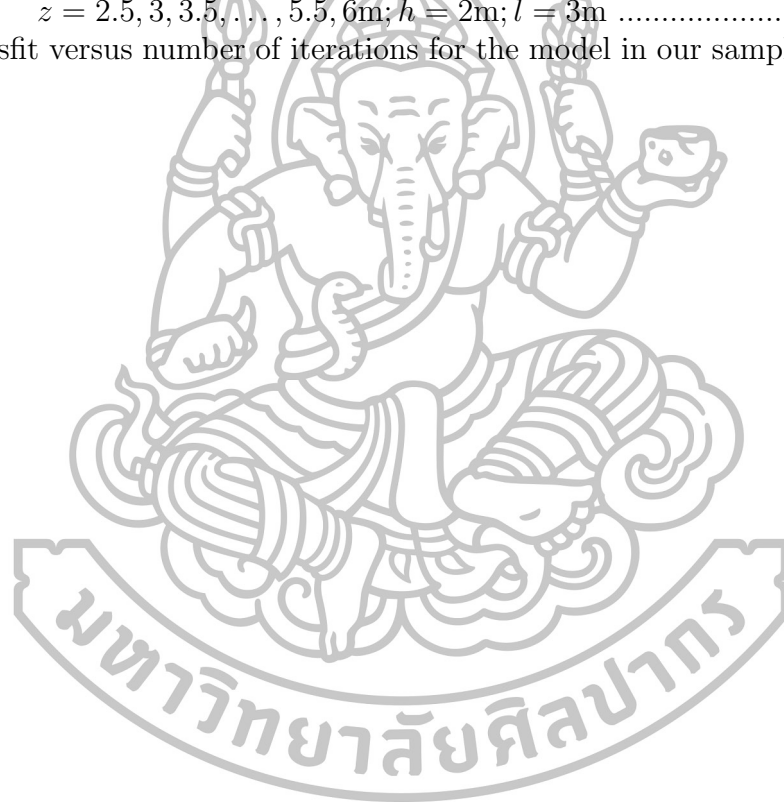
Chapter	Page
Sample Tests	73
Synthesis Data	73
Discussions	74
Summary and Conclusions	75
5 Conclusions and Future Works	76
Conclusions of the Thesis	76
Future Works	77
References	78
Publications of the Thesis	81
Plagiarism Checking Report	96
Biography	97



List of Figures

Figures	Page
2.1 The model of conductivity profile	11
2.2 Boundary condition of the earth structure	15
2.3 Reference and transformed coordinates of the boundary	16
2.4 The graph of potential when $10 \leq r \leq 100$ and $0 \leq z \leq 90\text{m}$ and $l = 0\text{m}$	33
2.5 The graph of potential against r when z is fixed, i.e. $z = 0, 10, 20, \dots, 90\text{m}$ and $l = 0\text{m}$	34
2.6 The graph of potential against z when r is fixed, i.e. $r = 10, 20, \dots, 100\text{m}$ and $l = 0\text{m}$	35
2.7 The graph of potential when $10 \leq r \leq 100$ and $0 \leq z \leq 90\text{m}$ and $l = 5\text{m}$	36
2.8 The graph of potential against r when z is fixed, i.e. $z = 0, 10, 20, \dots, 90\text{m}$ and $l = 5\text{m}$	37
2.9 The graph of potential against z when r is fixed, i.e. $r = 10, 20, \dots, 100\text{m}$ and $l = 5\text{m}$	38
2.10 The graph of potential when $10 \leq r \leq 100$ and $0 \leq z \leq 90\text{m}$ and $l = 10\text{m}$	39
2.11 The graph of potential against r when z is fixed, i.e. $z = 0, 10, 20, \dots, 90\text{m}$ and $l = 10\text{m}$	40
2.12 The graph of potential against z when r is fixed, i.e. $r = 10, 20, \dots, 100\text{m}$ and $l = 10\text{m}$	41
2.13 The graph of potential when $10 \leq r \leq 100$ and $0 \leq z \leq 90\text{m}$ and $l = 30\text{m}$	42
2.14 The graph of potential against r when z is fixed, i.e. $z = 0, 10, 20, \dots, 90\text{m}$ and $l = 30\text{m}$	43
2.15 The graph of potential against z when r is fixed, i.e. $r = 10, 20, \dots, 100\text{m}$ and $l = 30\text{m}$	44
2.16 The graph of potential when $10 \leq r \leq 100$ and $0 \leq z \leq 90\text{m}$ and $l = 50\text{m}$	45
2.17 The graph of potential against r when z is fixed, i.e. $z = 0, 10, 20, \dots, 90$ meters and $l = 50$ meters	46
2.18 The graph of potential against z when r is fixed, i.e. $r = 10, 20, \dots, 100\text{m}$ and $l = 50\text{m}$	47
3.1 Configuration of electrode array over an overburden of thickness d	54
3.2 The curve of normalized apparent resistivity against electrode spacing, $d = 5\text{m}$; $b = 0.01, 0.03\text{m}^{-2}$; $l = 1, 2, \dots, 5\text{m}$	57
3.3 The curve of normalized apparent resistivity against electrode spacing, $d = 10\text{m}$; $b = 0.003, 0.005\text{m}^{-2}$; $l = 2, 4, \dots, 10\text{m}$	57
3.4 The curve of normalized apparent resistivity against electrode spacing, $d = 20\text{m}$; $b = 0.0005, 0.001\text{m}^{-2}$; $l = 4, 8, \dots, 20\text{m}$	57
3.5 The curve of normalized apparent resistivity against electrode spacing, $d = 5, 10\text{m}$; $l = 1\text{m}$; $b = 0.01, 0.02, \dots, 0.05\text{m}^{-2}$	58

Figures	Page
3.6 The curve of normalized apparent resistivity against electrode spacing, $b = 0.01, 0.03\text{m}^{-2}$; $l = 1\text{m}$; $d = 1, 2, \dots, 5\text{m}$	58
3.7 Misfit versus number of iterations for the model in our sample test ...	60
4.1 Geometric model for 2-layered earth	68
4.2 The behavior of magnetic field against r at different depth $z = 0.5, 1, 1.5, \dots, 3.5, 4\text{m}$; $h = 5\text{m}$; $l = 3\text{m}$	71
4.3 The behavior of magnetic field against r at different depth $z = 0.5, 1, 1.5, \dots, 3.5, 4\text{m}$; $h = 3\text{m}$; $l = 5\text{m}$	71
4.4 The behavior of magnetic field against r at different depth $z = 2.5, 3, 3.5, \dots, 5.5, 6\text{m}$; $h = 2\text{m}$; $l = 1\text{m}$	72
4.5 The behavior of magnetic field against r at different depth $z = 2.5, 3, 3.5, \dots, 5.5, 6\text{m}$; $h = 2\text{m}$; $l = 3\text{m}$	72
4.6 Misfit versus number of iterations for the model in our sample test	74



List of Tables

Tables	Page
3.1 Model parameters used in our sample tests	59
3.2 Successive iterations for finding a conductivity parameter of the model in our sample tests	59
4.1 Model parameters used in our sample tests	73
4.2 Successive iterations for finding a conductivity parameter of the model in our sample tests	73



Chapter 1

Introduction

Nowadays, the natural resources are very useful for human. Most of the natural resources buried under the earth surface which are difficult to explore. Geomathematic is the science which applies the principles of mathematics and physics to explore the ore under the earth surface. The subject involves taking measurements at or near the earth's surface those are influenced by the internal distribution of physical properties. In the past few decade, there are many methods used in geophysical explorations, such as gravitational, magnetic, seismic, electrical, electromagnetic, radioactivity, and well logging. The most commonly used in mineral exploration are direct current resistivity and the magnetic methods because they are far less expensive than the most other investigation methods.

1.1 DC Resistivity Methods and Their Applications

Electrical prospecting method detects the ore under ground surface. The method is produced by electric current flow under the ground. Using electrical method, one may measure potential, current, and electromagnetic field that occur naturally or are introduced artificially in the ground. The measurements data can be made in a variety of ways to determine a variety of results. There is a much greater variety of electrical and electromagnetic techniques available than in the other prospecting methods, where only a single field of force or anomalous property is used. Basically, it is the enormous variation in electrical resistivity found in different minerals that makes these techniques possible [36].

Electrical method using direct current resistivity and induced polarization (IP) are probably the most widely used near-surface geophysical techniques, particularly for environmental investigations [1]. In the early part of 20th century, electromagnetic and direct current resistivity methods were brought first time to use. The direct current resistivity method gained early acceptance because of less requirement theoretical and instrumentation considerations. Direct current resistivity methods have become the most popularly used geoelectrical method. These

techniques are widely understood and accepted in term of the capabilities, and limitations and the standardized.

The direct current resistivity method employ an artificial source of current, which is introduced into the ground through point electrodes or long line contacts. The procedure is to measure potentials at other electrodes in the vicinity of the current flow. Because the current is measured as well, it is possible to determine an effective or apparent resistivity of the surface [36]. The analysis and interpretation are done on the basis of direct currents. The distribution of potential can be related theoretically to ground resistivity. Their distribution for some simple cases, notably, the case of a horizontally is stratified ground. The case of homogeneous masses are separated by vertical planes. Direct current resistivity survey can be useful in detecting bodies of anomalous materials or in estimating the depths of ground surfaces. Data from direct current resistivity surveys are customarily presented and interpreted in the form of values of apparent resistivity. Apparent resistivity is defined as the resistivity of an electrically homogeneous and isotropic half-space that would yield the measured relationship between the applied current and the potential difference for a particular arrangement and spacing of electrodes.

The direct current resistivity surveying problem is the use of apparent resistivity values from field observations at various locations and with various electrode configurations to estimate the true resistivities of the several earth materials present at a site and to locate their boundaries spatially below the surface of the site. An electrode array with constant spacing is used to investigate lateral changes in apparent resistivity reflecting lateral geologic variability or localized anomalous features. To investigate changes in resistivity with depth, the size of the electrode array is varied. The apparent resistivity is affected by material at increasingly greater depth as the electrode spacing is increased. Because of this effect, a plot of apparent resistivity against electrode spacing can be used to indicate vertical variations in resistivity. Schlumberger, Wenner, and dipole-dipole are the types of electrode array that are most commonly used. There are other electrode configurations that are used experimentally or for non-geotechnical problems or are not in wide popularity today. The Wenner array configuration is used in our thesis. It consists of four electrodes in line which is separated by equal intervals and all four electrodes are moved between successive observations. The Wenner array was used more extensively than Schlumberger array in the United States. This electrode array demands less instrument sensitivity and reduction of data is marginally easier.

The traditional direct current resistivity method maps the electrical properties of the earth by measuring differences in potential at the earth's surface caused by galvanic current flow between two current electrodes. The magnetic fields associated with these currents can also be measured with a class of geophysical techniques referred to here as magnetometric methods. These include magnetometric resistivity (MMR) and magnetic induced polarization (MIP), and a set of related 'total-field' techniques known as sub-audio magnetics (SAM). The

magnetometric resistivity method differs from the traditional method in that the potential electrodes are replaced by a highly sensitive coil or magnetometer and one or more the horizontal components of the magnetic field are recorded [23]. Magnetometric resistivity is an electrical exploration method based on the measurement of the low-level, low-frequency static magnetic fields associated with noninductive current flow in the ground. The current electrodes may be located on the surface or, for areas where targets are beneath conductive overburden which penetrate the bedrock in order to increase current flow below the cover.

1.2 Outline of the Thesis

This thesis deals with development and application of mathematics techniques for enhanced investigation in geophysical explorations. A horizontally stratified structure of the earth is studied in this research work.

Chapter 2 presents a mathematical model for the scalar potential at various positions. We assume that the earth structure is only one layer having exponential conductivity. Four probes are located on the ground surface. Two of them are direct current source and the another two probes are used for Voltage measurements. The electrode spacing starts from 10m to 100m. We use Finite Element Method (FEM) by applying Galerkin's Method of Weighted Residuals to solve the partial differential equation. Maple program is used to calculate and plot graphs of the scalar potential at different depths and different electrode spacing.

Chapter 3, the analytical solution of normalized apparent resistivity from DC source located on a two-layered earth model is formulated. Two-layered earth structure with an overburden having exponentially varying conductivity is considered. The Hankel transforms and power series method are used to solve the partial differential equation to find the potential functions. The expression for the Wenner configuration is introduced to formulate the normalized apparent resistivity. Numerical solutions are computed to show the behavior of the normalized apparent resistivity by using Chave's algorithm while some parameters are given. The curves of computation results of normalized apparent resistivity are plotted against electrode spacing. The inversion process, using the Newton-Raphson method, is conducted to estimate the conductivity variation parameter.

In Chapter 4, presents an electrical method used for investigation of two-layered earth structure. The method proposed here is based on the measurement of low-level, low-frequency static magnetic fields associated with noninductive current flow between two current electrodes on the earth's surface. Analytical solutions of the steady state magnetic field response from DC source located on a two-layered are derived in this study. The earth structure having exponentially varying conductivity is considered. The Hankel transform is applied to our problem and analytical result is obtained. Our solutions are expressed in the form of integral expressions. Numerical solutions are computed to show the behavior

of the magnetic field while some parameter are given approximately. An inverse problem via the use of the Newton-Raphson optimization technique is introduced for finding a conductivity parameter of the ground.

Finally, in Chapter 5, we summarize the results and contributions of this thesis, and indicate future research directions.



Chapter 2

Finite Element Method for the Scalar Potential Over an Exponential Conductive Earth

2.1 Introduction

Nowadays, many countries try to make economy grows rapidly. One of the ways to improve their economy is to use the natural resources. As a result, the earth surface has been studied widely in order to utilize the natural resources embedded beneath the earth. They use knowledge of geophysics which is a branch of science concerned with the earth survey. The survey uses mathematics, physics and the physical properties of the earth such as the resistivity, conductivity, electric potential, magnetic field and electric field to search for the natural resources. Since the most natural resources embedded beneath the earth is hard to find, we use a survey method to search for the natural resources beneath the earth surface to differentiate the minerals from the others. We process the data obtained from a geophysics survey to identify the location of minerals correctly. This geophysics survey can be costly, so we seek for a mathematical model which is a method that became famous because it is economical and costs less than the direct survey [36].

We formulate a mathematical model by using electromagnetic method to determine the value of scalar potential beneath the earth surface. We assume that the earth structure consists of horizontally stratified layers having exponential conductivities at certain depths except the last layer where the conductivity having the same varying through the rest of the layer which was presented by Chaladgarn and Yooyuanyong [32]. They derived the normalized apparent resistivity by formulating the problem from the electric field as the gradient of a scalar potential then solve a boundary value problem of a horizontally stratified layered earth with homogeneous layers. Stoyer and Wait [7] studied the problem of computing apparent resistivity for a structure with a homogeneous overburden and a medium whose resistivity varies exponentially with depth. Banerjee et al.[5] gave expressions for apparent resistivity of a multilayered earth with a layer having ex-

ponentially varying conductivity. Kim and Lee [16] derived a new resistivity kernel function to calculate the apparent resistivity of a multilayered earth with layers having exponentially varying conductivities. Chen and Oldenburg [18] derived the magnetic field directly by solving a boundary value problem of a horizontally stratified layered earth with homogeneous layers. However, in the real situation there are cases where the subsurface conductivities vary exponentially, linearly or binomially with depth. There exists a considerable amount of research about mathematical modeling which assumes that the earth structure consists of horizontally stratified multilayer with one or more layers having exponentially, linearly or binomially varying conductivities at certain depths except the last layer where the conductivity having the same varying through the rest of the layer. Siew and Yooyuanyong [24] studied the electromagnetic response of a thin disk beneath an inhomogeneous conductive overburden and expressions for the electric fields in the overburden. Ketchanwit [25] studied the earth surface layers using time-domain electromagnetic field by constructing three mathematical models having exponentially varying and constant varying conductivities. Sripunya [34] derived solutions of the steady state magnetic field due to a DC current source in a layered earth with some layer having exponentially or binomially or linearly varying conductivity.

We present our mathematical model by using electromagnetic method. We assume that the earth structure contains only one layer having exponentially varying conductivity. We use Finite Element Method (FEM) to find the numerical solution of the scalar potential under the earth surface. We are seeking the scalar potential at different depths and distances from the probe. This method is different from the Hankel transform which is difficult to solve for some complex problems such as all the research mentioned above. There are a few research used FEM by applying the Galerkin's Method of Weighted Residuals to find the solution of the scalar potential. Therefore, we are interested finding the numerical solution of our problem by using the Galerkin's Method of Weighted Residuals.

2.2 Galerkin's Method of Weighted Residuals

In this section, the method of weighted residuals is described and Galerkin's method of weighted residuals is emphasized as a tool for the finite element formulation for any field problem governed by differential equations from Hutton (2004)[9].

2.2.1 Method of Weighted Residuals

The *method of weighted residuals*(MWR) is an approximate technique for solving boundary value problems that utilizes *trial functions* satisfying the prescribed boundary conditions and integral formulation to minimize error, in an average sense, over the problem domain [8]. The general concept is described here in terms of the one-dimensional case. Given a differential equation of the general

form

$$D[y(x), x] = 0 \quad a < x < b \quad (2.1)$$

where D is differential operator subject to homogeneous boundary condition

$$y(a) = y(b) = 0 \quad (2.2)$$

the method of weighted residuals seeks an approximate solution in the form

$$y^*(x) = \sum_{i=1}^n c_i N_i(x) \quad (2.3)$$

where y^* is the approximate solution expressed as the product of the unknown, constant, c_i to be determined and the trial function, $N_i(x)$. The major requirement placed on the trial functions is that they are *admissible function*; that is, the trial functions are continuous over the domain of interest and satisfy the specified boundary conditions. In addition, the trial functions should be selected to satisfy the “physics” of the problem in a general sense. Given these somewhat lax conditions, it is highly unlikely that the solution represented by equation (2.3) is exact. Instead, on substitution of the assumed solution into the differential equation (2.1), a residual error (hereafter simply called *residual*) results such that

$$R(x) = D[y^*(x), x] \neq 0 \quad (2.4)$$

where $R(x)$ is the residual. Note that the residual is also a function of the unknown parameters c_i . The method of weighted residuals requires that the unknown parameters c_i be evaluated such that

$$\int_a^b w_i(x) R(x) dx = 0 \quad i = 1, \dots, n \quad (2.5)$$

where $w_i(x)$ represents n arbitrary weighting functions. We observe that, on integration, equation (2.5) results in n algebraic equations, which can be solved for the n values of c_i . Equation (2.5) expresses that the sum (integral) of the weighted residual error over the domain of the problem is zero. Owing to the requirements placed on the trial functions, the solution is exact at the end points (the boundary conditions must be satisfied) but, in general, at any interior point the residual error is nonzero. As is subsequently discussed, the MWR map capture the exact solution under certain conditions, but this occurrence is the exception rather than the rule.

Several variations of MWR exist and the techniques vary primarily in how the weighting factors are determined or selected. The most common techniques are point collocation, subdomain collocation, least squares, and Galerkin’s method. As it is quite simple to use and readily adaptable to the finite element method, we discuss only Galerkin’s method.

In Galerkin's weighted residual method, the weighting functions are chosen to be identical to the trial functions; that is,

$$w_i(x) = N_i(x) \quad i = 1, \dots, n. \quad (2.6)$$

Therefore, the unknown parameters are determined via

$$\int_a^b w_i(x)R(x)dx = \int_a^b N_i(x)R(x)dx = 0 \quad i = 1, \dots, n \quad (2.7)$$

again resulting in n algebraic equations for evaluation of the unknown parameters.

2.2.2 Elliptic Boundary Value Problems

In this section, we consider an elliptic-typed boundary value problems (BVP)[6, 10]. Our goal is to determine a finite element solution of the problem.

$$\begin{aligned} -\nabla \cdot [k(\mathbf{x})\nabla u] + b(\mathbf{x})u &= f(\mathbf{x}), \quad \mathbf{x} \in \Omega, \\ u(s) &= \hat{u}(s), \quad s \in \partial\Omega_1, \\ -k(s)\frac{\partial u(s)}{\partial n} &= p(s)[u(s) - \hat{u}(s)] = \sigma(s), \quad s \in \partial\Omega_2 \end{aligned} \quad (2.8)$$

Variational Statement

Consider the residual

$$R(\mathbf{x}) = -\nabla \cdot [k(\mathbf{x})\nabla u] + b(\mathbf{x})u - f(\mathbf{x}).$$

Method of weighted residual:

$$\begin{aligned} \int_{\Omega} R(\mathbf{x})v d\mathbf{x} &= 0, \quad v \in V \subset H^1(\Omega), \\ \int_{\Omega} [-\nabla \cdot [k\nabla u] + bu - f] v d\Omega &= 0, \\ \int_{\Omega} (-\nabla \cdot [k\nabla u] v + bu v - f v) d\Omega &= 0, \end{aligned} \quad (2.9)$$

where

$$H^1(\Omega) = \{v \mid v \in L^2(\Omega), \nabla v \in L^2(\Omega)\} \text{ and } L^2(\Omega) = \{v \mid \int_{\Omega} |v|^2 d\mathbf{x} < \infty\}.$$

We aim to reduce the 2nd - order terms to the 1st order by integration by parts. Using the product rule for differentiation

$$\nabla \cdot (vk\nabla u) = k\nabla u \cdot \nabla v + v\nabla \cdot (k\nabla u)$$

equation (2.9) becomes

$$\int_{\Omega} [k\nabla u \cdot \nabla v - \nabla \cdot (vk\nabla u) + buv - fv] d\Omega = 0.$$

From the divergence theorem,

$$\begin{aligned} \int_{\Omega} \nabla \cdot (vk\nabla u) d\Omega &= \oint_{\partial\Omega} vk\nabla u \cdot n ds \\ &= \oint_{\partial\Omega} vk \frac{\partial u}{\partial n} ds \\ \int_{\Omega} [k\nabla u \cdot \nabla v + buv - fv] d\Omega - \oint_{\partial\Omega} vk \frac{\partial u}{\partial n} ds &= 0. \end{aligned}$$

Choosing $v(x)$ such that $v(x) = 0$ on $\partial\Omega_1$, i.e. Choose $V = \{v \in H^1(\Omega) : v = 0 \text{ on } \partial\Omega_1\}$ and using the boundary condition, we obtain

$$\int_{\Omega} [k\nabla u \cdot \nabla v + buv - fv] d\Omega + \int_{\partial\Omega_2} puv ds - \int_{\partial\Omega_2} p\hat{u}v ds = 0, \quad \forall v \in V. \quad (2.10)$$

Variational statement :

Find $u \in H^1(\Omega)$ such that

$$\int_{\Omega} [k\nabla u \cdot \nabla v + buv - fv] d\Omega + \int_{\partial\Omega_2} puv ds - \int_{\partial\Omega_2} p\hat{u}v ds = 0, \quad \forall v \in V. \quad (2.11)$$

Finite Element Approximation

We pose the variational statement on a finite dimensional subspaces $V_h \subset V$ and $\tilde{V}_h \subset H^1(\Omega)$ to formulate a finite element approximation of u .

Finite element approximation:

Find $u_h \in \tilde{V}_h$ such that

$$\int_{\Omega} (k\nabla u_h \cdot \nabla v + bu_h v - fv) d\Omega + \int_{\partial\Omega_2} pu_h v ds - \int_{\partial\Omega_2} p\hat{u}v ds = 0, \quad \forall v \in V_h. \quad (2.12)$$

Let $\{\varphi_i(x)\}_{i=1}^n$ be the basis functions of \tilde{V}_h and V_h such that

$$\varphi_j(x_i) = \delta_{ij} = \begin{cases} 1, & \text{if } i = j, \\ 0, & \text{if } i \neq j. \end{cases}$$

Then our solution u_h and v can be expressed as

$$u_h(x) = \sum_{j=1}^n u_j \varphi_j(x), \quad v(x) = \sum_{i=1}^n \beta_i \varphi_i(x).$$

By choosing suitable set of values for β_i 's, the finite element approximation becomes

$$\begin{aligned} \sum_{j=1}^n \int_{\Omega} (k \nabla \varphi_j \cdot \nabla \varphi_i + b \varphi_j \varphi_i) u_j - f \varphi_i d\Omega + \sum_{j=1}^n \int_{\partial\Omega_2} p \varphi_j \varphi_i u_j ds - \int_{\partial\Omega_2} p \hat{u} \varphi_i ds &= 0, \\ &\text{for each } i = 1, \dots, n, \\ \sum_{j=1}^n \left[\int_{\Omega} (k \nabla \varphi_j \cdot \nabla \varphi_i + b \varphi_j \varphi_i) d\Omega + \int_{\partial\Omega_2} p \varphi_j \varphi_i ds \right] u_j &= \int_{\Omega} f \varphi_i d\Omega + \int_{\partial\Omega_2} p \hat{u} \varphi_i ds, \\ &\text{for each } i = 1, \dots, n. \end{aligned} \quad (2.13)$$

Equation (2.13) can be represented by a linear system

$$AU = F, \quad (2.14)$$

where

$$\begin{aligned} A &= \left[\int_{\Omega} (k \nabla \varphi_j \cdot \nabla \varphi_i + b \varphi_j \varphi_i) d\Omega + \int_{\partial\Omega_2} p \varphi_j \varphi_i ds \right]_{(n \times n)}, \\ U &= [u_j]_{(n \times 1)}, \\ F &= \left[\int_{\Omega} f \varphi_i d\Omega + \int_{\partial\Omega_2} p \hat{u} \varphi_i ds \right]_{(n \times 1)}. \end{aligned}$$

2.3 Mathematical Modeling

2.3.1 Formulation of the Problem

In this section, we introduce a mathematical model and find a numerical approximation of the scalar potential at various positions by using Finite Element Method (FEM). Assuming that the earth structure contains only one layer having exponential conductivities. There are a source providing a direct-current (DC) voltage and a receiver on the ground surface which is assumed to contain only homogeneous surface layer. In this model, we follow Wenner array method which used nodes 1 and 4 for current electrodes, nodes 2 and 3 for potential electrodes; and a is the electrode spacing which is the distance for which the receiver picks up to signal. From Figure 2.1, the receiver picks up the signal at node $r = 10, 20, \dots, 100m$ where r is the electrode spacing which picks up the signal.

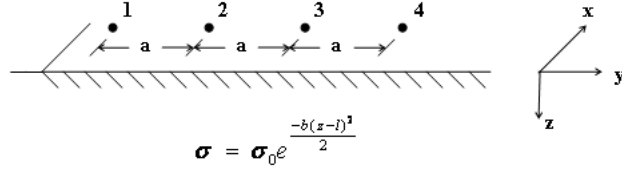


Figure 2.1: The model of conductivity profile

Since we are considering DC voltage, we may represent the electric field as the gradient of a scalar potential:

$$\vec{E} = -\nabla\psi, \quad (2.15)$$

where \vec{E} is the electric field in Volts per meter (V/m), ∇ is the gradient operator, and ψ is the scalar potential. Since the divergence of the current density is zero [7], by using Ohm's law, $\vec{J} = \sigma\vec{E}$, we obtain that

$$\begin{aligned} \nabla \cdot \vec{J} &= 0, \\ \nabla \cdot \sigma\vec{E} &= 0, \\ -\nabla \cdot \sigma\nabla\psi &= 0, \end{aligned} \quad (2.16)$$

where \vec{J} is the current density in Ampere per square meters (A/m^2), σ is the electrical conductivity of the medium in Siemens per meter (S/m) which is assumed to be a function of z only.

Thus, we have

$$\nabla \cdot \sigma\nabla\psi = 0$$

this yields

$$\sigma\nabla \cdot \nabla\psi + (\nabla\psi) \cdot (\nabla\sigma) = 0. \quad (2.17)$$

Since

$$\begin{aligned} \nabla \cdot \nabla\psi &= \left(\frac{\partial}{\partial x} \vec{i} + \frac{\partial}{\partial y} \vec{j} + \frac{\partial}{\partial z} \vec{k} \right) \cdot \left(\frac{\partial}{\partial x} \psi \vec{i} + \frac{\partial}{\partial y} \psi \vec{j} + \frac{\partial}{\partial z} \psi \vec{k} \right), \\ &= \left(\frac{\partial^2 \psi}{\partial x^2} + \frac{\partial^2 \psi}{\partial y^2} + \frac{\partial^2 \psi}{\partial z^2} \right), \\ &= \nabla^2 \psi, \end{aligned}$$

and

$$\begin{aligned} (\nabla\psi) \cdot (\nabla\sigma) &= \left(\frac{\partial}{\partial x} \psi \vec{i} + \frac{\partial}{\partial y} \psi \vec{j} + \frac{\partial}{\partial z} \psi \vec{k} \right) \cdot \left(\frac{\partial}{\partial x} \sigma \vec{i} + \frac{\partial}{\partial y} \sigma \vec{j} + \frac{\partial}{\partial z} \sigma \vec{k} \right), \\ &= \frac{\partial \psi}{\partial z} \frac{\partial \sigma}{\partial z}, \end{aligned}$$

thus, we have

$$\sigma \nabla^2 \psi + \frac{\partial \psi}{\partial z} \frac{\partial \sigma}{\partial z} = 0. \quad (2.18)$$

We define the residual for the problem as

$$\begin{aligned} R(\mathbf{x}) &= \sigma \nabla^2 \psi + \frac{\partial \psi}{\partial z} \frac{\partial \sigma}{\partial z} - 0 \\ &= \sigma \nabla^2 \psi + \frac{\partial \psi}{\partial z} \frac{\partial \sigma}{\partial z}. \end{aligned}$$

Method of weighted residual :

$$\int R(\mathbf{x}) v d\mathbf{x} = 0. \quad (2.19)$$

In a cylindrical coordinate system (r, ϕ, z) , we have

$$\begin{aligned} \nabla^2 \psi &= \frac{1}{r} \frac{\partial}{\partial r} \left(r \frac{\partial \psi}{\partial r} \right) + \frac{1}{r^2} \frac{\partial^2 \psi}{\partial \phi^2} + \frac{\partial^2 \psi}{\partial z^2}, \\ &= \frac{1}{r} \left(r \frac{\partial^2 \psi}{\partial r^2} + \frac{\partial \psi}{\partial r} \right) + \frac{1}{r^2} \frac{\partial^2 \psi}{\partial \phi^2} + \frac{\partial^2 \psi}{\partial z^2}. \end{aligned}$$

The probe is used and located on the ground surface. The potential around the probe is symmetric and independent of ϕ , i.e. $\frac{\partial \psi}{\partial \phi} = 0$. It follows that $\frac{\partial^2 \psi}{\partial \phi^2} = 0$ in the real physical situation.

Therefore,

$$\nabla^2 \psi = \frac{1}{r} \left(r \frac{\partial^2 \psi}{\partial r^2} + \frac{\partial \psi}{\partial r} \right) + \frac{\partial^2 \psi}{\partial z^2}.$$

Hence from the equation (2.18), we have,

$$\begin{aligned} \sigma \nabla^2 \psi + \frac{\partial \psi}{\partial z} \frac{\partial \sigma}{\partial z} &= 0, \\ \sigma \left[\frac{1}{r} \left(r \frac{\partial^2 \psi}{\partial r^2} + \frac{\partial \psi}{\partial r} \right) + \frac{\partial^2 \psi}{\partial z^2} \right] + \frac{\partial \psi}{\partial z} \frac{\partial \sigma}{\partial z} &= 0, \\ \frac{1}{r} \left(r \frac{\partial^2 \psi}{\partial r^2} + \frac{\partial \psi}{\partial r} \right) + \frac{\partial^2 \psi}{\partial z^2} + \frac{1}{\sigma} \frac{\partial \psi}{\partial z} \frac{\partial \sigma}{\partial z} &= 0, \\ \frac{\partial^2 \psi}{\partial r^2} + \frac{1}{r} \frac{\partial \psi}{\partial r} + \frac{\partial^2 \psi}{\partial z^2} + \frac{1}{\sigma} \frac{\partial \psi}{\partial z} \frac{\partial \sigma}{\partial z} &= 0. \end{aligned} \quad (2.20)$$

The next step, we use finite element method to establish a numerical solution of our problem by applying the Galerkin's Method of Weighted Residuals to equation (2.20). Recall the Laplace equation in three-dimension with the electric charge on the cylinder

$$\nabla^2 \psi = \Delta \psi = \frac{1}{r} \frac{\partial \psi}{\partial r} + \frac{\partial^2 \psi}{\partial r^2} + \frac{1}{r} \frac{\partial^2 \psi}{\partial \phi^2} + \frac{\partial^2 \psi}{\partial z^2}. \quad (2.21)$$

Since the potential is independent of ϕ . Substituting (2.21) into (2.20), we obtain

$$\Delta\psi + \frac{1}{\sigma} \frac{\partial\psi}{\partial\sigma} \frac{\partial\sigma}{\partial z} = 0 \quad (2.22)$$

where $r \in [10, 100]$, $z \in [0, 90]$.

Let

$$V = \{v \in H_0^1 : v \text{ is a continuous function on } \Omega, \frac{\partial v}{\partial r} \text{ and } \frac{\partial v}{\partial z} \text{ are piecewise continuous on } \Omega \text{ and } v = 0 \text{ on } \partial\Omega\}.$$

By transforming the system into cylindrical coordinates (r, ϕ, z) [11] and use (2.22), the weighted residual in (2.19) becomes

$$\int R(r, \phi, z) v r dr d\phi dz = 0. \quad (2.23)$$

The weak formulation of (2.22) is

$$(\Delta\psi, v) + \left(\frac{1}{\sigma} \frac{\partial\psi}{\partial z} \frac{\partial\sigma}{\partial z}, v \right) = 0, \quad v \in V,$$

or

$$\int_{\Omega} \Delta\psi v d\Omega + \int_{\Omega} \frac{1}{\sigma} \frac{\partial\psi}{\partial z} \frac{\partial\sigma}{\partial z} v d\Omega = 0. \quad (2.24)$$

Since $\nabla^2\psi = \Delta\psi$ and from equation (2.24), we have

$$\int_{\Omega} \Delta\psi v d\Omega = \int_{\Omega} \nabla^2\psi v d\Omega = \int_{\Omega} v \nabla^2\psi d\Omega.$$

Note that $\int_{\Omega} v \nabla^2\psi d\Omega = \int_{\Omega} v \nabla \cdot \nabla\psi d\Omega$ together with the product rule for differentiation

$$\begin{aligned} \nabla \cdot (v \nabla\psi) &= \nabla\psi \cdot \nabla v + v \nabla \cdot \nabla\psi \\ v \nabla \cdot \nabla\psi &= \nabla \cdot (v \nabla\psi) - \nabla\psi \cdot \nabla v, \end{aligned}$$

we have

$$\int_{\Omega} v \nabla^2\psi d\Omega = \int_{\Omega} (\nabla \cdot (v \nabla\psi) - \nabla\psi \cdot \nabla v) d\Omega.$$

From the divergence theorem,

$$\int_{\Omega} \nabla \cdot (v \nabla\psi) d\Omega = \oint_{\partial\Omega} v \nabla\psi \cdot \vec{n} ds.$$

Therefore,

$$\begin{aligned}
\int_{\Omega} \Delta \psi v d\Omega &= \int_{\partial\Omega} v (\nabla \psi \cdot \vec{n}) ds - \int_{\Omega} \nabla v \cdot \nabla \psi d\Omega \\
&= \int_{\partial\Omega_1} v (\nabla \psi \cdot \vec{n}) ds + \int_{\partial\Omega_2} v (\nabla \psi \cdot \vec{n}) ds + \int_{\partial\Omega_3} v (\nabla \psi \cdot \vec{n}) ds \\
&\quad + \int_{\partial\Omega_4} v (\nabla \psi \cdot \vec{n}) ds - \int_{\Omega} \nabla v \cdot \nabla \psi d\Omega.
\end{aligned}$$

Since $v \in V$, $v = 0$ on $\partial\Omega_1, \partial\Omega_2, \partial\Omega_3$ and $\partial\Omega_4$, then

$$\int_{\Omega} \Delta \psi v d\Omega = - \int_{\Omega} \nabla v \cdot \nabla \psi d\Omega. \quad (2.25)$$

Substituting equation (2.25) into equation (2.24), we obtain

$$- \int_{\Omega} \nabla v \cdot \nabla \psi d\Omega + \int_{\Omega} \frac{1}{\sigma} \frac{\partial \psi}{\partial z} \frac{\partial \sigma}{\partial z} v d\Omega = 0. \quad (2.26)$$

$$- \int_{\Omega} r \nabla \psi \cdot \nabla v dr d\phi dz + \int_{\Omega} r \frac{1}{\sigma} \frac{\partial \psi}{\partial z} \frac{\partial \sigma}{\partial z} v dr d\phi dz = 0. \quad (2.27)$$

Since the problem is axisymmetric and independent of ϕ in cylindrical coordinate we divide equation (2.27) by 2π and derive the following formulation in the cylindrical coordinate (r, z) :

$$- \int_{\tilde{\Omega}} r \nabla \psi \cdot \nabla v dr dz + \int_{\tilde{\Omega}} r \frac{1}{\sigma} \frac{\partial \psi}{\partial z} \frac{\partial \sigma}{\partial z} v dr dz = 0 \quad (2.28)$$

where $\tilde{\Omega}$ is the two-dimensional cross-section of domain Ω (ϕ is fixed); i.e. $\tilde{\Omega} = \{(r, z) \in R^2 | 10 \leq r \leq 100, 0 \leq z \leq 90\}$. The boundary conditions (BC) of problem (2.22) and the notation of the potential in the domain which is refined using bilinear rectangular elements are shown in Figure 2.2

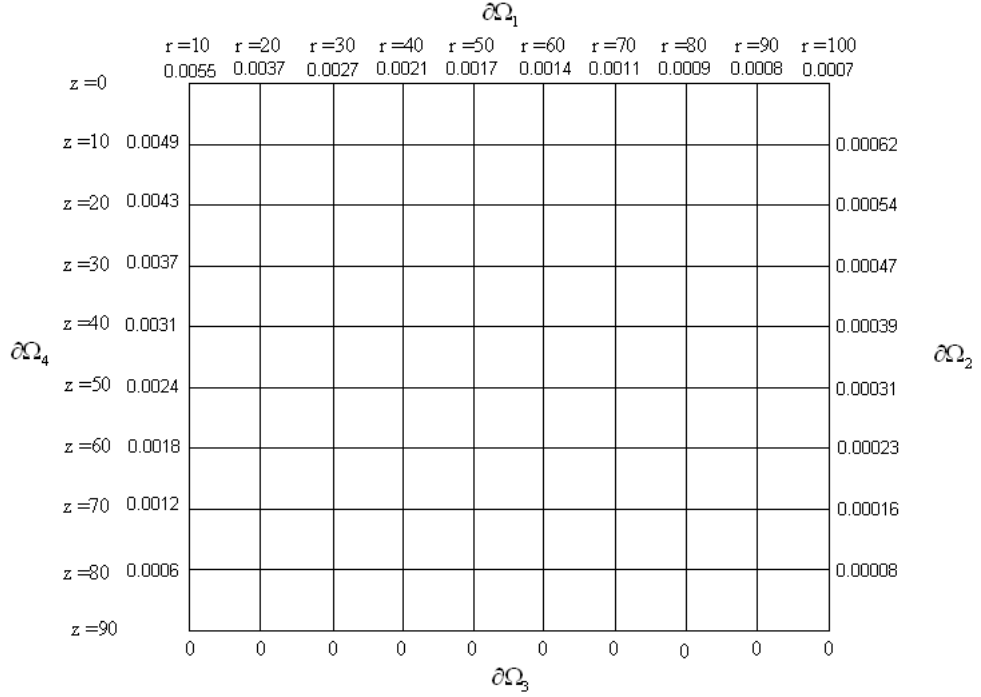


Figure 2.2: Boundary condition of the earth structure.

The values of potential on the surface at $z = 0\text{m}$ are obtained by generating the potential from the mathematical model of Chaladgarn and Yooyuanyong, (2013)[32] when $b = 0.0005\text{m}^{-2}$, $l = 10\text{m}$, $d = 90\text{m}$ (the thickness of the earth layer). The potential decreases to zero as the depth increases, i.e we assume that the potential is zero at $z = 90\text{m}$. The values of the potential on $\partial\Omega_2$ and $\partial\Omega_4$ are obtained from the approximation by linear function, $g_1(r, z) = -6.11 \times 10^{-5}z + 0.0055$ on $\partial\Omega_4$ and $g_2(r, z) = -7.78 \times 10^{-6}z + 0.0007$ on $\partial\Omega_2$, respectively.

Next, we consider the domain of equation (2.28) in two-dimensions. By dividing the domain into rectangular elements. We discretize r into 9 subintervals and, discretize z into 9 subintervals equally. Let (r_i, z_j) be a node of Ω on the non-overlapping rectangular grids such that the horizontal and vertical edges of these rectangles are parallel to the r - and z - coordinate axes, respectively. As a result,

$$\begin{aligned} r_k &= 10k, \\ z_k &= 10(k-1), \quad k = 1, \dots, 10. \end{aligned}$$

Since the form of equation (2.28) suggests that the finite elements can have an arbitrary shape and position in space computing integrals over their element domains is a bit tricky. To overcome this difficulty one uses a projection method which maps the coordinates of a well known reference element to the coordinates of an arbitrary element in space. Computing an integral on the local reference element

(e.g. it's area) is easy. One just has to capture the effect of the mapping (deformation, stretching, shearing) to get the right value of the integral for the global element domain. During the mapping process the points in the local coordinate system ξ, η (here : parent domain) get mapped to points in the global coordinate system r, z by a mapping the values range from -1 to +1, and the reference coordinates are transformed to $(\xi_1, \eta_1) = (-1, -1)$, $(\xi_2, \eta_2) = (1, -1)$, $(\xi_3, \eta_3) = (1, 1)$, $(\xi_4, \eta_4) = (-1, 1)$, as shown in Figure 2.3(b).

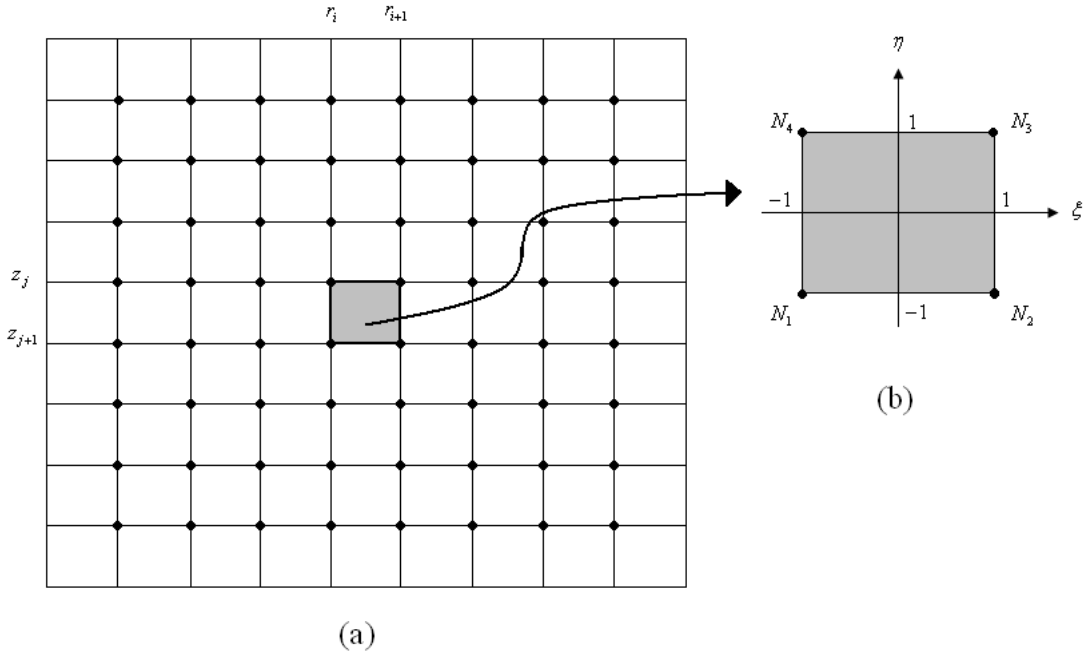


Figure 2.3: Reference and transformed coordinates of the boundary.

By using a transformation in Figure 2.3, we have

$$r = r_k + \frac{h}{2}(1 + \xi), \quad dr = \frac{h}{2}d\xi$$

$$z = z_k + \frac{h}{2}(1 + \eta), \quad dz = \frac{h}{2}d\eta.$$

And from Figure 2.3(b), the basis functions $N_\gamma, \gamma = 1, 2, 3, 4$ in (ξ, η) coordinates which have the relationship with coordinate (r, z) are defined as

$$\begin{aligned} r &= N_1 r_1 + N_2 r_2 + N_3 r_3 + N_4 r_4, \\ z &= N_1 z_1 + N_2 z_2 + N_3 z_3 + N_4 z_4 \end{aligned} \quad (2.29)$$

such that basis functions can be written in the form of ξ and η as follows

$$\begin{aligned} N_1(\xi, \eta) &= \frac{1}{4}(1 - \xi)(1 - \eta), \\ N_2(\xi, \eta) &= \frac{1}{4}(1 + \xi)(1 - \eta), \\ N_3(\xi, \eta) &= \frac{1}{4}(1 + \xi)(1 + \eta), \\ N_4(\xi, \eta) &= \frac{1}{4}(1 - \xi)(1 + \eta). \end{aligned} \quad (2.30)$$

For convenience, we rename the potential at the node (r_i, z_j) to Ψ_i , so we have $\{\Psi\}_{i=1}^{100}$ as the potential at the nodes of the element in Ω . For simplicity and to avoid any confusion, we use Ψ_i for $\Psi(X_i)$, $1 \leq i \leq 100$. In other words, we define nodes X_i for (r_i, z_j) , $1 \leq i, j \leq 10$. For each X_i , $i = 1, 2, \dots, 100$, we define the basis function β_j such that

$$\beta_j(X_i) = \begin{cases} 1, & \text{if } i = j \\ 0, & \text{if } i \neq j \end{cases}$$

and function $v \in V$ can be written in the form of linear combination of trial function β_i

$$v(X) = \sum_{i=1}^{100} \alpha_i \beta_i(X).$$

We obtain $v(X_i) = \alpha_i$, by choosing appropriate values of α_i and equation (2.28) becomes

$$-\int_{\tilde{\Omega}} r \nabla \psi \cdot \nabla \beta_i dr dz + \int_{\tilde{\Omega}} r \frac{1}{\sigma} \frac{\partial \psi}{\partial z} \frac{\partial \sigma}{\partial z} \beta_i dr dz = 0 \quad (2.31)$$

and from $\sigma(z) = \sigma_0 e^{-\frac{b(z-l)^2}{2}}$ such that σ_0 , b , and l are constants, we have

$$-\int_{\tilde{\Omega}} r \nabla \psi \cdot \nabla \beta_i dr dz + \int_{\tilde{\Omega}} r b (l - z) \frac{\partial \psi}{\partial z} \beta_i dr dz = 0 \quad (2.32)$$

for $i = 1, 2, \dots, 100$. Next, we consider the solution in the form of linear combination of trial function β_j

$$\psi(X) = \sum_{j=1}^{100} \Psi_j \beta_j(X)$$

when Ψ_j is the unknown. The equation (2.32) can be written in the form of linear combination as follows for each $i = 1, 2, \dots, 100$,

$$\sum_{j=1}^{100} \Psi_j \left[-\int_{\tilde{\Omega}} r \nabla \beta_j \cdot \nabla \beta_i dr dz + \int_{\tilde{\Omega}} r b (l - z) \frac{\partial \beta_j}{\partial z} \beta_i dr dz \right] = 0. \quad (2.33)$$

After that by using a transformation in Figure 2.3, we will consider the value of $\int_{\tilde{\Omega}} r \nabla \beta_j \cdot \nabla \beta_i dr dz$ by using Chain rule, thus

$$\begin{aligned}
\int_{\tilde{\Omega}} r \nabla \beta_j \cdot \nabla \beta_i dr dz &= \int_{\tilde{\Omega}} r \left[\frac{\partial \beta_j}{\partial r} \frac{\partial \beta_i}{\partial r} + \frac{\partial \beta_j}{\partial z} \frac{\partial \beta_i}{\partial z} \right] dr dz, \\
&= \int_{-1}^1 \int_{-1}^1 r \left[\left(\frac{\partial \hat{\beta}_j}{\partial \xi} \frac{\partial \xi}{\partial r} + \frac{\partial \hat{\beta}_j}{\partial \eta} \frac{\partial \eta}{\partial r} \right) \left(\frac{\partial \hat{\beta}_i}{\partial \xi} \frac{\partial \xi}{\partial r} + \frac{\partial \hat{\beta}_i}{\partial \eta} \frac{\partial \eta}{\partial r} \right) \right. \\
&\quad \left. + r \left[\left(\frac{\partial \hat{\beta}_j}{\partial \xi} \frac{\partial \xi}{\partial z} + \frac{\partial \hat{\beta}_j}{\partial \eta} \frac{\partial \eta}{\partial z} \right) \left(\frac{\partial \hat{\beta}_i}{\partial \xi} \frac{\partial \xi}{\partial z} + \frac{\partial \hat{\beta}_i}{\partial \eta} \frac{\partial \eta}{\partial z} \right) \right] \left(\frac{h}{2} \right)^2 d\xi d\eta, \\
&= \int_{-1}^1 \int_{-1}^1 \left(\frac{2}{h} \right)^2 r \left[\left(\frac{\partial \hat{\beta}_j}{\partial \xi} \frac{\partial \hat{\beta}_i}{\partial \xi} \right) + \left(\frac{\partial \hat{\beta}_j}{\partial \eta} \frac{\partial \hat{\beta}_i}{\partial \eta} \right) \right] \left(\frac{h}{2} \right)^2 d\xi d\eta, \\
&= \int_{-1}^1 \int_{-1}^1 \left(r_k + \frac{h}{2} (1 + \xi) \right) \left[\left(\frac{\partial \hat{\beta}_j}{\partial \xi} \frac{\partial \hat{\beta}_i}{\partial \xi} \right) + \left(\frac{\partial \hat{\beta}_j}{\partial \eta} \frac{\partial \hat{\beta}_i}{\partial \eta} \right) \right] d\xi d\eta
\end{aligned} \tag{2.34}$$

where $k = 1, 2, \dots, 9$.

Consider the value of $\int_{\tilde{\Omega}} r b (l - z) \frac{\partial \beta_j}{\partial z} \beta_i dr dz$ by using chain rule and Jacobian transform, we obtain

$$\begin{aligned}
\int_{\tilde{\Omega}} r b (l - z) \frac{\partial \beta_j}{\partial z} \beta_i dr dz &= \int_{-1}^1 \int_{-1}^1 r b (l - z) \left[\left(\frac{\partial \hat{\beta}_j}{\partial \xi} \frac{\partial \xi}{\partial z} + \frac{\partial \hat{\beta}_j}{\partial \eta} \frac{\partial \eta}{\partial z} \right) \right] \hat{\beta}_j \left(\frac{h}{2} \right)^2 d\xi d\eta, \\
&= \int_{-1}^1 \int_{-1}^1 r b (l - z) \left[\left(\frac{\partial \hat{\beta}_j}{\partial \xi} (0) + \frac{\partial \hat{\beta}_j}{\partial \eta} \left(\frac{2}{h} \right) \right) \right] \hat{\beta}_j \left(\frac{h}{2} \right)^2 d\xi d\eta, \\
&= \int_{-1}^1 \int_{-1}^1 r b (l - z) \left(\frac{h}{2} \right) \frac{\partial \hat{\beta}_j}{\partial \eta} \hat{\beta}_j d\xi d\eta, \\
&= \left(\frac{bh}{2} \right) \int_{-1}^1 \int_{-1}^1 r (l - z) \frac{\partial \hat{\beta}_j}{\partial \eta} \hat{\beta}_j d\xi d\eta,
\end{aligned}$$

thus,

$$\begin{aligned}
& \int_{\bar{\Omega}} rb(l-z) \frac{\partial \beta_j}{\partial z} \beta_i dr dz \\
&= \left(\frac{bh}{2}\right) \int_{-1}^1 \int_{-1}^1 \left(r_k + \frac{h}{2}(1+\xi)\right) \left(l - z_k - \frac{h}{2}(1+\eta)\right) \frac{\partial \hat{\beta}_j}{\partial \eta} \hat{\beta}_j d\xi d\eta
\end{aligned} \tag{2.35}$$


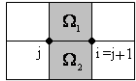
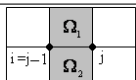
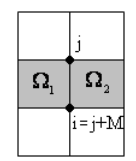
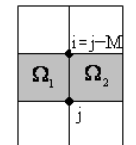
where $k = 1, 2, \dots, 9$. Therefore,

$$\begin{aligned}
& - \int_{\bar{\Omega}} r \nabla \beta_j \cdot \nabla \beta_i dr dz + \int_{\bar{\Omega}} rb(l-z) \frac{\partial \beta_j}{\partial z} \beta_i dr dz \\
&= - \int_{-1}^1 \int_{-1}^1 \left(r_k + \frac{h}{2}(1+\xi)\right) \left[\left(\frac{\partial \hat{\beta}_j}{\partial \xi} \frac{\partial \hat{\beta}_i}{\partial \xi}\right) + \left(\frac{\partial \hat{\beta}_j}{\partial \eta} \frac{\partial \hat{\beta}_i}{\partial \eta}\right) \right] d\xi d\eta \\
&+ \left(\frac{bh}{2}\right) \int_{-1}^1 \int_{-1}^1 \left(r_k + \frac{h}{2}(1+\xi)\right) \left(l - z_k - \frac{h}{2}(1+\eta)\right) \frac{\partial \hat{\beta}_j}{\partial \eta} \hat{\beta}_j d\xi d\eta
\end{aligned} \tag{2.36}$$

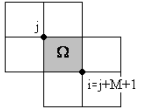
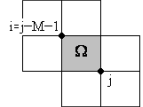
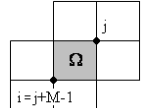
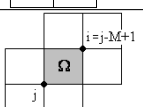
where $k = 1, 2, \dots, 9$.

Consider the value of $\int_{-1}^1 \int_{-1}^1 \left(r_k + \frac{h}{2}(1+\xi)\right) \left[\left(\frac{\partial \hat{\beta}_j}{\partial \xi} \frac{\partial \hat{\beta}_i}{\partial \xi}\right) + \left(\frac{\partial \hat{\beta}_j}{\partial \eta} \frac{\partial \hat{\beta}_i}{\partial \eta}\right) \right] d\xi d\eta$ in (ξ, η) coordinate, for the corresponding Linear rectangular elements on $[-1, 1] \times [-1, 1]$, the approximation $\int_{-1}^1 \int_{-1}^1 \left(r_k + \frac{h}{2}(1+\xi)\right) \left[\left(\frac{\partial \hat{\beta}_j}{\partial \xi} \frac{\partial \hat{\beta}_i}{\partial \xi}\right) + \left(\frac{\partial \hat{\beta}_j}{\partial \eta} \frac{\partial \hat{\beta}_i}{\partial \eta}\right) \right] d\xi d\eta$ can be divided into nine cases which in following table.

The values of $\int \int_{\tilde{\Omega}} \left(r_k + \frac{h}{2} (1 + \xi) \right) \left[\left(\frac{\partial \hat{\beta}_j}{\partial \xi} \frac{\partial \hat{\beta}_i}{\partial \xi} \right) + \left(\frac{\partial \hat{\beta}_j}{\partial \eta} \frac{\partial \hat{\beta}_i}{\partial \eta} \right) \right] d\xi d\eta$ in coordinate (ξ, η)

Elements	Cases	The values of $\int \int_{\tilde{\Omega}} \left(r_k + \frac{h}{2} (1 + \xi) \right) \left[\left(\frac{\partial \hat{\beta}_j}{\partial \xi} \frac{\partial \hat{\beta}_i}{\partial \xi} \right) + \left(\frac{\partial \hat{\beta}_j}{\partial \eta} \frac{\partial \hat{\beta}_i}{\partial \eta} \right) \right] d\xi d\eta$ in coordinate (ξ, η)	Solutions
	$i = j$	$\int_{-1}^1 \int_{-1}^1 \left(r_k + \frac{h}{2} (1 + \xi) \right) \left[\left(\frac{\partial N_3}{\partial \xi} \frac{\partial N_3}{\partial \xi} + \frac{\partial N_3}{\partial \eta} \frac{\partial N_3}{\partial \eta} \right) + \left(\frac{\partial N_2}{\partial \xi} \frac{\partial N_2}{\partial \xi} + \frac{\partial N_2}{\partial \eta} \frac{\partial N_2}{\partial \eta} \right) \right] d\xi d\eta$ $+ \int_{-1}^1 \int_{-1}^1 \left(r_{k+1} + \frac{h}{2} (1 + \xi) \right) \left[\left(\frac{\partial N_4}{\partial \xi} \frac{\partial N_4}{\partial \xi} + \frac{\partial N_4}{\partial \eta} \frac{\partial N_4}{\partial \eta} \right) + \left(\frac{\partial N_1}{\partial \xi} \frac{\partial N_1}{\partial \xi} + \frac{\partial N_1}{\partial \eta} \frac{\partial N_1}{\partial \eta} \right) \right] d\xi d\eta$	$\frac{1}{6} (80 + 160k + 8h)$
	$i = j + 1$	$\int_{-1}^1 \int_{-1}^1 \left(r_k + \frac{h}{2} (1 + \xi) \right) \left[\left(\frac{\partial N_4}{\partial \xi} \frac{\partial N_3}{\partial \xi} + \frac{\partial N_4}{\partial \eta} \frac{\partial N_3}{\partial \eta} \right) + \left(\frac{\partial N_1}{\partial \xi} \frac{\partial N_2}{\partial \xi} + \frac{\partial N_1}{\partial \eta} \frac{\partial N_2}{\partial \eta} \right) \right] d\xi d\eta$	$-\frac{1}{6} (20k + h)$
	$i = j - 1$	$\int_{-1}^1 \int_{-1}^1 \left(r_k + \frac{h}{2} (1 + \xi) \right) \left[\left(\frac{\partial N_3}{\partial \xi} \frac{\partial N_4}{\partial \xi} + \frac{\partial N_3}{\partial \eta} \frac{\partial N_4}{\partial \eta} \right) + \left(\frac{\partial N_2}{\partial \xi} \frac{\partial N_1}{\partial \xi} + \frac{\partial N_2}{\partial \eta} \frac{\partial N_1}{\partial \eta} \right) \right] d\xi d\eta$	$-\frac{1}{6} (20k + h)$
	$i = j + M$	$\int_{-1}^1 \int_{-1}^1 \left(r_k + \frac{h}{2} (1 + \xi) \right) \left[\left(\frac{\partial N_3}{\partial \xi} \frac{\partial N_2}{\partial \xi} + \frac{\partial N_3}{\partial \eta} \frac{\partial N_2}{\partial \eta} \right) \right] d\xi d\eta$ $+ \int_{-1}^1 \int_{-1}^1 \left(r_{k+1} + \frac{h}{2} (1 + \xi) \right) \left[\left(\frac{\partial N_4}{\partial \xi} \frac{\partial N_1}{\partial \xi} + \frac{\partial N_4}{\partial \eta} \frac{\partial N_1}{\partial \eta} \right) \right] d\xi d\eta$	$-\frac{1}{6} (10 + 20k + h)$
	$i = j - M$	$\int_{-1}^1 \int_{-1}^1 \left(r_k + \frac{h}{2} (1 + \xi) \right) \left[\left(\frac{\partial N_2}{\partial \xi} \frac{\partial N_3}{\partial \xi} + \frac{\partial N_2}{\partial \eta} \frac{\partial N_3}{\partial \eta} \right) \right] d\xi d\eta$ $+ \int_{-1}^1 \int_{-1}^1 \left(r_{k+1} + \frac{h}{2} (1 + \xi) \right) \left[\left(\frac{\partial N_1}{\partial \xi} \frac{\partial N_4}{\partial \xi} + \frac{\partial N_1}{\partial \eta} \frac{\partial N_4}{\partial \eta} \right) \right] d\xi d\eta$	$-\frac{1}{6} (10 + 20k + h)$

The values of $\int \int_{\tilde{\Omega}} \left(r_k + \frac{h}{2} (1 + \xi) \right) \left[\left(\frac{\partial \hat{\beta}_j}{\partial \xi} \frac{\partial \hat{\beta}_i}{\partial \xi} \right) + \left(\frac{\partial \hat{\beta}_j}{\partial \eta} \frac{\partial \hat{\beta}_i}{\partial \eta} \right) \right] d\xi d\eta$ in coordinate (ξ, η)

Elements	Cases	The values of $\int \int_{\tilde{\Omega}} \left(r_k + \frac{h}{2} (1 + \xi) \right) \left[\left(\frac{\partial \hat{\beta}_j}{\partial \xi} \frac{\partial \hat{\beta}_i}{\partial \xi} \right) + \left(\frac{\partial \hat{\beta}_j}{\partial \eta} \frac{\partial \hat{\beta}_i}{\partial \eta} \right) \right] d\xi d\eta$ in coordinate (ξ, η)	Solutions
	$i = j + M + 1$	$\int_{-1}^1 \int_{-1}^1 \left(r_k + \frac{h}{2} (1 + \xi) \right) \left[\left(\frac{\partial N_4}{\partial \xi} \frac{\partial N_2}{\partial \xi} + \frac{\partial N_4}{\partial \eta} \frac{\partial N_2}{\partial \eta} \right) \right] d\xi d\eta$	$-\frac{1}{6} (20k + h)$
	$i = j - M - 1$	$\int_{-1}^1 \int_{-1}^1 \left(r_k + \frac{h}{2} (1 + \xi) \right) \left[\left(\frac{\partial N_2}{\partial \xi} \frac{\partial N_4}{\partial \xi} + \frac{\partial N_2}{\partial \eta} \frac{\partial N_4}{\partial \eta} \right) \right] d\xi d\eta$	$-\frac{1}{6} (20k + h)$
	$i = j + M - 1$	$\int_{-1}^1 \int_{-1}^1 \left(r_k + \frac{h}{2} (1 + \xi) \right) \left[\left(\frac{\partial N_3}{\partial \xi} \frac{\partial N_1}{\partial \xi} + \frac{\partial N_3}{\partial \eta} \frac{\partial N_1}{\partial \eta} \right) \right] d\xi d\eta$	$-\frac{1}{6} (20k + h)$
	$i = j - M + 1$	$\int_{-1}^1 \int_{-1}^1 \left(r_k + \frac{h}{2} (1 + \xi) \right) \left[\left(\frac{\partial N_1}{\partial \xi} \frac{\partial N_3}{\partial \xi} + \frac{\partial N_1}{\partial \eta} \frac{\partial N_3}{\partial \eta} \right) \right] d\xi d\eta$	$-\frac{1}{6} (20k + h)$

where $k = 1, 2, \dots, 9$.



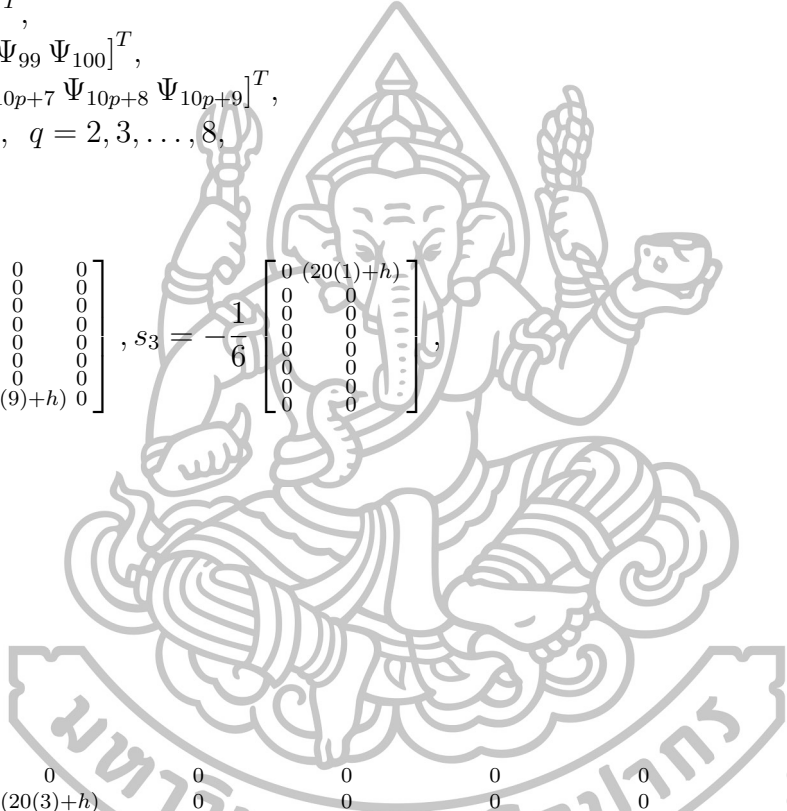
$\hat{U} = [ub_1 u_1 ub_2 u_2 ub_3 u_3 ub_4 u_4 ub_5 u_5 ub_6 u_6 ub_7 u_7 ub_8 u_8 ub_9]^T$ and $0 = [0]_{1 \times 100}$ such that

$$\begin{aligned} ub_1 &= [\Psi_1 \Psi_2 \Psi_3 \Psi_4 \Psi_5 \Psi_6 \Psi_7 \Psi_8 \Psi_9 \Psi_{10} \Psi_{11}]^T, \\ ub_9 &= [\Psi_{90} \Psi_{91} \Psi_{92} \Psi_{93} \Psi_{94} \Psi_{95} \Psi_{96} \Psi_{97} \Psi_{98} \Psi_{99} \Psi_{100}]^T, \\ u_p &= [\Psi_{10p+2} \Psi_{10p+3} \Psi_{10p+4} \Psi_{10p+5} \Psi_{10p+6} \Psi_{10p+7} \Psi_{10p+8} \Psi_{10p+9}]^T, \\ ub_q &= [\Psi_{10q} \Psi_{10p+1}]^T, \text{ for all } p = 1, 2, \dots, 8, \quad q = 2, 3, \dots, 8, \end{aligned}$$

$$s_1 = -\frac{1}{6} \begin{bmatrix} 0 & (20(1)+h) \\ 0 & 0 \\ 0 & 0 \\ 0 & 0 \\ 0 & 0 \\ 0 & 0 \\ (20(9)+h) & 0 \end{bmatrix}, s_2 = -\frac{1}{6} \begin{bmatrix} 0 & 0 \\ 0 & 0 \\ 0 & 0 \\ 0 & 0 \\ 0 & 0 \\ 0 & 0 \\ (20(9)+h) & 0 \end{bmatrix}, s_3 = -\frac{1}{6} \begin{bmatrix} 0 & (20(1)+h) \\ 0 & 0 \\ 0 & 0 \\ 0 & 0 \\ 0 & 0 \\ 0 & 0 \\ 0 & 0 \\ 0 & 0 \\ 0 & 0 \end{bmatrix},$$

$$A_1 = \begin{bmatrix} 1 & 0 & 0 & 0 & 0 & 0 & 0 & 0 & 0 & 0 & 0 \\ 0 & 1 & 0 & 0 & 0 & 0 & 0 & 0 & 0 & 0 & 0 \\ 0 & 0 & 1 & 0 & 0 & 0 & 0 & 0 & 0 & 0 & 0 \\ 0 & 0 & 0 & 1 & 0 & 0 & 0 & 0 & 0 & 0 & 0 \\ 0 & 0 & 0 & 0 & 1 & 0 & 0 & 0 & 0 & 0 & 0 \\ 0 & 0 & 0 & 0 & 0 & 1 & 0 & 0 & 0 & 0 & 0 \\ 0 & 0 & 0 & 0 & 0 & 0 & 1 & 0 & 0 & 0 & 0 \\ 0 & 0 & 0 & 0 & 0 & 0 & 0 & 1 & 0 & 0 & 0 \\ 0 & 0 & 0 & 0 & 0 & 0 & 0 & 0 & 1 & 0 & 0 \\ 0 & 0 & 0 & 0 & 0 & 0 & 0 & 0 & 0 & 1 & 0 \\ 0 & 0 & 0 & 0 & 0 & 0 & 0 & 0 & 0 & 0 & 1 \end{bmatrix}, t = \begin{bmatrix} 1 & 0 \\ 0 & 1 \end{bmatrix},$$

$$A_2 = -\frac{1}{6} \begin{bmatrix} (20(1)+h) & (10+20(1)+h) & (20(2)+h) & 0 & 0 & 0 & 0 & 0 & 0 & 0 & 0 & (20(1)+h) \\ 0 & (20(2)+h) & (10+20(2)+h) & (20(3)+h) & 0 & 0 & 0 & 0 & 0 & 0 & 0 & 0 \\ 0 & 0 & 0 & (20(3)+h) & (10+20(3)+h) & (20(4)+h) & 0 & 0 & 0 & 0 & 0 & 0 \\ 0 & 0 & 0 & 0 & (20(4)+h) & (10+20(4)+h) & (20(5)+h) & 0 & 0 & 0 & 0 & 0 \\ 0 & 0 & 0 & 0 & 0 & (20(5)+h) & (10+20(5)+h) & (20(6)+h) & 0 & 0 & 0 & 0 \\ 0 & 0 & 0 & 0 & 0 & 0 & (20(6)+h) & (10+20(6)+h) & (20(7)+h) & 0 & 0 & 0 \\ 0 & 0 & 0 & 0 & 0 & 0 & 0 & (20(7)+h) & (10+20(7)+h) & (20(8)+h) & 0 & 0 \\ 0 & 0 & 0 & 0 & 0 & 0 & 0 & 0 & (20(8)+h) & (10+20(8)+h) & (20(9)+h) & 0 \end{bmatrix},$$



Since we know the value of the potential at the boundary $\Psi_1, \Psi_2, \Psi_3, \dots, \Psi_{11}, \Psi_{90}, \Psi_{91}, \Psi_{92}, \dots, \Psi_{100}$ and Ψ_{10q}, Ψ_{10q+1} for all $q = 2, 3, \dots, 8$ the system can be written as

$$\text{or } \begin{bmatrix} A_3 & A_4 & 0 & 0 & 0 & 0 & 0 & 0 \\ A_4 & A_3 & A_4 & 0 & 0 & 0 & 0 & 0 \\ 0 & A_4 & A_3 & A_4 & 0 & 0 & 0 & 0 \\ 0 & 0 & A_4 & A_3 & A_4 & 0 & 0 & 0 \\ 0 & 0 & 0 & A_4 & A_3 & A_4 & 0 & 0 \\ 0 & 0 & 0 & 0 & A_4 & A_3 & A_4 & 0 \\ 0 & 0 & 0 & 0 & 0 & A_4 & A_3 & A_4 \\ 0 & 0 & 0 & 0 & 0 & 0 & A_4 & A_3 \end{bmatrix} \begin{bmatrix} u_1 \\ u_2 \\ u_3 \\ u_4 \\ u_5 \\ u_6 \\ u_7 \\ u_8 \end{bmatrix} = \begin{bmatrix} a_1 \\ a_2 \\ a_3 \\ a_4 \\ a_5 \\ a_6 \\ a_7 \\ a_8 \end{bmatrix}$$

where

$$A = \begin{bmatrix} A_3 & A_4 & 0 & 0 & 0 & 0 & 0 & 0 \\ A_4 & A_3 & A_4 & 0 & 0 & 0 & 0 & 0 \\ 0 & A_4 & A_3 & A_4 & 0 & 0 & 0 & 0 \\ 0 & 0 & A_4 & A_3 & A_4 & 0 & 0 & 0 \\ 0 & 0 & 0 & A_4 & A_3 & A_4 & 0 & 0 \\ 0 & 0 & 0 & 0 & A_4 & A_3 & A_4 & 0 \\ 0 & 0 & 0 & 0 & 0 & A_4 & A_3 & A_4 \\ 0 & 0 & 0 & 0 & 0 & 0 & A_4 & A_3 \end{bmatrix}$$

and $U = u_p = [\Psi_{10p+2} \Psi_{10p+3} \Psi_{10p+4} \Psi_{10p+5} \Psi_{10p+6} \Psi_{10p+7} \Psi_{10p+8} \Psi_{10p+9}]^T$,
 $P = [a_1, \dots, a_8]^T$ for all $p = 1, 2, \dots, 8$
 and

$$a_1 = -\frac{1}{6} \begin{bmatrix} (20(1)+h)(0.0055)+(10+20(1)+h)(0.0037)+(20(2)+h)(0.0027)+(20(1)+h)(0.0049)+(20(1)+h)(0.0043) \\ (20(2)+h)(0.0037)+(10+20(2)+h)(0.0027)+(20(3)+h)(0.0021) \\ (20(3)+h)(0.0027)+(10+20(3)+h)(0.0021)+(20(4)+h)(0.0017) \\ (20(4)+h)(0.0021)+(10+20(4)+h)(0.0017)+(20(5)+h)(0.0014) \\ (20(5)+h)(0.0017)+(10+20(5)+h)(0.0014)+(20(6)+h)(0.0011) \\ (20(6)+h)(0.0014)+(10+20(6)+h)(0.0011)+(20(7)+h)(0.0009) \\ (20(7)+h)(0.0011)+(10+20(7)+h)(0.0009)+(20(8)+h)(0.0008) \\ (20(8)+h)(0.0009)+(10+20(8)+h)(0.0008)+(20(9)+h)(0.0007)+(20(9)+h)(0.00062)+(20(9)+h)(0.00054) \end{bmatrix},$$

$$a_2 = -\frac{1}{6} \begin{bmatrix} (20(1)+h)(0.0049)+(20(1)+h)(0.0043)+(20(1)+h)(0.0037) \\ 0 \\ 0 \\ 0 \\ 0 \\ 0 \\ 0 \\ (20(9)+h)(0.00062)+(20(9)+h)(0.00054)+(20(9)+h)(0.00047) \end{bmatrix},$$

$$a_3 = -\frac{1}{6} \begin{bmatrix} (20(1)+h)(0.0043)+(20(1)+h)(0.0037)+(20(1)+h)(0.0031) \\ 0 \\ 0 \\ 0 \\ 0 \\ 0 \\ (20(9)+h)(0.00054)+(20(9)+h)(0.00047)+(20(9)+h)(0.00039) \end{bmatrix},$$

$$a_4 = -\frac{1}{6} \begin{bmatrix} (20(1)+h)(0.0037)+(20(1)+h)(0.0031)+(20(1)+h)(0.0024) \\ 0 \\ 0 \\ 0 \\ 0 \\ 0 \\ (20(9)+h)(0.00047)+(20(9)+h)(0.00039)+(20(9)+h)(0.00031) \end{bmatrix},$$

$$a_5 = -\frac{1}{6} \begin{bmatrix} (20(1)+h)(0.0031)+(20(1)+h)(0.0024)+(20(1)+h)(0.0018) \\ 0 \\ 0 \\ 0 \\ 0 \\ 0 \\ (20(9)+h)(0.00039)+(20(9)+h)(0.00031)+(20(9)+h)(0.00023) \end{bmatrix},$$

$$a_6 = -\frac{1}{6} \begin{bmatrix} (20(1)+h)(0.0024)+(20(1)+h)(0.0018)+(20(1)+h)(0.0012) \\ 0 \\ 0 \\ 0 \\ 0 \\ 0 \\ (20(9)+h)(0.00031)+(20(9)+h)(0.00023)+(20(9)+h)(0.00016) \end{bmatrix},$$

$$a_7 = -\frac{1}{6} \begin{bmatrix} (20(1)+h)(0.0018)+(20(1)+h)(0.0012)+(20(1)+h)(0.0006) \\ 0 \\ 0 \\ 0 \\ 0 \\ 0 \\ (20(9)+h)(0.00023)+(20(9)+h)(0.00016)+(20(9)+h)(0.00008) \end{bmatrix},$$

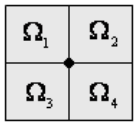
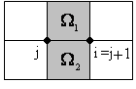
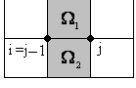
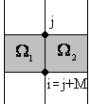
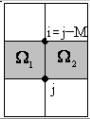
$$a_8 = -\frac{1}{6} \begin{bmatrix} (20(1)+h)(0.0012)+(20(1)+h)(0.0006) \\ 0 \\ 0 \\ 0 \\ 0 \\ 0 \\ (20(9)+h)(0.00016)+(20(9)+h)(0.00008) \end{bmatrix}.$$

Next we consider the value of

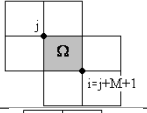
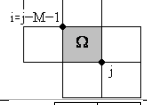
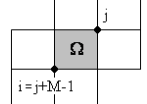
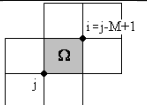
$$\left(\frac{bh}{2}\right) \int_{-1}^1 \int_{-1}^1 \left(r_k + \frac{h}{2}(1+\xi)\right) \left(l - z_k - \frac{h}{2}(1+\eta)\right) \frac{\partial \hat{\beta}_j}{\partial \eta} \hat{\beta}_j d\xi d\eta$$

in coordinates (ξ, η) as in the following tables

The values of $\left(\frac{bh}{2}\right) \int_{-1}^1 \int_{-1}^1 \left(r_k + \frac{h}{2}(1+\xi)\right) \left(l - z_k - \frac{h}{2}(1+\eta)\right) \frac{\partial \hat{\beta}_j}{\partial \eta} \hat{\beta}_j d\xi d\eta$ in coordinate (ξ, η)

Elements	Cases	The values of $\left(\frac{bh}{2}\right) \int_{-1}^1 \int_{-1}^1 \left(r_k + \frac{h}{2}(1+\xi)\right) \left(l - z_k - \frac{h}{2}(1+\eta)\right) \frac{\partial \hat{\beta}_j}{\partial \eta} \hat{\beta}_j d\xi d\eta$ in coordinate (ξ, η)	Solutions
	$i = j$	$\int_{-1}^1 \int_{-1}^1 \left(r_k + \frac{h}{2}(1+\xi)\right) \left[\left(l - z_k - \frac{h}{2}(1+\eta)\right) \frac{\partial N_2}{\partial \eta} N_2 + \left(l - z_{k+1} - \frac{h}{2}(1+\eta)\right) \frac{\partial N_3}{\partial \eta} N_3 \right] d\xi d\eta$ $+ \int_{-1}^1 \int_{-1}^1 \left(r_{k+1} + \frac{h}{2}(1+\xi)\right) \left[\left(l - z_k - \frac{h}{2}(1+\eta)\right) \frac{\partial N_1}{\partial \eta} N_1 + \left(l - z_{k+1} - \frac{h}{2}(1+\eta)\right) \frac{\partial N_4}{\partial \eta} N_4 \right] d\xi d\eta$	$-\frac{bh}{18} (30+h)(10+20k+h)$
	$i = j + 1$	$\int_{-1}^1 \int_{-1}^1 \left(r_k + \frac{h}{2}(1+\xi)\right) \left[\left(l - z_k - \frac{h}{2}(1+\eta)\right) \frac{\partial N_1}{\partial \eta} N_2 + \left(l - z_{k+1} - \frac{h}{2}(1+\eta)\right) \frac{\partial N_4}{\partial \eta} N_3 \right] d\xi d\eta$	$-\frac{bh}{72} (30+h)(20k+h)$
	$i = j - 1$	$\int_{-1}^1 \int_{-1}^1 \left(r_k + \frac{h}{2}(1+\xi)\right) \left[\left(l - z_k - \frac{h}{2}(1+\eta)\right) \frac{\partial N_2}{\partial \eta} N_1 + \left(l - z_{k+1} - \frac{h}{2}(1+\eta)\right) \frac{\partial N_3}{\partial \eta} N_4 \right] d\xi d\eta$	$-\frac{bh}{72} (30+h)(20k+h)$
	$i = j + M$	$\int_{-1}^1 \int_{-1}^1 \left(l - z_k - \frac{h}{2}(1+\eta)\right) \left[\left(r_k + \frac{h}{2}(1+\xi)\right) \frac{\partial N_3}{\partial \eta} N_2 + \left(r_{k+1} + \frac{h}{2}(1+\xi)\right) \frac{\partial N_4}{\partial \eta} N_1 \right] d\xi d\eta$	$-\frac{bh}{18} (h-3l+30m-30)(10+20k+h)$
	$i = j - M$	$\int_{-1}^1 \int_{-1}^1 \left(l - z_k - \frac{h}{2}(1+\eta)\right) \left[\left(r_k + \frac{h}{2}(1+\xi)\right) \frac{\partial N_2}{\partial \eta} N_3 + \left(r_{k+1} + \frac{h}{2}(1+\xi)\right) \frac{\partial N_1}{\partial \eta} N_4 \right] d\xi d\eta$	$\frac{bh}{18} (2h-3l+30m-30)(10+20k+h)$

The values of $\left(\frac{bh}{2}\right) \int_{-1}^1 \int_{-1}^1 \left(r_k + \frac{h}{2}(1+\xi)\right) \left(l - z_k - \frac{h}{2}(1+\eta)\right) \frac{\partial \hat{\beta}_j}{\partial \eta} \hat{\beta}_j d\xi d\eta$ in coordinate (ξ, η)

Elements	Cases	The values of $\left(\frac{bh}{2}\right) \int_{-1}^1 \int_{-1}^1 \left(r_k + \frac{h}{2}(1+\xi)\right) \left(l - z_k - \frac{h}{2}(1+\eta)\right) \frac{\partial \hat{\beta}_j}{\partial \eta} \hat{\beta}_j d\xi d\eta$ in coordinate (ξ, η)	Solutions
	$i = j + M + 1$	$\int_{-1}^1 \int_{-1}^1 \left(r_k + \frac{h}{2}(1+\xi)\right) \left(l - z_k - \frac{h}{2}(1+\eta)\right) \frac{\partial N_4}{\partial \eta} N_2 d\xi d\eta$	$-\frac{bh}{72} (h - 3l + 30m - 30) (20k + h)$
	$i = j - M - 1$	$\int_{-1}^1 \int_{-1}^1 \left(r_k + \frac{h}{2}(1+\xi)\right) \left(l - z_k - \frac{h}{2}(1+\eta)\right) \frac{\partial N_2}{\partial \eta} N_4 d\xi d\eta$	$\frac{bh}{72} (2h - 3l + 30m - 30) (20k + h)$
	$i = j + M - 1$	$\int_{-1}^1 \int_{-1}^1 \left(r_k + \frac{h}{2}(1+\xi)\right) \left(l - z_k - \frac{h}{2}(1+\eta)\right) \frac{\partial N_3}{\partial \eta} N_1 d\xi d\eta$	$-\frac{bh}{72} (h - 3l + 30m - 30) (20k + h)$
	$i = j - M + 1$	$\int_{-1}^1 \int_{-1}^1 \left(r_k + \frac{h}{2}(1+\xi)\right) \left(l - z_k - \frac{h}{2}(1+\eta)\right) \frac{\partial N_1}{\partial \eta} N_3 d\xi d\eta$	$\frac{bh}{72} (2h - 3l + 30m - 30) (20k + h)$

where $k = 1, 2, \dots, 9$ and $m = 1, 2, \dots, 9$.



The value of

$$\left(\frac{bh}{2}\right) \int_{-1}^1 \int_{-1}^1 \left(r_k + \frac{h}{2}(1+\xi)\right) \left(l - z_k - \frac{h}{2}(1+\eta)\right) \frac{\partial \hat{\beta}_j}{\partial \eta} \hat{\beta}_j d\xi d\eta$$

are obtained in the form of matrix as follows

$$\begin{bmatrix} B_1 & C_2 & 0 & 0 & 0 & 0 & 0 & 0 \\ D_2 & B_1 & C_3 & 0 & 0 & 0 & 0 & 0 \\ 0 & D_3 & B_1 & C_4 & 0 & 0 & 0 & 0 \\ 0 & 0 & D_4 & B_1 & C_5 & 0 & 0 & 0 \\ 0 & 0 & 0 & D_5 & B_1 & C_6 & 0 & 0 \\ 0 & 0 & 0 & 0 & D_6 & B_1 & C_7 & 0 \\ 0 & 0 & 0 & 0 & 0 & D_7 & B_1 & C_8 \\ 0 & 0 & 0 & 0 & 0 & 0 & D_8 & B_1 \end{bmatrix} \begin{bmatrix} u_1 \\ u_2 \\ u_3 \\ u_4 \\ u_5 \\ u_6 \\ u_7 \\ u_8 \end{bmatrix} = - \begin{bmatrix} c_1 \\ c_2 \\ c_3 \\ c_4 \\ c_5 \\ c_6 \\ c_7 \\ c_8 \end{bmatrix}$$

or

$$BU = Q$$

where

$$B = \begin{bmatrix} B_1 & C_2 & 0 & 0 & 0 & 0 & 0 & 0 \\ D_2 & B_1 & C_3 & 0 & 0 & 0 & 0 & 0 \\ 0 & D_3 & B_1 & C_4 & 0 & 0 & 0 & 0 \\ 0 & 0 & D_4 & B_1 & C_5 & 0 & 0 & 0 \\ 0 & 0 & 0 & D_5 & B_1 & C_6 & 0 & 0 \\ 0 & 0 & 0 & 0 & D_6 & B_1 & C_7 & 0 \\ 0 & 0 & 0 & 0 & 0 & D_7 & B_1 & C_8 \\ 0 & 0 & 0 & 0 & 0 & 0 & D_8 & B_1 \end{bmatrix}$$

and $U = u_p = [\Psi_{10p+2} \Psi_{10p+3} \Psi_{10p+4} \Psi_{10p+5} \Psi_{10p+6} \Psi_{10p+7} \Psi_{10p+8} \Psi_{10p+9}]^T$,
 $Q = [c_1, \dots, c_8]^T$ for all $p = 1, 2, \dots, 8$ and

$$B_1 = -\frac{bh}{72} \begin{bmatrix} 4b_1 & f_2 & 0 & 0 & 0 & 0 & 0 & 0 \\ f_2 & 4b_2 & f_3 & 0 & 0 & 0 & 0 & 0 \\ 0 & f_3 & 4b_3 & f_4 & 0 & 0 & 0 & 0 \\ 0 & 0 & f_4 & 4b_4 & f_5 & 0 & 0 & 0 \\ 0 & 0 & 0 & f_5 & 4b_5 & f_6 & 0 & 0 \\ 0 & 0 & 0 & 0 & f_6 & 4b_6 & f_7 & 0 \\ 0 & 0 & 0 & 0 & 0 & f_7 & 4b_7 & f_8 \\ 0 & 0 & 0 & 0 & 0 & 0 & f_8 & 4b_8 \end{bmatrix},$$

where $b_k = (30+h)(10+20(k)+h)$,
 $f_k = (30+h)(20(k)+h)$ for all $k = 1, 2, \dots, 8$,

$$C_g = \frac{bh}{72} \begin{bmatrix} 4b_{g,1} & f_{g,2} & 0 & 0 & 0 & 0 & 0 & 0 \\ f_{g,2} & 4b_{g,2} & f_{g,3} & 0 & 0 & 0 & 0 & 0 \\ 0 & f_{g,3} & 4b_{g,3} & f_{g,4} & 0 & 0 & 0 & 0 \\ 0 & 0 & f_{g,4} & 4b_{g,4} & f_{g,5} & 0 & 0 & 0 \\ 0 & 0 & 0 & f_{g,5} & 4b_{g,5} & f_{g,6} & 0 & 0 \\ 0 & 0 & 0 & 0 & f_{g,6} & 4b_{g,6} & f_{g,7} & 0 \\ 0 & 0 & 0 & 0 & 0 & f_{g,7} & 4b_{g,7} & f_{g,8} \\ 0 & 0 & 0 & 0 & 0 & 0 & f_{g,8} & 4b_{g,8} \end{bmatrix},$$

where $b_{g,k} = (2h - 3L + 30(g) - 30)(10 + 20(k) + h)$,
 $f_{g,k} = (2h - 3L + 30(g) - 30)(20(k) + h)$ for all $k = 1, 2, \dots, 8$, $g = 2, 3, \dots, 8$,

$$D_g = -\frac{bh}{72} \begin{bmatrix} 4E_{g,1} & F_{g,2} & 0 & 0 & 0 & 0 & 0 & 0 \\ F_{g,2} & 4E_{g,2} & F_{g,3} & 0 & 0 & 0 & 0 & 0 \\ 0 & F_{g,3} & 4E_{g,3} & F_{g,4} & 0 & 0 & 0 & 0 \\ 0 & 0 & F_{g,4} & 4E_{g,4} & F_{g,5} & 0 & 0 & 0 \\ 0 & 0 & 0 & F_{g,5} & 4E_{g,5} & F_{g,6} & 0 & 0 \\ 0 & 0 & 0 & 0 & F_{g,6} & 4E_{g,6} & F_{g,7} & 0 \\ 0 & 0 & 0 & 0 & 0 & F_{g,7} & 4E_{g,7} & F_{g,8} \\ 0 & 0 & 0 & 0 & 0 & 0 & F_{g,8} & 4E_{g,8} \end{bmatrix},$$

where $E_{g,k} = (h - 3L + 30(g) - 30)(10 + 20(k) + h)$,
 $F_{g,k} = (h - 3L + 30(g) - 30)(20(k) + h)$ for all $k = 1, 2, \dots, 9$,
and $g = 1, 2, 3, \dots, 8$.

$$c_1 = -\frac{bh}{72} \begin{bmatrix} F_{1,1}(0.0055) + E_{1,1}(0.0037) + F_{1,2}(0.0027) + f_1(0.0049) - f_{2,1}(0.0043) \\ F_{1,2}(0.0037) + E_{1,2}(0.0027) + F_{1,3}(0.0021) \\ F_{1,3}(0.0027) + E_{1,3}(0.0021) + F_{1,4}(0.0017) \\ F_{1,4}(0.0021) + E_{1,4}(0.0017) + F_{1,5}(0.0014) \\ F_{1,5}(0.0017) + E_{1,5}(0.0014) + F_{1,6}(0.0011) \\ F_{1,6}(0.0014) + E_{1,6}(0.0011) + F_{1,7}(0.0009) \\ F_{1,7}(0.0011) + E_{1,7}(0.0009) + F_{1,8}(0.0008) \\ F_{1,8}(0.0009) + E_{1,8}(0.0008) + F_{1,9}(0.0007) + f_9(0.00062) - f_{2,9}(0.00054) \end{bmatrix},$$

$$c_2 = -\frac{bh}{72} \begin{bmatrix} F_{2,1}(0.0049) + f_1(0.0043) - f_{3,1}(0.0037) \\ 0 \\ 0 \\ 0 \\ 0 \\ 0 \\ 0 \\ F_{2,9}(0.00062) + f_9(0.00054) - f_{3,9}(0.00047) \end{bmatrix},$$

$$c_3 = -\frac{bh}{72} \begin{bmatrix} F_{3,1}(0.0043) + f_1(0.0037) - f_{4,1}(0.0031) \\ 0 \\ 0 \\ 0 \\ 0 \\ 0 \\ 0 \\ F_{3,9}(0.00054) + f_9(0.00047) - f_{4,9}(0.00039) \end{bmatrix},$$

$$c_4 = -\frac{bh}{72} \begin{bmatrix} F_{4,1}(0.0037) + f_1(0.0031) - f_{5,1}(0.0024) \\ 0 \\ 0 \\ 0 \\ 0 \\ 0 \\ 0 \\ F_{4,9}(0.00047) + f_9(0.00039) - f_{5,9}(0.00031) \end{bmatrix},$$

$$c_5 = -\frac{bh}{72} \begin{bmatrix} F_{5,1}(0.0031) + f_1(0.0024) - f_{6,1}(0.0018) \\ 0 \\ 0 \\ 0 \\ 0 \\ 0 \\ 0 \\ F_{5,9}(0.00039) + f_9(0.00031) - f_{6,9}(0.00023) \end{bmatrix},$$

$$c_6 = -\frac{bh}{72} \begin{bmatrix} F_{6,1}(0.0024) + f_1(0.0018) - f_{7,1}(0.0012) \\ 0 \\ 0 \\ 0 \\ 0 \\ 0 \\ 0 \\ F_{6,9}(0.00031) + f_9(0.00023) - f_{7,9}(0.00016) \end{bmatrix},$$

$$c_7 = -\frac{bh}{72} \begin{bmatrix} F_{7,1}(0.0018) + f_1(0.0012) - f_{8,1}(0.0006) \\ 0 \\ 0 \\ 0 \\ 0 \\ 0 \\ 0 \\ F_{7,9}(0.00023) + f_9(0.00016) - f_{8,9}(0.00008) \end{bmatrix},$$

$$c_8 = -\frac{bh}{72} \begin{bmatrix} F_{8,1}(0.0012) + f_1(0.0006) \\ 0 \\ 0 \\ 0 \\ 0 \\ 0 \\ 0 \\ F_{8,9}(0.00016) + f_9(0.00008) \end{bmatrix}$$

Therefore, equation (2.36) can be written in the form of matrix as follows

$$(-A + B) \begin{bmatrix} u_1 \\ u_2 \\ u_3 \\ u_4 \\ u_5 \\ u_6 \\ u_7 \\ u_8 \end{bmatrix} = \begin{bmatrix} a_1 - c_1 \\ a_2 - c_2 \\ a_3 - c_3 \\ a_4 - c_4 \\ a_5 - c_5 \\ a_6 - c_6 \\ a_7 - c_7 \\ a_8 - c_8 \end{bmatrix}$$

or

$$(-A + B) u_p = (a - c)$$

where $u_p = [\Psi_{10p+2} \Psi_{10p+3} \Psi_{10p+4} \Psi_{10p+5} \Psi_{10p+6} \Psi_{10p+7} \Psi_{10p+8} \Psi_{10p+9}]^T$,
 $P = [a_1, \dots, a_8]^T$,
 $Q = [c_1, \dots, c_8]^T$ for all $p = 1, 2, \dots, 8$.

2.3.2 Numerical Experiments

Numerical result of potential at various positions of the earth's structure with one layer having exponentially conductivity $\sigma(z) = \sigma_0 e^{\frac{-b(z-l)^2}{2}}$ from equation (2.20) are obtained by using the finite element method. We use the potential at the ground surface together with linear approximation to find the value of the scalar potential in the domain $\tilde{\Omega}$. There are a source providing a DC voltage and a receiver on the ground surface which picks up the signal from

$r = 10\text{m}$ to $r = 100\text{m}$. We discretize the depth into 9 subintervals equally of the size $h = 10\text{m}$, i.e. we consider $z = 0, 10, 20, \dots, 90\text{m}$. We use constant $b = 0.0001, 0.0005, 0.001, 0.005 \text{ m}^{-2}$ and $l = 0, 5, 10, 30, 50\text{m}$. The suitable range for b in our program is $0 < b < 0.01 \text{ m}^{-2}$. The numerical solution of the potential at each node is calculated by using Maple program version 14 which is used in laboratory of the Department of Mathematics, Faculty of Science, Silpakorn University.

Figures 2.4, 2.5 and 2.6 show the graphs of the relationship between the values of potential and the distance between two probes at various depths as $b = 0.0001, 0.0005, 0.001, 0.005 \text{ m}^{-2}$ where $l = 0\text{m}$.

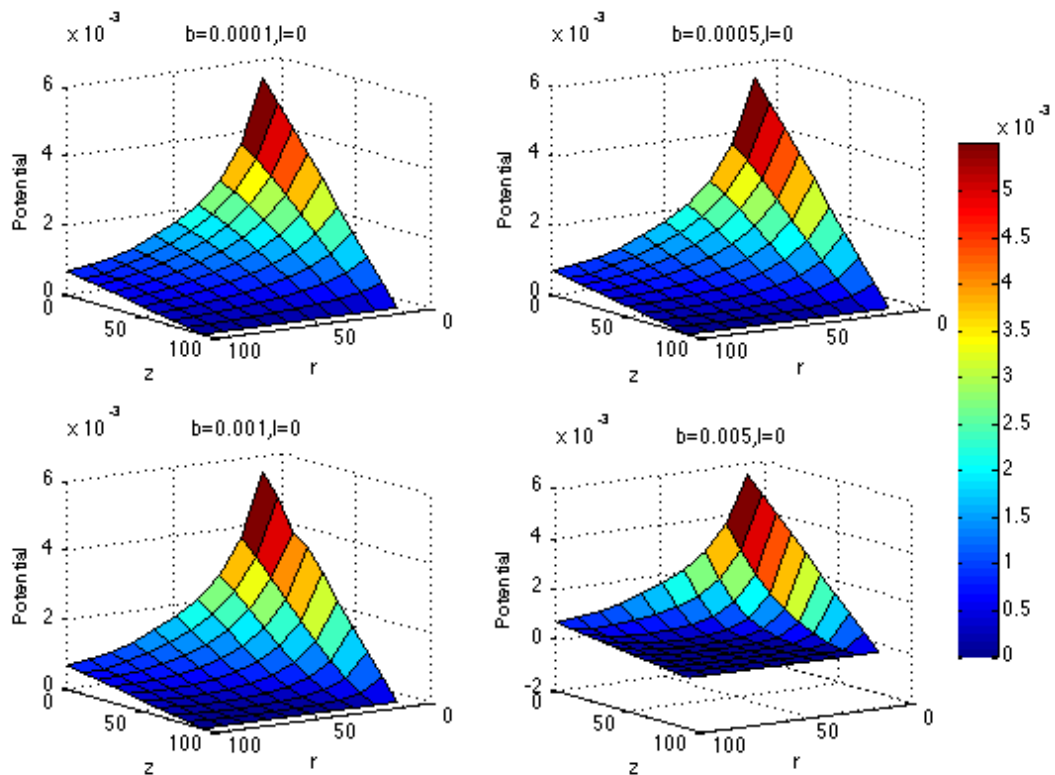


Figure 2.4: The graph of potential when $10 \leq r \leq 100\text{m}$ and $0 \leq z \leq 90\text{m}$

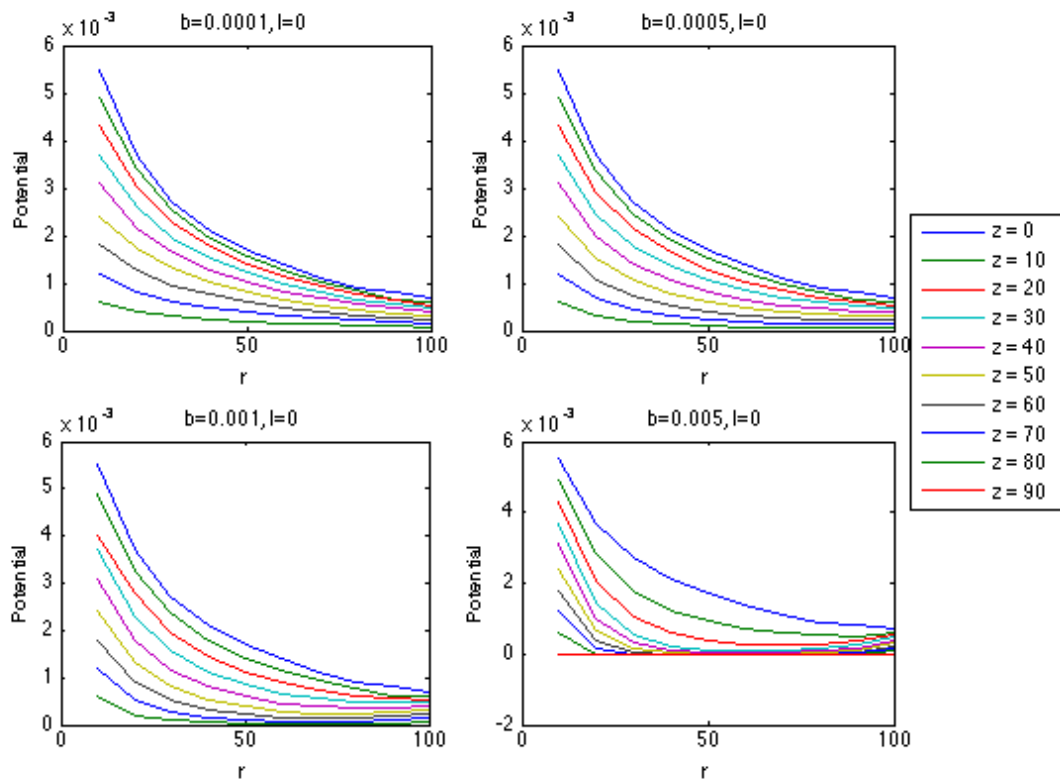


Figure 2.5: The graph of potential against r when z is fixed, i.e. $z = 0, 10, 20, \dots, 90\text{m}$



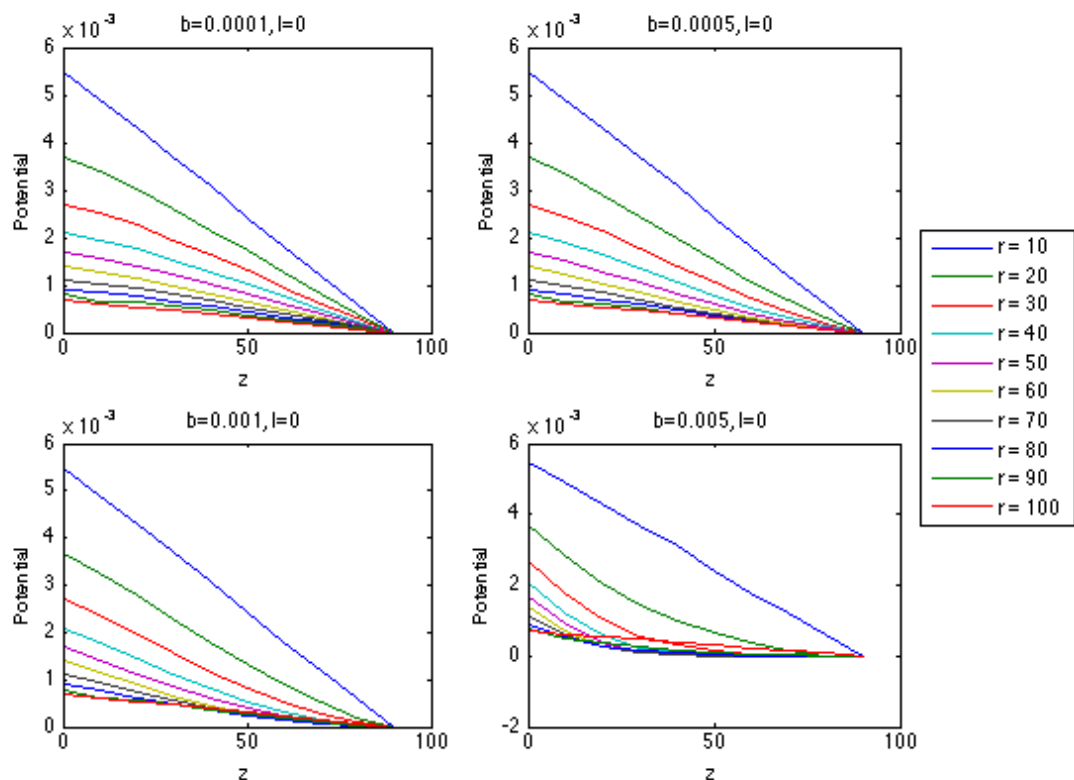


Figure 2.6: The graph of potential against z when r is fixed, i.e. $r = 10, 20, \dots, 100\text{m}$

Figure 2.4 represents the scalar potential as r and z vary. It shows the behavior of the value of scalar potential while the value of b is adjusted but the value of l is fixed ($l = 0\text{m}$). For the small values of b , all of the potential surfaces are in the same exponential pattern except the case when $b = 0.005\text{ m}^{-2}$, some of the value of potential surfaces becomes negative. In each graph, the potential is at its highest when $r = 10\text{m}$, $z = 0\text{m}$ which is the closet location on the ground surface to the probe. It then decreases exponentially as shown in Figure 2.4. Figure 2.5 represent the scalar potential against electrodes spacing. It shows ten curves of scalar potential while the value of b and z are adjusted but l is fixed. All of our curves give very large response in the scalar potential when z is at the smallest. The value of potential decrease exponentially as r increases and it is a straight line where $z = 90\text{m}$ (the bottom edge of the domain). It starts decreasing rapidly at the small values of r and then decreases slowly at the large value of r . Figure 2.6 shows the value of scalar potential against depth (z). The curves when $r = 10, 100\text{m}$ (at the boundary) decrease linearly as z increases and they decrease exponentially for the cases when $r = 20, 30, \dots, 90\text{m}$. For $b = 0.005\text{ m}^{-2}$, the curves have a different behavior from the other values of b . We can see that some of curves intersect and some of the values of scalar potential are less than zero.

Figures 2.7, 2.8 and 2.9 show the graphs of the relationship between the values of potential and the distance between two probes at various depths as $b = 0.0001, 0.0005, 0.001, 0.005 \text{ m}^{-2}$ where $l = 5\text{m}$.

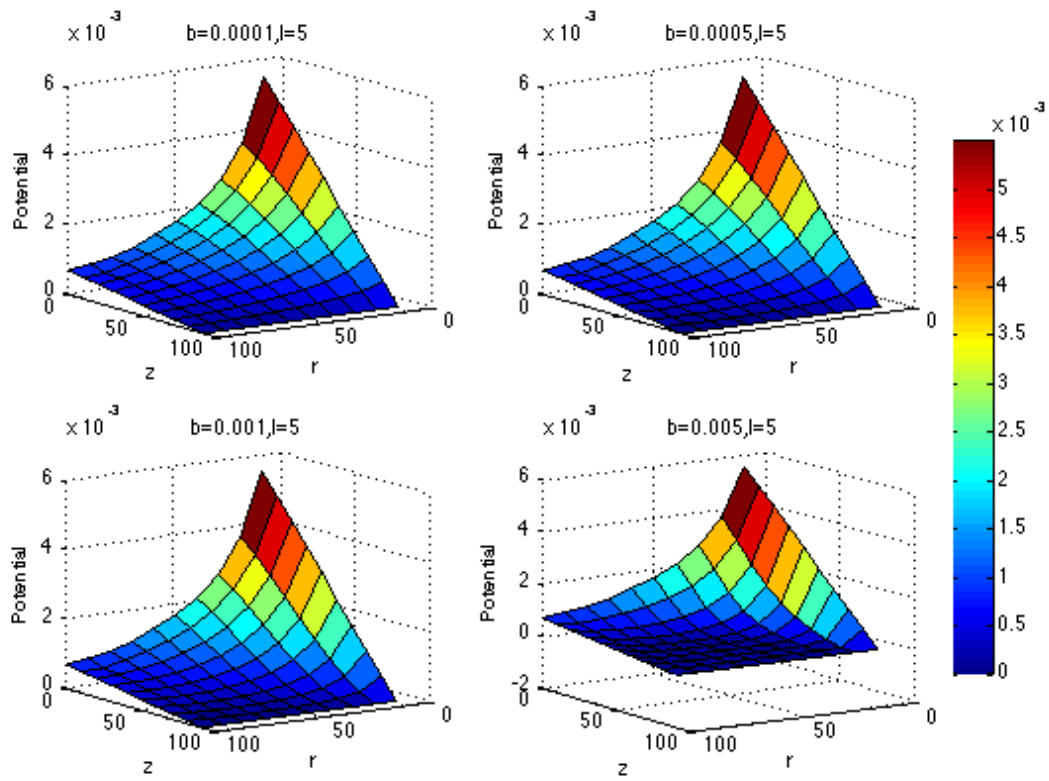
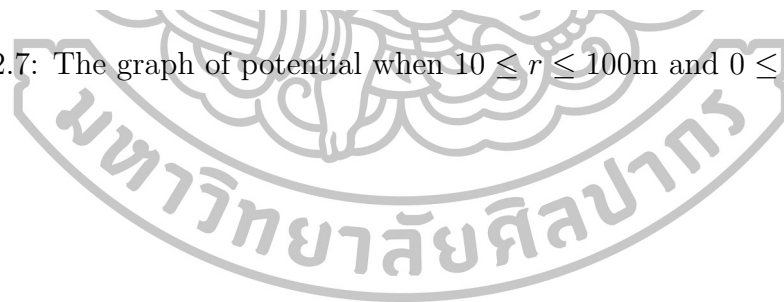


Figure 2.7: The graph of potential when $10 \leq r \leq 100\text{m}$ and $0 \leq z \leq 90\text{m}$.



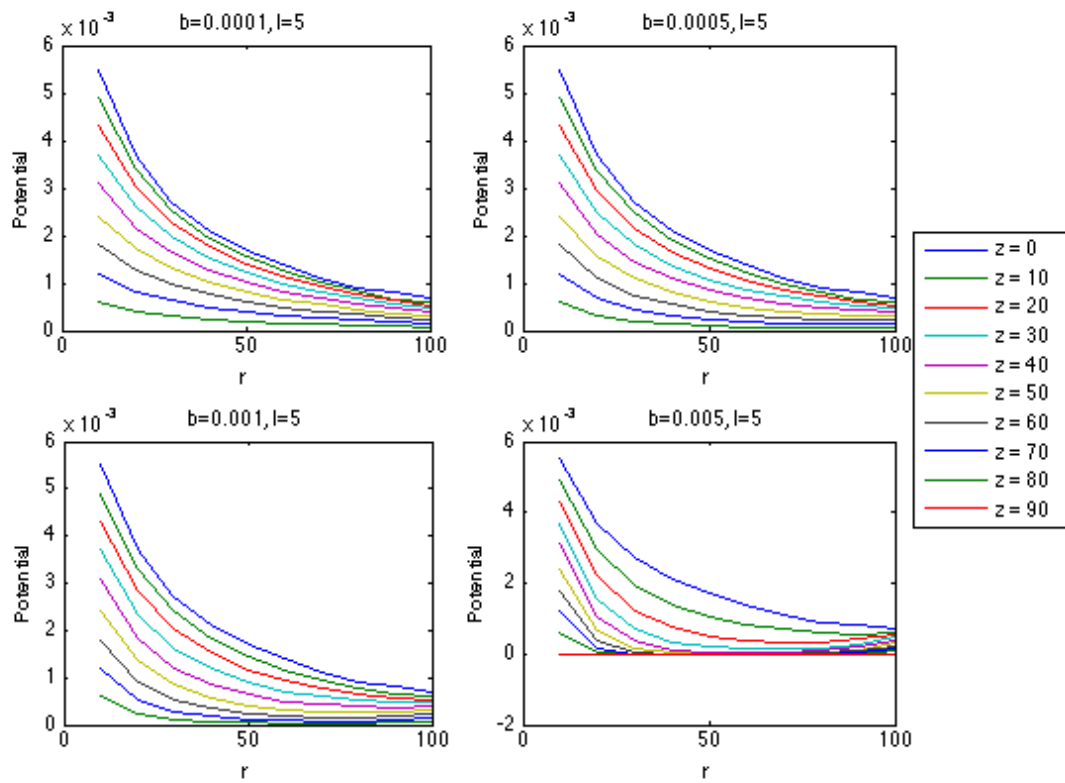


Figure 2.8: The graph of potential against r when z is fixed, i.e. $z = 0, 10, 20, \dots, 90$ m.



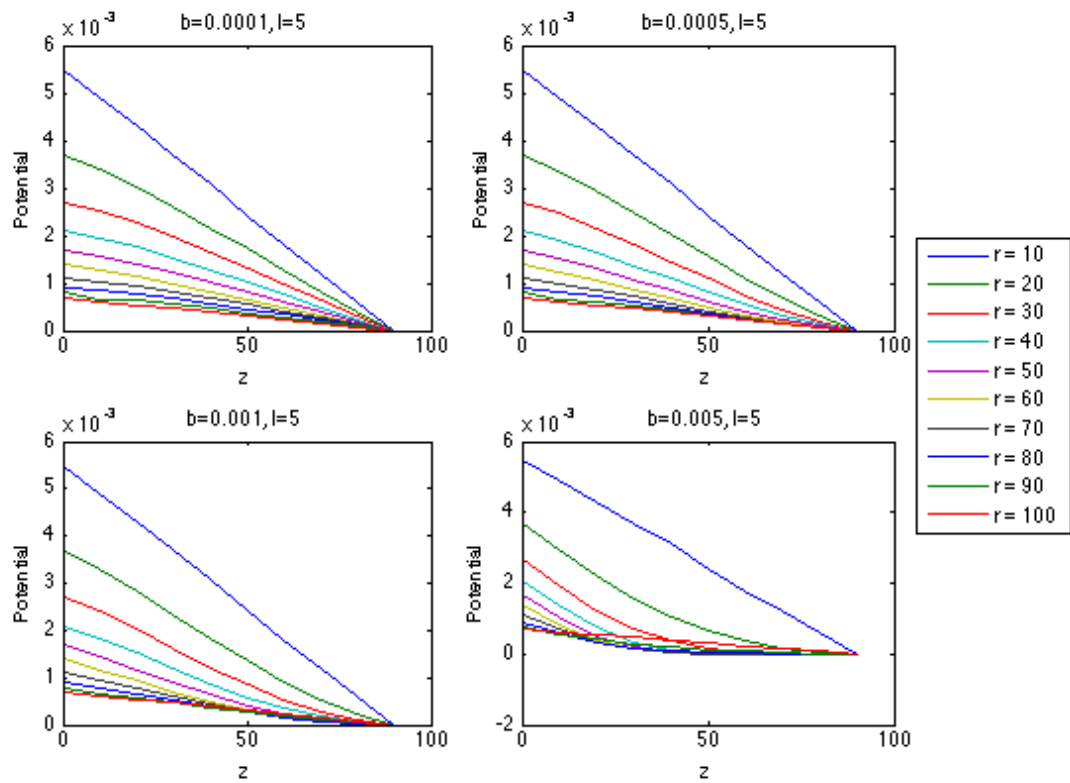


Figure 2.9: The graph of potential against z when r is fixed, i.e. $r = 10, 20, \dots, 100m$.

In this case, the graphs show the behavior of the scalar potential while the value of l is fixed at $5m$ but the value of b is adjusted. Curves of the scalar potential have similar response to the previous case when $l = 0m$ but the values of the scalar potential when $l = 5m$ are greater than as $l = 0m$.

Figures 2.10, 2.11 and 2.12 show the graphs of the relationship between the values of potential and the distance between two probes at various depths as $b = 0.0001, 0.0005, 0.001, 0.005 \text{ m}^{-2}$ where $l = 10\text{m}$.

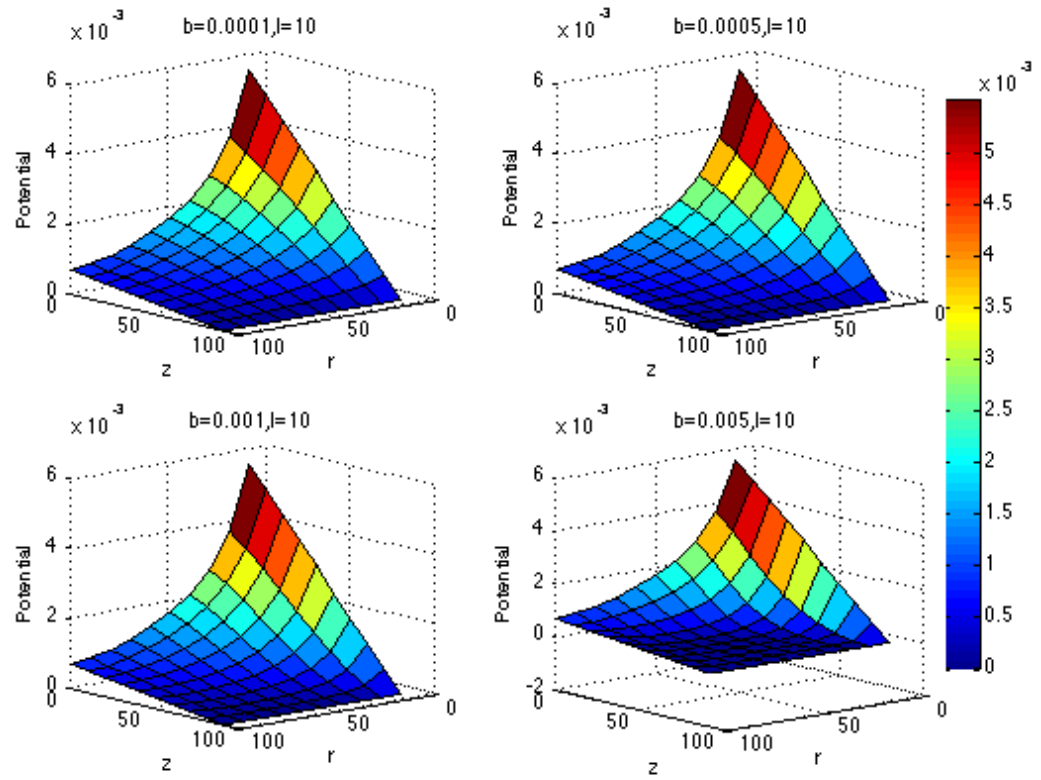
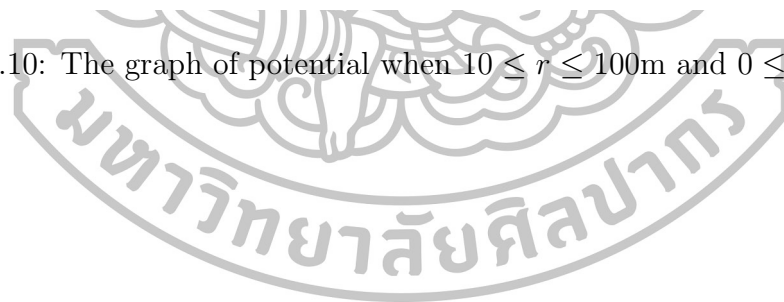


Figure 2.10: The graph of potential when $10 \leq r \leq 100\text{m}$ and $0 \leq z \leq 90\text{m}$.



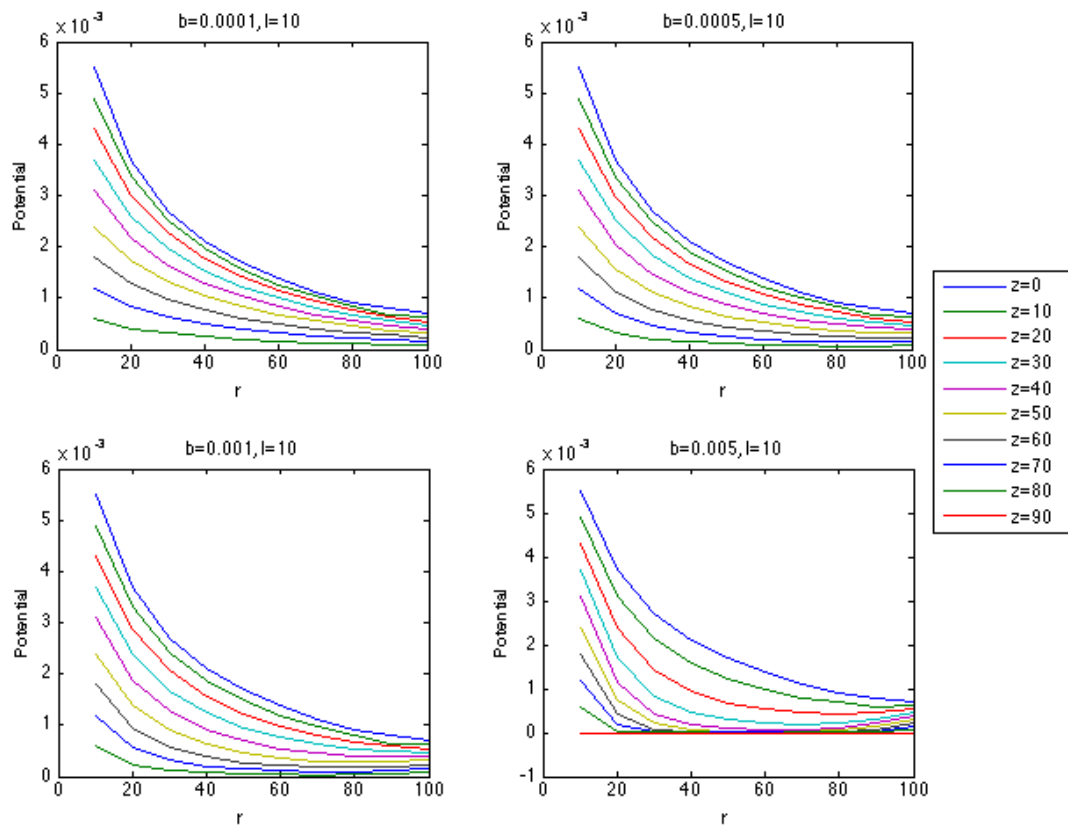
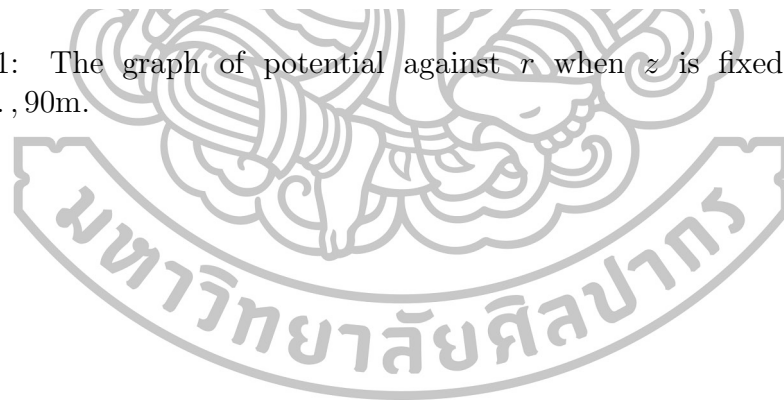


Figure 2.11: The graph of potential against r when z is fixed, i.e. $z = 0, 10, 20, \dots, 90\text{m}$.



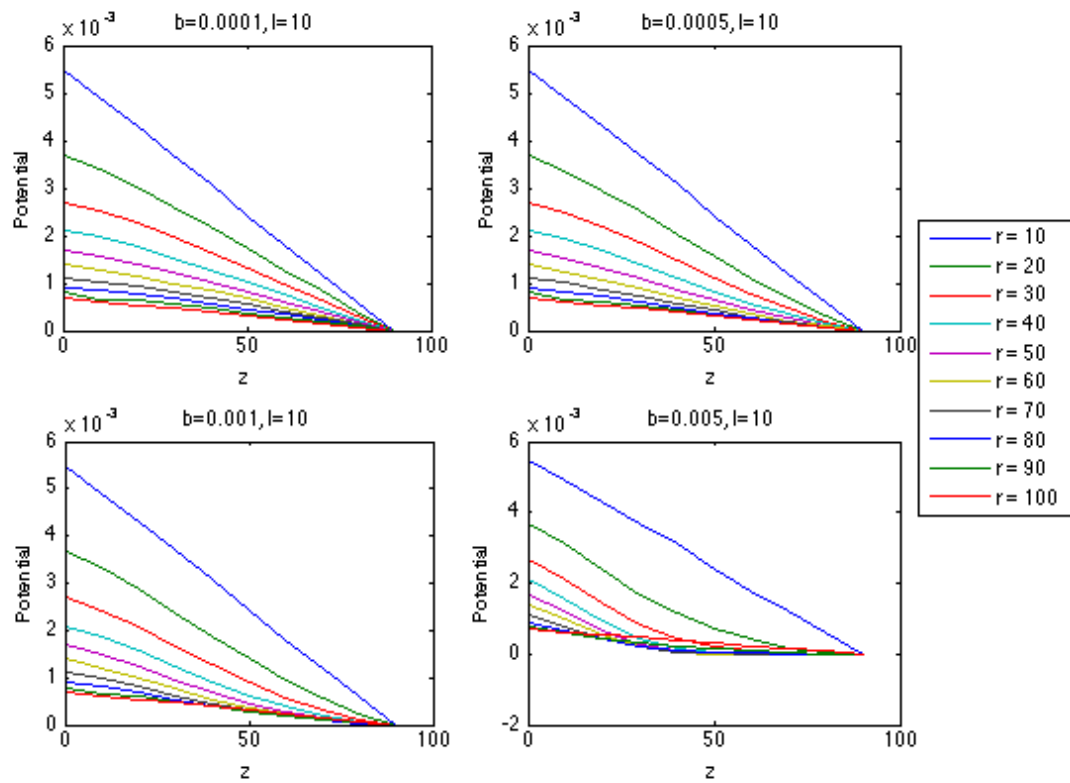


Figure 2.12: The graph of potential against z when r is fixed, i.e. $r = 10, 20, \dots, 100$ m.

Figure 2.10 through 2.12 represent the behavior of the scalar potential while the value of l is fixed at 10m but the value of b is adjusted. The behavior of all values of the scalar potential are similar when l is fixed at 0m and 5m and the values of the scalar potential are greater than as $l = 0$ m and $l = 5$ m.

Figures 2.13, 2.14 and 2.15 show the graphs of the relationship between the values of potential and the distance between two probes at various depths as $b = 0.0001, 0.0005, 0.001, 0.005 \text{ m}^{-2}$ where $l = 30\text{m}$.

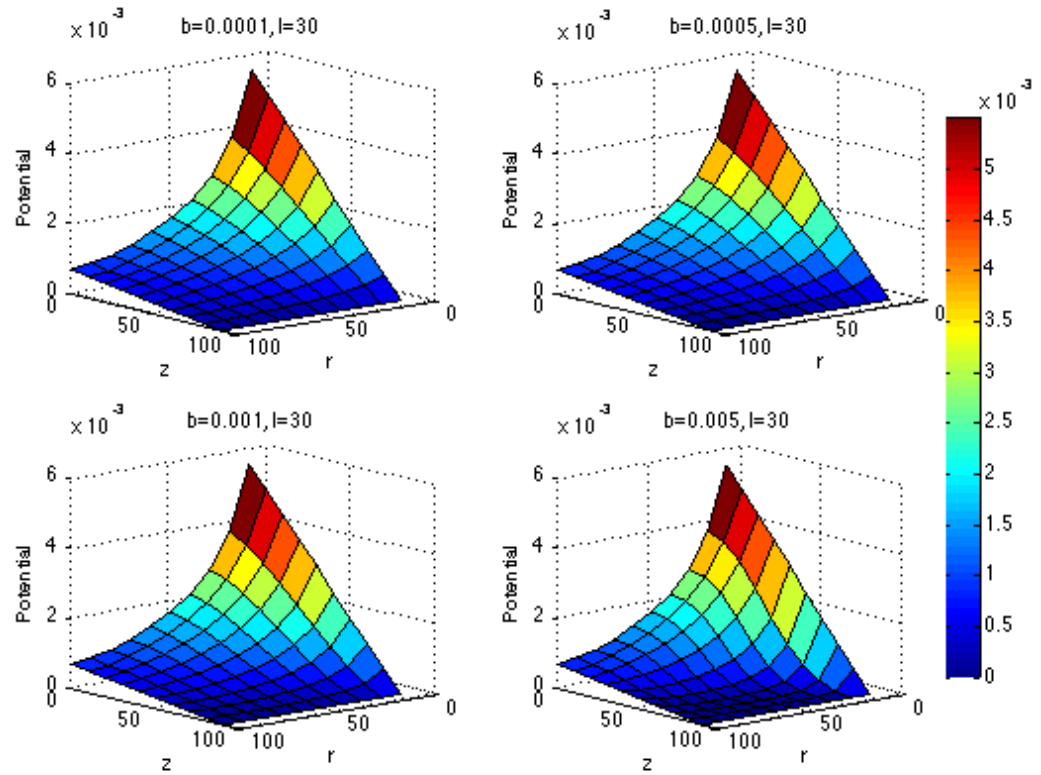
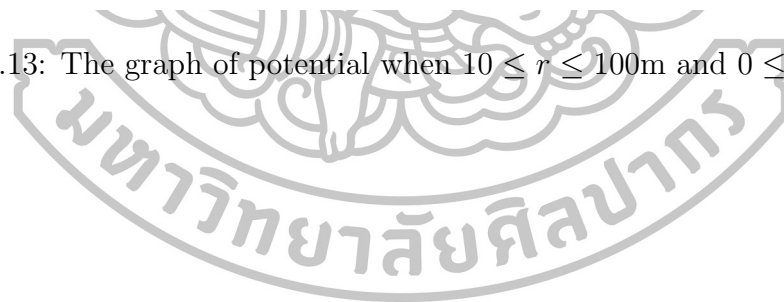


Figure 2.13: The graph of potential when $10 \leq r \leq 100\text{m}$ and $0 \leq z \leq 90\text{m}$.



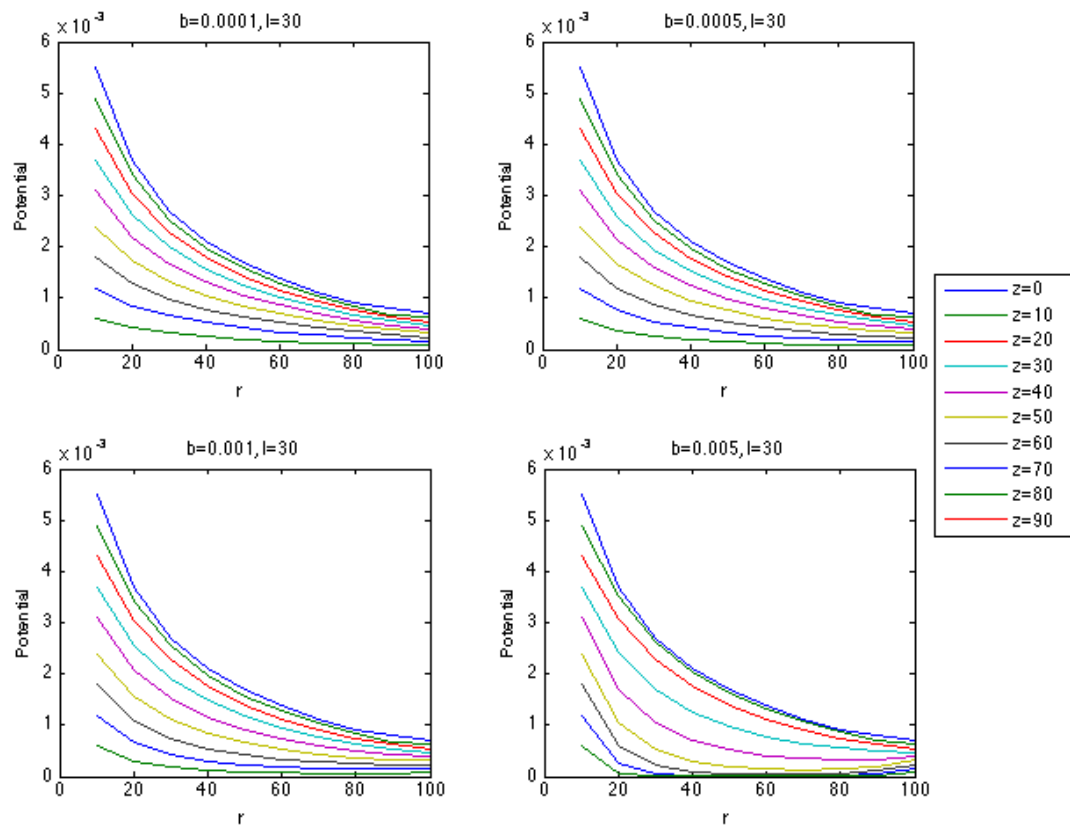
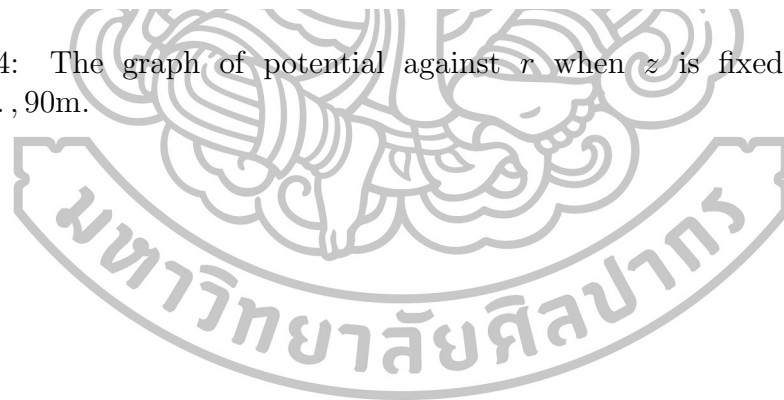


Figure 2.14: The graph of potential against r when z is fixed, i.e. $z = 0, 10, 20, \dots, 90m$.



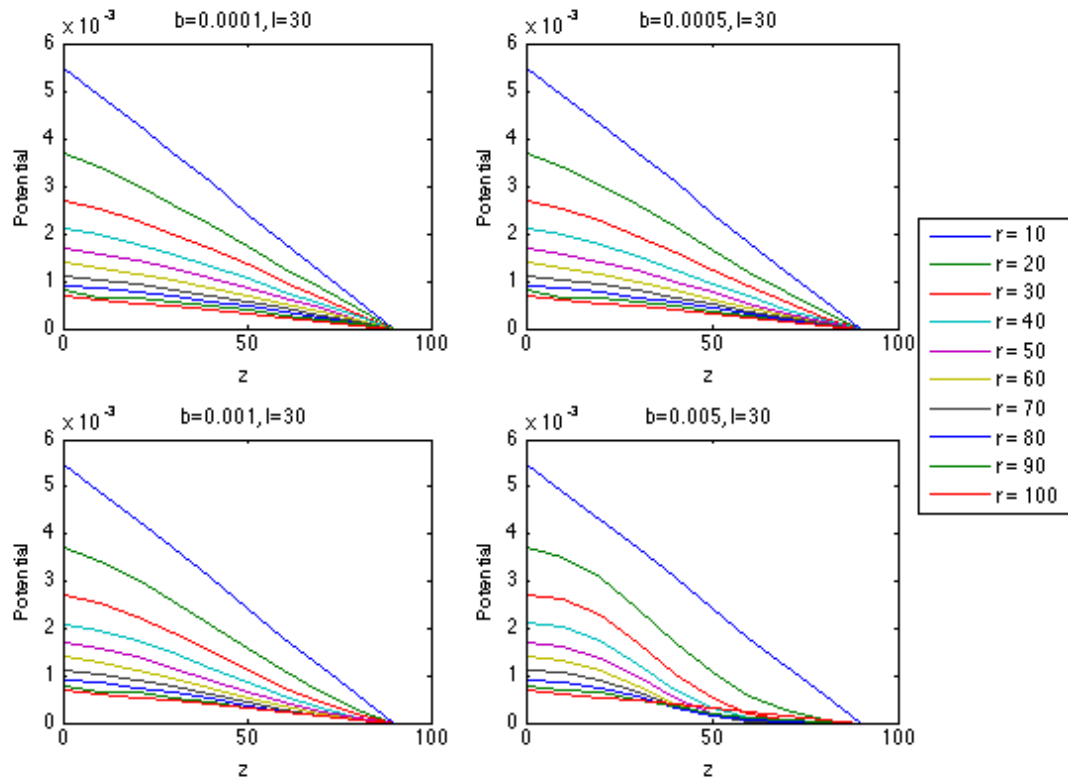


Figure 2.15: The graph of potential against z when r is fixed, i.e. $r = 10, 20, \dots, 100$ m.

Figure 2.13 through Figure 2.15 show the behavior of the value of scalar potential while the value of l is fixed at 30m but the value of b is adjusted. For the small value of b , all of our curves are of the same pattern. In Figure 2.14, the value of potential decreases exponentially as r increase and it is a straight line when $z = 90$ m. In Figure 2.15, our curves decrease linearly where $r = 10$ m and $r = 100$ m as z increases while the value of scalar potential of other r decreases exponentially as z increases. Note that in Figure 2.15, for $b = 0.005 \text{ m}^{-2}$, we see that the value of the scalar potential decreases rapidly when the value of z is greater than l , ($z > 30$ m).

Figures 2.16, 2.17 and 2.18 show the graphs of the relationship between the values of potential and the distance between two probes at various depths as $b = 0.0001, 0.0005, 0.001, 0.005 \text{ m}^{-2}$ where $l = 50\text{m}$.

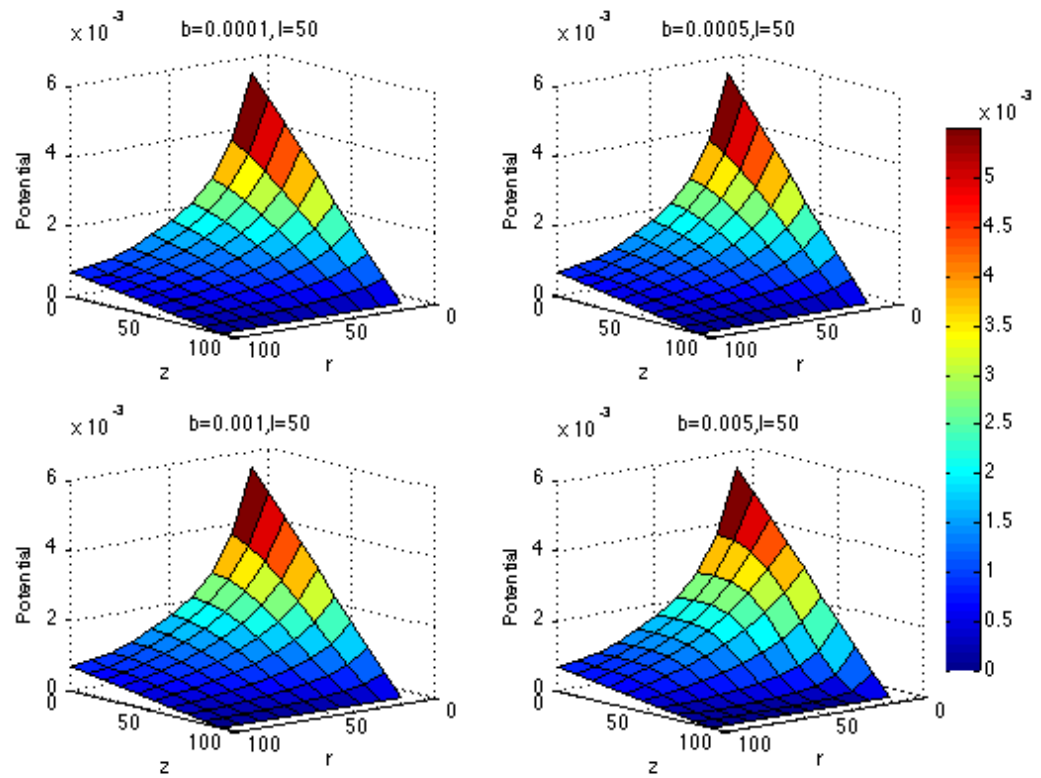
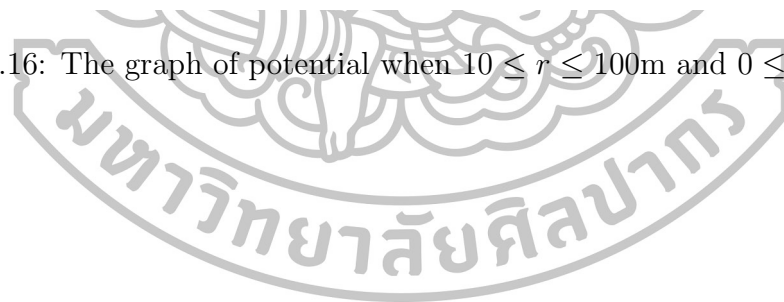


Figure 2.16: The graph of potential when $10 \leq r \leq 100\text{m}$ and $0 \leq z \leq 90\text{m}$.



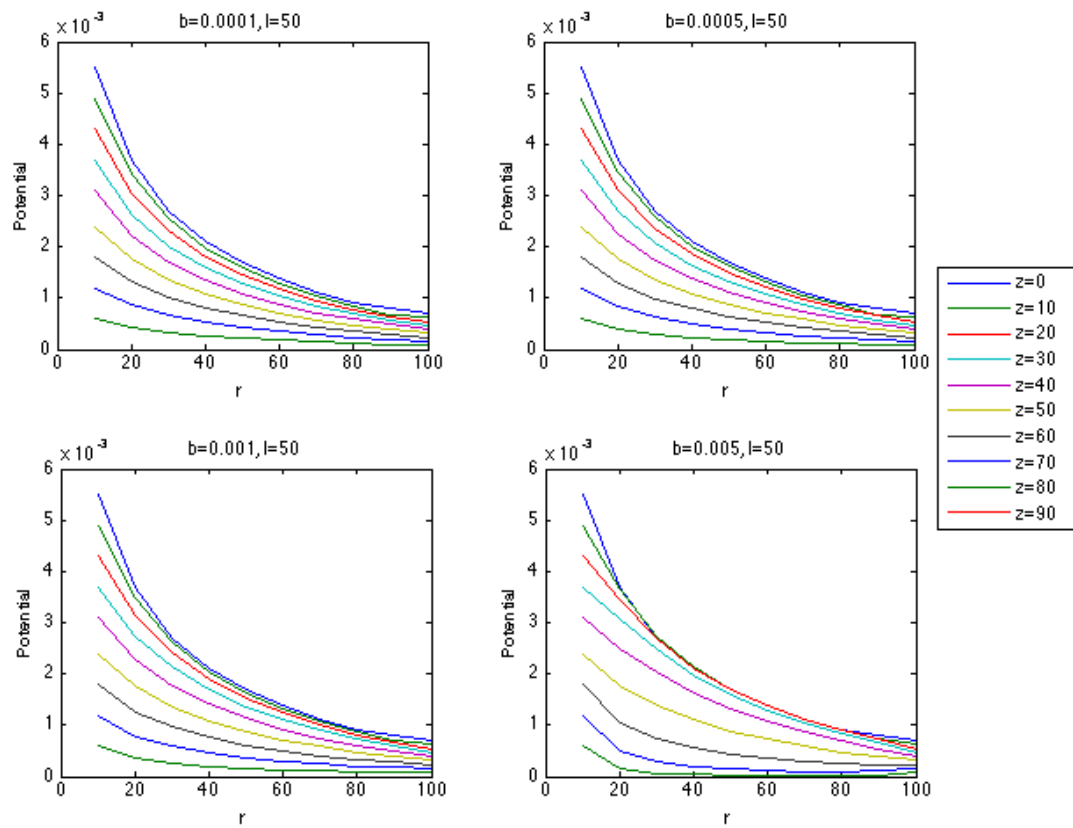
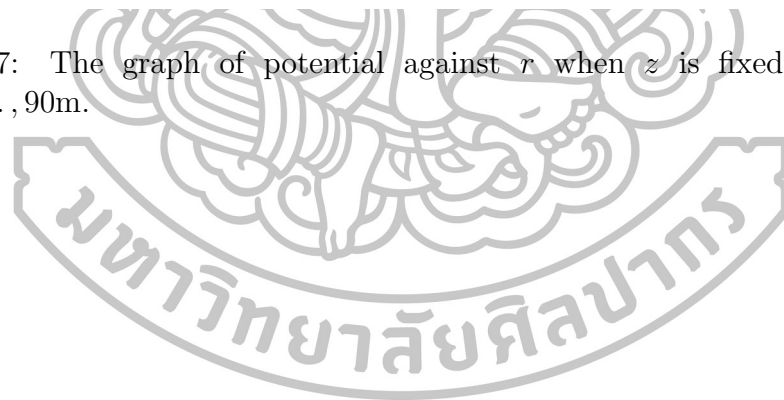


Figure 2.17: The graph of potential against r when z is fixed, i.e. $z = 0, 10, 20, \dots, 90$ m.



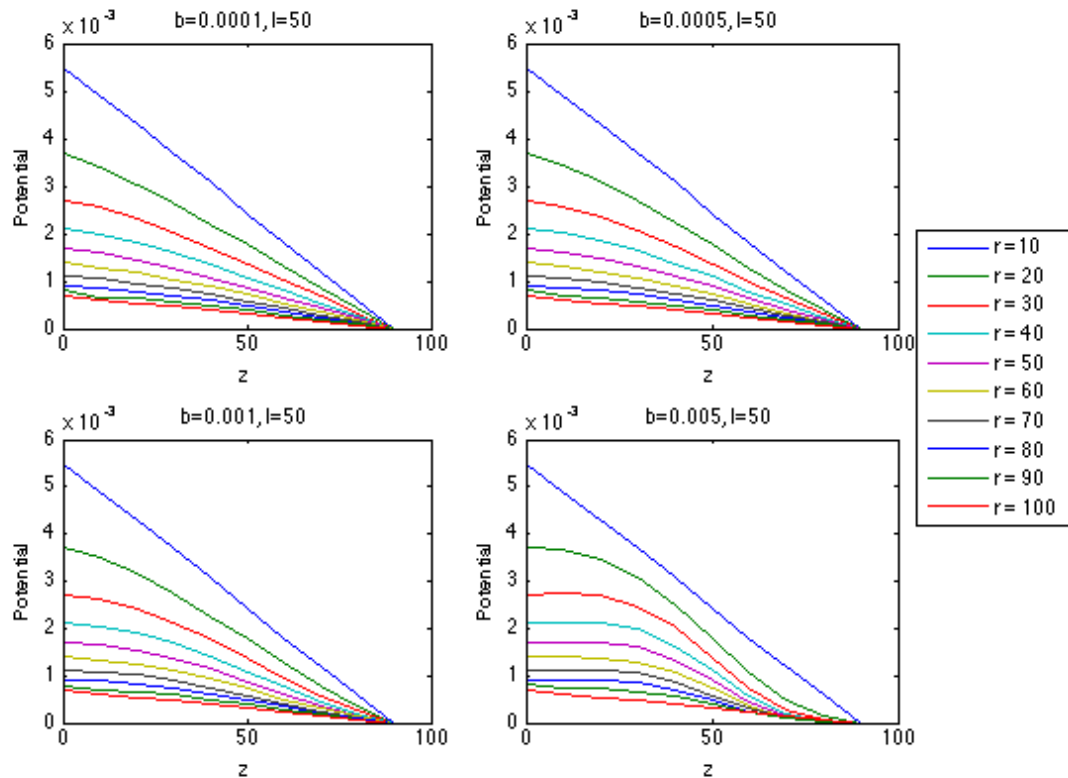


Figure 2.18: The graph of potential against z when r is fixed, i.e. $r = 10, 20, \dots, 100$ m.

In the last case, all the graphs show the behavior of the scalar potential while the value of l is fixed at 50m, but the value of b is adjusted. For the small values of b , the curves are of similar pattern as in the previous case when $l = 30$ m. However, the values of the scalar potential in this case are greater than that when $l = 30$ m. The values of the scalar potential decreases rapidly when the value of z is greater than l , ($z > 50$ m).

2.4 Conclusions and Discussion

The value of scalar potential decreases exponentially to zero as the depth of ground increases whereas it decreases exponentially to zero as the electrode spacing on the ground surface increases. For $l = 0, 5, 10$ m, the value of scalar potential decreases when b increases whereas for $l = 30, 50$ m meters, it increases when b increases.

When z is fixed, the value of scalar potential decreases exponentially as r increases and it starts to decrease rapidly at the early of r and then decreases slowly at the lately of r .

When r is fixed, the value of scalar potential decreases linearly on the boundary and decreases exponentially for the case when $10 < r < 100$ m (not

at the boundary). The curves drop down slowly when depth is small and they decrease rapidly when the value of z is greater than l .



Chapter 3

Inversion of Direct Current for a Conductive Host with a Bulge Overburden

3.1 Introduction

The direct current resistivity method is introduced to investigate the ground structure for geo-informatic data through point electrodes. The procedure is to measure potentials at other electrodes in the vicinity of the current flow. Because the current is measured, it is possible to determine an apparent resistivity of the subsurface [36]. The mathematical models for the preparation of curves for the normalized apparent resistivity response from the earth's surface layer are considered. The earth structure usually can be denoted by horizontally stratified earth [5], where each layer having homogeneous and isotropic electrical properties. In this chapter, two layered earth model is considered. The conductivity of overburden is denoted by $\sigma_{over}(z) = \sigma_0 e^{-b(z-l)^2/2}$, $0 \leq z \leq d$, where b and l are positive constants and l is used to locate the peak of the bulge, d is the thickness of overburden and σ_0 is a positive constant. This bulge conductivity profile could be used to inform the subsurface that rich with water table according to the canal, pond and river nearby [29]. The conductivity of host medium, $z > d$, is denoted by a constant and is given by $\sigma_{host}(z) = \sigma_0$. The curves of normalized apparent resistivity against electrode spacing can be used to predict the depth of the underground water that could damage to the foundation of old building.

3.2 Formulation of the Problem

We now consider an essentially Direct Current sounding method. We may represent the electric field as the gradient of a scalar potential [7] as

$$\vec{E} = -\nabla\psi, \quad (3.1)$$

where \vec{E} is the vector electric field, ∇ is the vector gradient operator, and ψ is the scalar potential.

The divergence of the current density is zero, and we can express this in terms of the electric field, using Ohm's law, $\vec{J} = \sigma \vec{E}$. Thus, the governing equation can be denoted by

$$\begin{aligned}\nabla \cdot \vec{J} &= 0, \\ \nabla \cdot \sigma \nabla \psi &= 0,\end{aligned}\tag{3.2}$$

where \vec{J} is the current density in Ampere per square meters (A/m^2), σ is the electrical conductivity of the medium in Siemens per meter (S/m) which is assumed to be a function of z only. Using vector calculus, the left hand side of equation (3.2) can be rewritten as

$$\begin{aligned}\nabla \cdot \sigma \nabla \psi &= \left(\frac{\partial}{\partial x} \vec{i} + \frac{\partial}{\partial y} \vec{j} + \frac{\partial}{\partial z} \vec{k} \right) \cdot \left[\sigma \left(\frac{\partial}{\partial x} \psi \vec{i} + \frac{\partial}{\partial y} \psi \vec{j} + \frac{\partial}{\partial z} \psi \vec{k} \right) \right], \\ &= \left(\frac{\partial}{\partial x} \vec{i} + \frac{\partial}{\partial y} \vec{j} + \frac{\partial}{\partial z} \vec{k} \right) \cdot \left(\sigma \frac{\partial}{\partial x} \psi \vec{i} + \sigma \frac{\partial}{\partial y} \psi \vec{j} + \sigma \frac{\partial}{\partial z} \psi \vec{k} \right), \\ &= \frac{\partial}{\partial x} \left(\sigma \frac{\partial}{\partial x} \psi \right) + \frac{\partial}{\partial y} \left(\sigma \frac{\partial}{\partial y} \psi \right) + \frac{\partial}{\partial z} \left(\sigma \frac{\partial}{\partial z} \psi \right), \\ \nabla \cdot \sigma \nabla \psi &= \sigma \frac{\partial^2 \psi}{\partial x^2} + \sigma \frac{\partial^2 \psi}{\partial y^2} + \sigma \frac{\partial^2 \psi}{\partial z^2} + \frac{\partial \psi}{\partial z} \frac{\partial \sigma}{\partial z}, \\ &= \sigma \left(\frac{\partial^2 \psi}{\partial x^2} + \frac{\partial^2 \psi}{\partial y^2} + \frac{\partial^2 \psi}{\partial z^2} \right) + \frac{\partial \psi}{\partial z} \frac{\partial \sigma}{\partial z}, \\ &= \sigma \left(\frac{\partial}{\partial x} \vec{i} + \frac{\partial}{\partial y} \vec{j} + \frac{\partial}{\partial z} \vec{k} \right) \cdot \left(\frac{\partial}{\partial x} \psi \vec{i} + \frac{\partial}{\partial y} \psi \vec{j} + \frac{\partial}{\partial z} \psi \vec{k} \right) \\ &\quad + \left(\frac{\partial}{\partial x} \psi \vec{i} + \frac{\partial}{\partial y} \psi \vec{j} + \frac{\partial}{\partial z} \psi \vec{k} \right) \cdot \left(\frac{\partial}{\partial x} \sigma \vec{i} + \frac{\partial}{\partial y} \sigma \vec{j} + \frac{\partial}{\partial z} \sigma \vec{k} \right), \\ &= \sigma \nabla \cdot \nabla \psi + (\nabla \psi) \cdot (\nabla \sigma),\end{aligned}$$

this yields

$$\sigma \nabla \cdot \nabla \psi + (\nabla \psi) \cdot (\nabla \sigma) = 0.\tag{3.3}$$

For simply, since we denote σ as a function of z only, thus, the above equation

becomes

$$\begin{aligned}\nabla \cdot \nabla \psi &= \left(\frac{\partial}{\partial x} \vec{i} + \frac{\partial}{\partial y} \vec{j} + \frac{\partial}{\partial z} \vec{k} \right) \cdot \left(\frac{\partial}{\partial x} \psi \vec{i} + \frac{\partial}{\partial y} \psi \vec{j} + \frac{\partial}{\partial z} \psi \vec{k} \right), \\ &= \left(\frac{\partial^2 \psi}{\partial x^2} + \frac{\partial^2 \psi}{\partial y^2} + \frac{\partial^2 \psi}{\partial z^2} \right), \\ &= \nabla^2 \psi,\end{aligned}$$

and

$$\begin{aligned}(\nabla \psi) \cdot (\nabla \sigma) &= \left(\frac{\partial}{\partial x} \psi \vec{i} + \frac{\partial}{\partial y} \psi \vec{j} + \frac{\partial}{\partial z} \psi \vec{k} \right) \cdot \left(\frac{\partial}{\partial x} \sigma \vec{i} + \frac{\partial}{\partial y} \sigma \vec{j} + \frac{\partial}{\partial z} \sigma \vec{k} \right), \\ &= \frac{\partial \psi}{\partial z} \frac{\partial \sigma}{\partial z},\end{aligned}$$

thus, we obtain

$$\sigma \nabla^2 \psi + \frac{\partial \psi}{\partial z} \frac{\partial \sigma}{\partial z} = 0. \quad (3.4)$$

In cylindrical coordinate system (ρ, ϕ, z) , the probe is used and located on the ground surface. The potential around the probe is symmetry and independent of ϕ . Thus, we can rewrite the equation (3.4) as

$$\frac{\partial^2 \psi}{\partial \rho^2} + \frac{1}{\rho} \frac{\partial \psi}{\partial \rho} + \frac{\partial^2 \psi}{\partial z^2} + \frac{1}{\sigma} \frac{\partial \psi}{\partial z} \frac{\partial \sigma}{\partial z} = 0. \quad (3.5)$$

We shall use the Hankel transforms [2] defined by

$$f(\lambda, z) = \int_0^{\infty} \lambda \rho \psi(\rho, z) J_0(\lambda \rho) d\rho, \quad (3.6)$$

and the inverse Hankel transforms of $f(\lambda, z)$ which is defined as

$$\psi(\rho, z) = \int_0^{\infty} f(\lambda, z) J_0(\lambda \rho) d\lambda, \quad (3.7)$$

where J_0 is the Bessel function of the first kind of order zero and λ is the Hankel variable. Taking the transformation on both sides of equation (3.5), we obtain

$$\int_0^{\infty} \lambda \rho \left(\frac{\partial^2 \psi}{\partial \rho^2} + \frac{1}{\rho} \frac{\partial \psi}{\partial \rho} + \frac{\partial^2 \psi}{\partial z^2} + \frac{1}{\sigma} \frac{\partial \psi}{\partial z} \frac{\partial \sigma}{\partial z} \right) J_0(\lambda \rho) d\rho = \int_0^{\infty} \lambda \rho (0) J_0(\lambda \rho) d\rho,$$

or

$$\int_0^{\infty} \lambda \left(\rho \frac{\partial^2 \psi}{\partial \rho^2} + \frac{\partial \psi}{\partial \rho} \right) J_0(\lambda \rho) d\rho + \int_0^{\infty} \lambda \rho \frac{\partial^2 \psi}{\partial z^2} J_0(\lambda \rho) d\rho + \frac{1}{\sigma} \frac{\partial \sigma}{\partial z} \int_0^{\infty} \lambda \rho \frac{\partial \psi}{\partial z} J_0(\lambda \rho) d\rho = 0,$$

or

$$\int_0^{\infty} \lambda \frac{\partial}{\partial \rho} \left(\rho \frac{\partial \psi}{\partial \rho} \right) J_0(\lambda \rho) d\rho + \int_0^{\infty} \lambda \rho \frac{\partial^2 \psi}{\partial z^2} J_0(\lambda \rho) d\rho + \frac{1}{\sigma} \frac{\partial \sigma}{\partial z} \int_0^{\infty} \lambda \rho \frac{\partial \psi}{\partial z} J_0(\lambda \rho) d\rho = 0,$$

or

$$\lim_{a \rightarrow 0^+} \int_a^1 \lambda \frac{\partial}{\partial \rho} \left(\rho \frac{\partial \psi}{\partial \rho} \right) J_0(\lambda \rho) d\rho + \lim_{b \rightarrow \infty} \int_1^b \lambda \frac{\partial}{\partial \rho} \left(\rho \frac{\partial \psi}{\partial \rho} \right) J_0(\lambda \rho) d\rho + \int_0^{\infty} \lambda \rho \frac{\partial^2 \psi}{\partial z^2} J_0(\lambda \rho) d\rho + \frac{1}{\sigma} \frac{\partial \sigma}{\partial z} \int_0^{\infty} \lambda \rho \frac{\partial \psi}{\partial z} J_0(\lambda \rho) d\rho = 0.$$

Integrating by parts on the first and second terms of the above equation yields

$$\begin{aligned} & \lim_{a \rightarrow 0^+} \left(\lambda \rho \frac{\partial \psi}{\partial \rho} J_0(\lambda \rho) \right) \Big|_a^1 - \lim_{a \rightarrow 0^+} \int_a^1 \lambda \rho \frac{\partial \psi}{\partial \rho} \frac{d}{d\rho} J_0(\lambda \rho) d\rho \\ & + \lim_{b \rightarrow \infty} \left(\lambda \rho \frac{\partial \psi}{\partial \rho} J_0(\lambda \rho) \right) \Big|_1^b - \lim_{b \rightarrow \infty} \int_1^b \lambda \rho \frac{\partial \psi}{\partial \rho} \frac{d}{d\rho} J_0(\lambda \rho) d\rho \\ & + \int_0^{\infty} \lambda \rho \frac{\partial^2 \psi}{\partial z^2} J_0(\lambda \rho) d\rho + \frac{1}{\sigma} \frac{\partial \sigma}{\partial z} \int_0^{\infty} \lambda \rho \frac{\partial \psi}{\partial z} J_0(\lambda \rho) d\rho = 0, \end{aligned}$$

or

$$\begin{aligned} & \int_0^{\infty} \lambda \rho \frac{\partial^2 \psi}{\partial z^2} J_0(\lambda \rho) d\rho + \frac{1}{\sigma} \frac{\partial \sigma}{\partial z} \int_0^{\infty} \lambda \rho \frac{\partial \psi}{\partial z} J_0(\lambda \rho) d\rho \\ & - \lim_{a \rightarrow 0^+} \int_a^1 \lambda \rho \frac{\partial \psi}{\partial \rho} \frac{d}{d\rho} J_0(\lambda \rho) d\rho - \lim_{b \rightarrow \infty} \int_1^b \lambda \rho \frac{\partial \psi}{\partial \rho} \frac{d}{d\rho} J_0(\lambda \rho) d\rho = 0. \end{aligned}$$

Integrating by parts again on the third and fourth terms of the above equation, we obtain

$$\begin{aligned} & \int_0^{\infty} \lambda \rho \frac{\partial^2 \psi}{\partial z^2} J_0(\lambda \rho) d\rho + \frac{1}{\sigma} \frac{\partial \sigma}{\partial z} \int_0^{\infty} \lambda \rho \frac{\partial \psi}{\partial z} J_0(\lambda \rho) d\rho \\ & - \lim_{a \rightarrow 0^+} \left(\lambda \rho \psi \frac{d}{d\rho} J_0(\lambda \rho) \right) \Big|_a^1 + \lim_{a \rightarrow 0^+} \int_a^1 \lambda \psi \frac{d}{d\rho} \left(\rho \frac{d}{d\rho} J_0(\lambda \rho) \right) d\rho \\ & - \lim_{b \rightarrow \infty} \left(\lambda \rho \psi \frac{d}{d\rho} J_0(\lambda \rho) \right) \Big|_1^b + \lim_{b \rightarrow \infty} \int_1^b \lambda \psi \frac{d}{d\rho} \left(\rho \frac{d}{d\rho} J_0(\lambda \rho) \right) d\rho = 0, \end{aligned}$$

or

$$\begin{aligned} & \int_0^{\infty} \lambda \rho \frac{\partial^2 \psi}{\partial z^2} J_0(\lambda \rho) d\rho + \frac{1}{\sigma} \frac{\partial \sigma}{\partial z} \int_0^{\infty} \lambda \rho \frac{\partial \psi}{\partial z} J_0(\lambda \rho) d\rho \\ & + \lim_{a \rightarrow 0^+} \int_a^1 \lambda \psi \frac{d}{d\rho} \left(\rho \frac{d}{d\rho} J_0(\lambda \rho) \right) d\rho + \lim_{b \rightarrow \infty} \int_1^b \lambda \psi \frac{d}{d\rho} \left(\rho \frac{d}{d\rho} J_0(\lambda \rho) \right) d\rho = 0, \end{aligned}$$

or

$$\begin{aligned} & \int_0^{\infty} \lambda \rho \frac{\partial^2 \psi}{\partial z^2} J_0(\lambda \rho) d\rho + \frac{1}{\sigma} \frac{\partial \sigma}{\partial z} \int_0^{\infty} \lambda \rho \frac{\partial \psi}{\partial z} J_0(\lambda \rho) d\rho \\ & + \int_0^{\infty} \lambda \psi \frac{d}{d\rho} \left(\rho \frac{d}{d\rho} J_0(\lambda \rho) \right) d\rho = 0, \end{aligned}$$

or

$$\begin{aligned} & \int_0^{\infty} \lambda \rho \frac{\partial^2 \psi}{\partial z^2} J_0(\lambda \rho) d\rho + \frac{1}{\sigma} \frac{\partial \sigma}{\partial z} \int_0^{\infty} \lambda \rho \frac{\partial \psi}{\partial z} J_0(\lambda \rho) d\rho \\ & + \int_0^{\infty} \lambda \psi \left(\rho \frac{d^2}{d\rho^2} J_0(\lambda \rho) + \frac{d}{d\rho} J_0(\lambda \rho) \right) d\rho = 0, \end{aligned}$$

or

$$\begin{aligned} & \int_0^{\infty} \lambda \rho \frac{\partial^2 \psi}{\partial z^2} J_0(\lambda \rho) d\rho + \frac{1}{\sigma} \frac{\partial \sigma}{\partial z} \int_0^{\infty} \lambda \rho \frac{\partial \psi}{\partial z} J_0(\lambda \rho) d\rho \\ & + \int_0^{\infty} \lambda \psi \left(\lambda^2 \rho J_0''(\lambda \rho) + \lambda J_0'(\lambda \rho) \right) d\rho = 0, \end{aligned}$$

or

$$\int_0^{\infty} \lambda \rho \frac{\partial^2 \psi}{\partial z^2} J_0(\lambda \rho) d\rho + \frac{1}{\sigma} \frac{\partial \sigma}{\partial z} \int_0^{\infty} \lambda \rho \frac{\partial \psi}{\partial z} J_0(\lambda \rho) d\rho + \int_0^{\infty} \lambda \rho \psi \left(\lambda^2 J_0''(\lambda \rho) + \frac{\lambda}{\rho} J_0'(\lambda \rho) \right) d\rho = 0.$$

Since J_0 is the solution of Bessel's differential equation, we now have

$$\lambda^2 J_0''(\lambda \rho) + \frac{\lambda}{\rho} J_0'(\lambda \rho) = -\lambda^2 J_0(\lambda \rho).$$

This yields

$$\int_0^{\infty} \lambda \rho \frac{\partial^2 \psi}{\partial z^2} J_0(\lambda \rho) d\rho + \frac{1}{\sigma} \frac{\partial \sigma}{\partial z} \int_0^{\infty} \lambda \rho \frac{\partial \psi}{\partial z} J_0(\lambda \rho) d\rho - \lambda^2 \int_0^{\infty} \lambda \rho \psi J_0(\lambda \rho) d\rho = 0.$$

Hence, the Hankel transform of equation (3.5) results in

$$\frac{\partial^2 f}{\partial z^2} + \frac{1}{\sigma} \frac{\partial \sigma}{\partial z} \frac{\partial f}{\partial z} - \lambda^2 f = 0. \quad (3.8)$$

Therefore, the electric potential in each layer can be obtained by taking the inverse Hankel transform to the solution of equation (3.8), which satisfies the boundary conditions.

3.3 Apparent Resistivity of Two-Layered Earth

We now consider the two-layered earth model denoted by overburden and host medium. For the first layer, the conductivity of overburden is denoted by $\sigma_{over}(z) = \sigma_0 e^{-b(z-l)^2/2}$ and for the host medium, the conductivity is defined by $\sigma_{host}(z) = \sigma_0$ where σ_0 , l and b are positive constants.

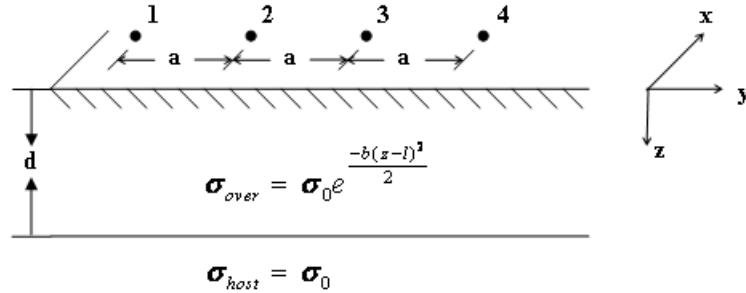


Figure 3.1: Configuration of electrode array over an overburden of thickness d

As shown in Figure 3.1, the electrodes 1 and 4 are used for direct current injection of Wenner array configuration while the electrodes 2 and 3 are used for potential measurement. a is the electrode spacing. We have to determine the potential functions in the overburden ($f = f_1$, $0 \leq z \leq d$) and in the host medium ($f = f_2$, $z > d$). These can be found by substituting $\sigma_{over}(z) = \sigma_0 e^{-b(z-l)^2/2}$ and $\sigma_{host}(z) = \sigma_0$ into the equation (3.8), respectively. The power series method [4, 17, 26] is used to solve the partial differential equation and obtain the potential functions f_1 and f_2 , as

$$f_1 = a_0 \left(1 + \frac{\lambda^2 z^2}{2} \right) + a_1 \left(z - \frac{blz^2}{2} \right), \quad 0 \leq z \leq d, \quad (3.9)$$

and

$$f_2 = a_3 e^{-\lambda z}, \quad z > d, \quad (3.10)$$

where a_0 , a_1 and a_3 can be determined by using the boundary conditions at the interfaces [7, 16, 31, 34]. The first boundary condition is denoted by the continuity of normal current density at the ground surface

$$\lim_{z \rightarrow 0} \left(-\sigma_0 e^{-\frac{bt^2}{2}} \frac{\partial \psi_1}{\partial z} \right) = \frac{I \delta(\rho)}{2\pi \rho}, \quad (3.11)$$

where I is the current at the probe on the ground surface, and $\delta(\rho)$ is the Dirac Delta function denoted by $\delta(\rho) = \begin{cases} 0, & \text{if } \rho \neq 0 \\ 1, & \text{if } \rho = 0 \end{cases}$.

The second boundary condition is denoted by the continuity of normal current density at $z = d$ as

$$\lim_{z \rightarrow d^-} \left(\sigma_0 e^{-\frac{b(a-l)^2}{2}} \frac{\partial \psi_1}{\partial z} \right) = \lim_{z \rightarrow d^+} \left(\sigma_0 \frac{\partial \psi_2}{\partial z} \right). \quad (3.12)$$

The third boundary condition is the continuity of potential across the interface layer at $z = d$ as

$$\lim_{z \rightarrow d^-} \psi_1 = \lim_{z \rightarrow d^+} \psi_2. \quad (3.13)$$

From the first boundary condition as equation (3.11), we obtain

$$\lim_{z \rightarrow 0} \left\{ -\sigma_0 e^{-\frac{bt^2}{2}} \int_0^\infty (a_0 \lambda^2 z + a_1 - a_1 blz) J_0(\lambda \rho) d\lambda \right\} = \frac{I \delta(\rho)}{2\pi \rho}. \quad (3.14)$$

Since $\int_0^\infty \lambda J_0(\lambda \rho) d\lambda = \frac{\delta(\rho)}{\rho}$, then the equation (3.14) becomes

$$\int_0^\infty \left(-\sigma_0 e^{-\frac{bt^2}{2}} a_1 \right) J_0(\lambda \rho) d\lambda = \int_0^\infty \frac{I}{2\pi} \lambda J_0(\lambda \rho) d\lambda. \quad (3.15)$$

From equations (3.7) and (3.15), we now have

$$a_1 = -\frac{I\lambda}{2\pi\sigma_0 e^{-\frac{bl^2}{2}}}. \quad (3.16)$$

Using the boundary condition in equations (3.12) and (3.13), we now have

$$e^{-\frac{b(d-l)^2}{2}} (a_0\lambda^2 d + a_1 - a_1 bld) = -\lambda a_3 e^{-\lambda d} \quad (3.17)$$

and

$$a_0 \left(1 + \frac{\lambda^2 d^2}{2}\right) + a_1 \left(d - \frac{bld^2}{2}\right) = a_3 e^{-\lambda d}, \quad (3.18)$$

respectively. Simultaneous solution of the equations (3.17) and (3.18) yields,

$$a_0 = \frac{a_1 \left(2e^{-\frac{b(d-l)^2}{2}} (bld - 1) - 2\lambda d + bl\lambda d^2\right)}{\lambda^3 d^2 + 2\lambda^2 d e^{-\frac{b(d-l)^2}{2}} + 2\lambda}. \quad (3.19)$$

Therefore, substituting equation (3.16) into equation (3.19), we obtain

$$a_0 = -\frac{I\lambda}{2\pi\sigma_0 e^{-\frac{bl^2}{2}}} \left[\frac{2e^{-\frac{b(d-l)^2}{2}} (bld - 1) - 2\lambda d + bl\lambda d^2}{\lambda^3 d^2 + 2\lambda^2 d e^{-\frac{b(d-l)^2}{2}} + 2\lambda} \right]. \quad (3.20)$$

The surface potential is then

$$\psi(\rho, 0) = \frac{I}{2\pi\sigma_0 e^{-\frac{bl^2}{2}}} \int_0^\infty \left(\frac{2e^{-\frac{b(d-l)^2}{2}} (1 - bld) + 2\lambda d - bl\lambda d^2}{\lambda^2 d^2 + 2\lambda d e^{-\frac{b(d-l)^2}{2}} + 2} \right) J_0(\lambda\rho) d\lambda. \quad (3.21)$$

3.4 Normalized Apparent Resistivity

Although the knowledge of the potential function allows to compute the apparent resistivity for any electrode configuration, we shall present here the expression for the Wenner array configuration. The Wenner array formulation [7] is denoted by

$$(\nabla V)_W = 2[\psi(a) - \psi(2a)] \quad (3.22)$$

where $(\nabla V)_W$ is the Wenner's potential function and $\psi(a)$ is the scalar potential function. The apparent resistivity of Wenner, $(\rho_a)_W$, [7] can be computed from

$$(\rho_a)_W = \left(\frac{2\pi a}{I} \right) (\nabla V)_W. \quad (3.23)$$

Using equations (3.21), (3.22) and (3.23) we obtain

$$(\rho_a)_W = \frac{2a}{\sigma_0 e^{-\frac{bl^2}{2}}} \int_0^\infty \left(\frac{2e^{-\frac{b(d-l)^2}{2}} (1 - bld) + 2\lambda d - bl\lambda d^2}{\lambda^2 d^2 + 2\lambda d e^{-\frac{b(d-l)^2}{2}} + 2} \right) (J_0(\lambda a) - J_0(2\lambda a)) d\lambda. \quad (3.24)$$

Equation (3.24) can be rewritten as the normalized apparent resistivity

$$\left(\frac{\rho_a}{\rho_1}\right)_W = 2a \int_0^\infty \left(\frac{2e^{-\frac{b(d-l)^2}{2}} (1 - bld) + 2\lambda d - bl\lambda d^2}{\lambda^2 d^2 + 2\lambda d e^{-\frac{b(d-l)^2}{2}} + 2} \right) (J_0(\lambda a) - J_0(2\lambda a)) d\lambda \quad (3.25)$$

where $\rho_1 = \frac{1}{\sigma_0 e^{-\frac{bl^2}{2}}}$ is the resistivity at the ground surface.

3.5 Sounding Curves and Discussions

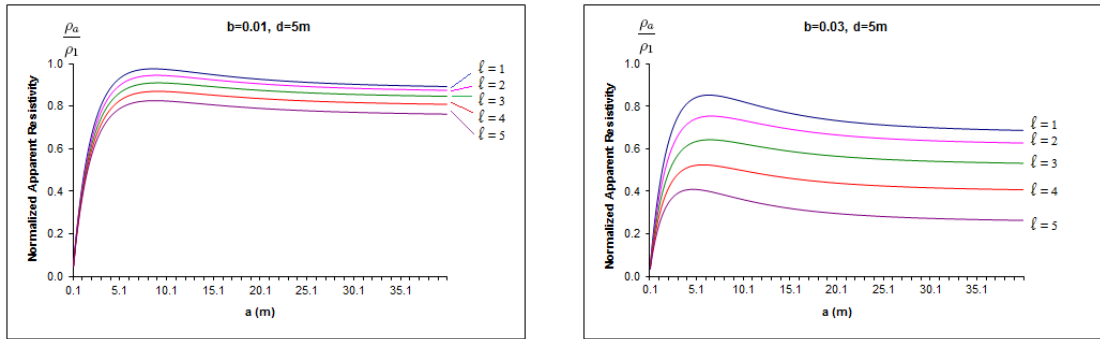


Figure 3.2: The curve of normalized apparent resistivity against electrode spacing, $d = 5\text{m}$; $b = 0.01$ and 0.03m^{-2} and $l = 1, 2, 3, 4$ and 5m .

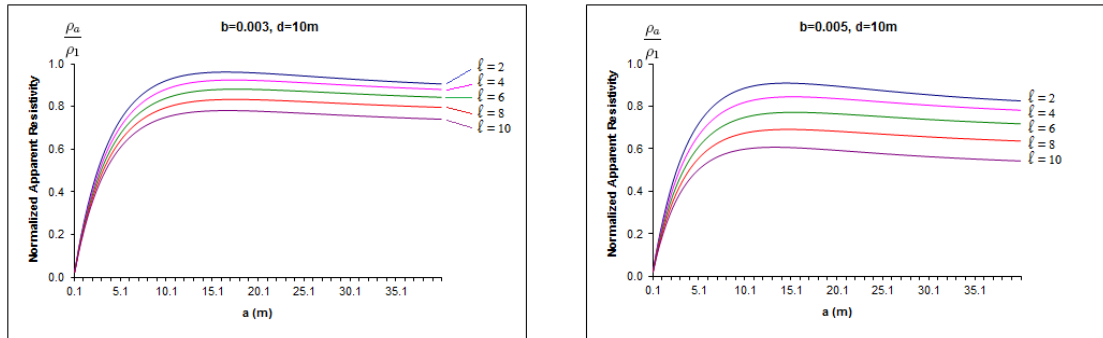


Figure 3.3: The curve of normalized apparent resistivity against electrode spacing, $d = 10\text{m}$; $b = 0.003$ and 0.005m^{-2} and $l = 2, 4, 6, 8$ and 10m .

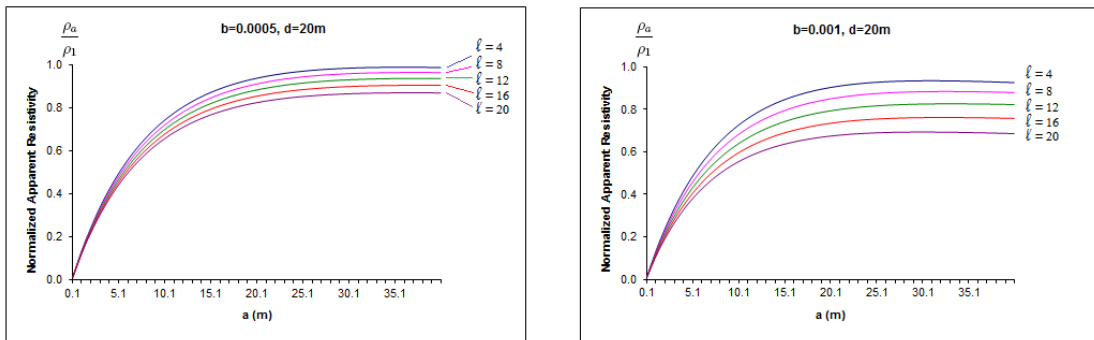


Figure 3.4: The curve of normalized apparent resistivity against electrode spacing, $d = 20\text{m}$; $b = 0.0005$ and 0.001m^{-2} and $l = 4, 8, 12, 16$ and 20m .

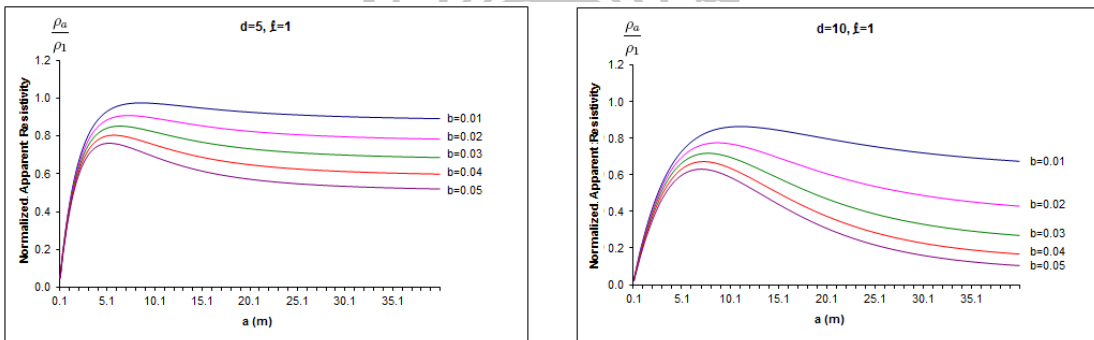


Figure 3.5: The curve of normalized apparent resistivity against electrode spacing, $d = 5, 10\text{m}$; $l = 1\text{m}$ and $b = 0.01, 0.02, \dots, 0.05\text{m}^{-2}$.

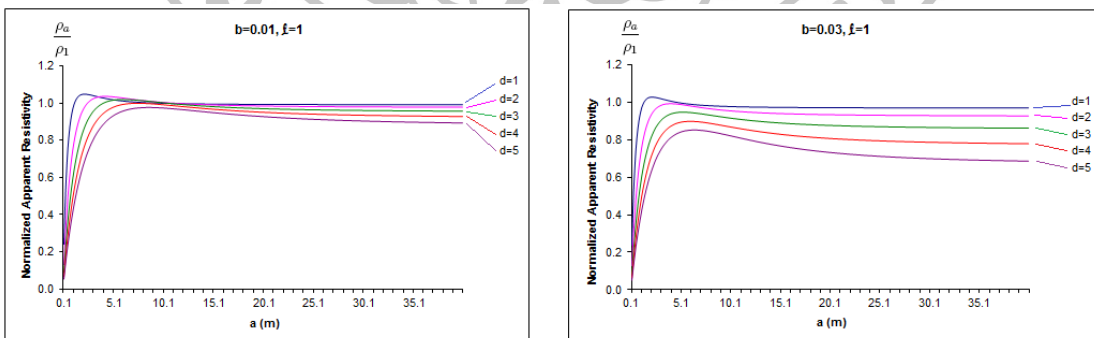


Figure 3.6: The curve of normalized apparent resistivity against electrode spacing, $b = 0.01$ and 0.03m^{-2} ; $l = 1\text{m}$ and $d = 1, 2, \dots, 5\text{m}$.

3.6 Inversion Process

Although, normalized apparent resistivity curve can be able to show a good pattern of conductivity profile of the ground, but however, we need more

accurate profile to explore the ground. Here, the inverse problem is introduced.

In our inverse model examples, we simulate array data of normalized apparent resistivity from our forward model of practical interest. The model of ground structures is used to investigate the conductivity profile. Chave's algorithm is used for numerically calculating the inverse Hankel transform of the normalized apparent resistivity solutions [3]. The special function is computed by using the Numerical Recipes source codes [33]. The electric current of 1 ampere is used in our computations. The Newton-Raphson method in optimization is applied to find a conductivity parameter of the ground.

3.6.1 Sample Tests

We firstly consider the normalized apparent resistivity data obtained from the model of simple case. The simple model test is the heterogeneous conductive half-space. The ground model has two layers. The overburden of the model has an exponentially varying conductivity denoted by $\sigma_{over}(z) = \sigma_0 e^{-b(z-l)^2/2}$ with thickness d , whereas the host has a constant conductivity denoted by $\sigma_{host}(z) = \sigma_0$ with infinite depth. The values of the model parameters are given in Table 3.1. The parameter l is a vertical location of the peak of the bulge for the model structure, which assumed to be sample test. This implies that the example model has only one unknown parameter, namely, b . The iterative procedure using the Newton-Raphson method [33] is applied to estimate the model parameter b of conductivity variation. We start the iterative process to find the value of the conductivity parameter with an initial guess $b = 0 \text{ m}^{-2}$. The optimal result is close to the true value with misfit less than $10^{-12} \text{ A} \cdot \text{m}^{-1}$ after using 3 iterations (see Table 3.2).

Table 3.1: Model parameters used in our sample tests.

Parameter		
d (m)	l (m)	b (m^{-2})
10	5	0.005

Table 3.2: Successive iterations for finding a conductivity parameter of the model in our sample tests.

Iteration	Parameter b (m^{-2})	Misfit ($\text{A} \cdot \text{m}^{-1}$)
0	0.0000000000000000	21.997686366243370
1	$4.846954974921935 \times 10^{-3}$	$1.922332776364707 \times 10^{-2}$
2	$4.999853700934837 \times 10^{-3}$	$1.752381931447662 \times 10^{-8}$
3	$4.999999999866227 \times 10^{-3}$	$1.106987846894784 \times 10^{-13}$

3.6.2 Simulated Real Data

We now consider the real data of normalized apparent resistivity obtained from the simulation model. The normalized apparent resistivity are generated by the forward problems of the model in our sample test. Random error up to 3% is superimposed on the normalized apparent resistivity to simulate the set of real data. The iterative procedures using the Newton-Raphson is applied to estimate the model parameter of conductivity variation for our model.

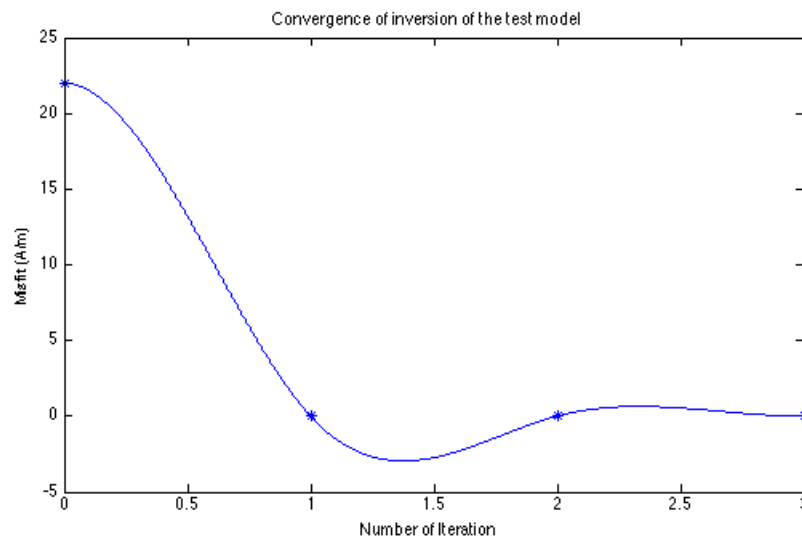


Figure 3.7: Curve of misfit versus number of iterations for the model in our sample test.

3.7 Discussions

In our calculation section, the equation (3.25) is used to compute the value of normalized apparent resistivity against electrode spacing by using Chave's algorithm [3]. Fortran programming is introduced under PC computer, Intel(R) Core(TM)2 Duo CPU P8600 @2.40GHz and 4GB of RAM. With the use of electric current 1 Ampere, $\sigma_0 = 2$ S/m, the results can be determined with the time used less than a second. The results are plotted to show some significant advantages in ground exploration.

The figures 3.2, 3.3, 3.4, 3.5 and 3.6 perform the normalized apparent resistivity against electrode spacing. Each of those figures show 5 curves of normalized apparent resistivity while the value of d , l and b are adjusted. The thickness of overburden used in our computation are 1, 2, 3, 4, 5, 10 and 20m. For small value of l and small value of b , all of our curves perform very large response in normalized apparent resistivity whereas for large value of l , the curves perform smaller response in normalized apparent resistivity. This supports the reason for the peak of conductive ground located near the ground surface, so it will reflect stronger re-

sponse than the case of large l from the ground surface according to the inverse square law of the distance between conductive source and ground surface. The top of the peaks of normalized apparent resistivity show a good relationship to the value of l . In Figure 3.5, the small value of d perform large response in normalized apparent resistivity while the value of l and b are fixed. It can be explained that as d is large the average conductive of overburden is lower than host. In Figure 3.6, as b is large, the conductive of overburden is low, thus, the response curves will be small. It can be said that the curve of normalized apparent resistivity could be able to predict the vertical location of conductivity profile of the ground structure.

Normalized apparent resistivity is good to show the pattern of conductivity profile of ground. However, the inverse problem via the use of optimization technique is introduced for better finding the conductivity parameter of the ground than normalized apparent resistivity. The test model is assumed that it has only one unknown parameter of the conductivity variation. The iterative procedure using the Newton-Raphson method is applied to estimate this unknown parameter. The optimal result of our sample test converges very fast to the true value with misfit less than $10^{-12} \text{A} \cdot \text{m}^{-1}$ after using only 3 iterations. These illustrate the advantage in using the Newton-Raphson method which give the result much better than using another method of inversion (e.g., Oldenburg [12], Vozoff and Jupp [21]). The inversion method leads to very good result and has high speed of convergence. This shows the robustness of our medel.

3.8 Summary and Conclusions

The normalized apparent resistivities of the earth having the electrical conductivity $\sigma_{over}(z) = \sigma_0 e^{-b(z-l)^2/2}$ for the depth $0 \leq z \leq d$, and $\sigma_{host}(z) = \sigma_0$ for the depth $z > d$, are considered. The integral expressions are derived and computed to determine the electric potential due to a point of direct current source on the ground surface. The value of electric potential will be used to determine the normalized apparent resistivity. We derive analytical solutions of the electric potential due to a direct current source by using Wenner array configuration on two-layered earth structure having exponentially varying conductivity. The Hankel transform is introduced to our problem and analytical result is obtained. Our solutions are achieved by solving a boundary value problem in the wave number domain and then transforming the solution back to the spatial domain. The power series technique is used to solve the problem. The curves of normalized apparent resistivity against electrode spacing are plotted and shown the advantage in the ground exploration. To find the accurate of conductivity profile solution, the inverse problem is considered. The inversion process, using the Newton-Raphson method, is conducted to estimate the conductivity variation parameter. The method perform very good result and have high speed of convergence.

Chapter 4

Mathematical Model of Magnetometric Resistivity Sounding for a Conductive Host with a Bulge Overburden

4.1 Introduction

The magnetometric resistivity method has recently become an additional electrical prospecting technique used for finding mineral resources. This technique is based on the measurement of low-level, low-frequency magnetic fields associated with non-inductive current flow in the ground. Chen and Oldenburg [18] derived the magnetic field directly from solving a boundary value problems which was similar to the approach used by Edward [27] and then discussed in a homogeneous and a 2-layered earth model. Yooyuanyong and Sripanya [30] derived the solutions of the steady state magnetic field due to a DC current source in three types of heterogeneous earth models. These solutions are critical to interpret the magnetometric resistivity (MMR) data.

In this chapter, 2-layered conductive earth model is considered similar to Chen and Oldenburg[18], but it is different in the conductivity profile. For first layer, the conductivity of overburden is denoted by $\sigma_1(z) = \sigma_0 e^{-b(z-l)^2/2}$, $0 \leq z \leq h$, where b is constant, l is positive which is used to locate the peak of the bulge, h is the thickness of overburden and σ_0 is positive constant. The second layer, the conductivity of host medium, $z > h$, is constant and is given by $\sigma_2(z) = \sigma_0$. The objective of this chapter is to show the behavior of the field while some parameters are given approximately. The another important objective is to investigate the conductivity parameter via the optimization technique.

4.2 Formulation of the Problem

The general steady state Maxwell's equations in the frequency domain [18] can be used to determine the magnetic field for this problem, namely

$$\nabla \times \vec{E} = \vec{0} \quad (4.1)$$

and

$$\nabla \times \vec{H} = \sigma \vec{E}, \quad (4.2)$$

where \vec{E} is the vector electric field, \vec{H} is the vector magnetic field, σ is the conductivity of the medium in Siemens per meter (S/m) which is assumed to be a function of z only and ∇ is the del operator. Eliminating \vec{E} from equations (4.1) and (4.2), we obtain

$$\nabla \times \frac{1}{\sigma} \nabla \times \vec{H} = \vec{0}. \quad (4.3)$$

This can be expressed in cylindrical coordinates (r, ϕ, z) as

$$\begin{aligned} 0 = & \left(\frac{1}{r} \frac{\partial}{\partial \phi} \frac{1}{\sigma} \left(\frac{1}{r} \frac{\partial}{\partial r} (r H_\phi) - \frac{1}{r} \frac{\partial H_r}{\partial \phi} \right) - \frac{\partial}{\partial z} \frac{1}{\sigma} \left(\frac{\partial H_r}{\partial z} - \frac{\partial H_z}{\partial r} \right) \right) e_r \\ & + \left(\frac{\partial}{\partial z} \frac{1}{\sigma} \left(\frac{1}{r} \frac{\partial H_z}{\partial \phi} - \frac{\partial H_\phi}{\partial z} \right) - \frac{\partial}{\partial r} \frac{1}{\sigma} \left(\frac{1}{r} \frac{\partial}{\partial r} (r H_\phi) - \frac{1}{r} \frac{\partial H_r}{\partial \phi} \right) \right) e_\phi \\ & + \left(\frac{1}{r} \frac{\partial}{\partial r} \left(\frac{r}{\sigma} \left(\frac{\partial H_r}{\partial z} - \frac{\partial H_z}{\partial r} \right) \right) - \frac{1}{r} \frac{\partial}{\partial \phi} \frac{1}{\sigma} \left(\frac{1}{r} \frac{\partial H_z}{\partial \phi} - \frac{\partial H_\phi}{\partial z} \right) \right) e_z, \end{aligned} \quad (4.4)$$

where H_r , H_ϕ and H_z are the components of \vec{H} in e_r , e_ϕ and e_z directions, respectively. Since the problem is axisymmetric and \vec{H} has only the azimuthal component in cylindrical coordinates, for simplicity, we use H to represent the azimuthal component H_ϕ in the following derivations. Simplifying equation (4.4) yields

$$\frac{\partial}{\partial z} \frac{1}{\sigma} \frac{\partial H}{\partial z} - \frac{\partial}{\partial r} \frac{1}{\sigma r} \frac{\partial}{\partial r} (r H) = 0,$$

or

$$\frac{1}{\sigma} \frac{\partial^2 H}{\partial z^2} + \frac{\partial}{\partial z} \left(\frac{1}{\sigma} \right) \frac{\partial H}{\partial z} + \frac{1}{\sigma} \left(\frac{1}{r} \frac{\partial^2}{\partial r^2} (r H) + \frac{\partial}{\partial r} \left(\frac{1}{r} \right) \frac{\partial}{\partial r} (r H) \right) + \frac{\partial}{\partial r} \left(\frac{1}{\sigma} \right) \frac{1}{r} \frac{\partial}{\partial r} (r H) = 0.$$

In our study, we denote σ as a function of only depth z , and we now have

$$\frac{\partial^2 H}{\partial z^2} + \sigma \frac{\partial}{\partial z} \left(\frac{1}{\sigma} \right) \frac{\partial H}{\partial z} + \frac{\partial^2 H}{\partial r^2} + \frac{1}{r} \frac{\partial H}{\partial r} - \frac{1}{r^2} H = 0. \quad (4.5)$$

The Hankel transform [2] is introduced and defined by

$$\tilde{H}(\lambda, z) = \int_0^\infty r H(r, z) J_1(\lambda r) dr, \quad (4.6)$$

and

$$H(r, z) = \int_0^{\infty} \lambda \tilde{H}(\lambda, z) J_1(\lambda r) d\lambda, \quad (4.7)$$

where J_1 is the Bessel function of the first kind of order one and λ is the Hankel variable. Taking the transformation on both sides of equation (4.5), we obtain

$$\int_0^{\infty} r \left(\frac{\partial^2 H}{\partial z^2} + \sigma \frac{\partial}{\partial z} \left(\frac{1}{\sigma} \right) \frac{\partial H}{\partial z} + \frac{\partial^2 H}{\partial r^2} + \frac{1}{r} \frac{\partial H}{\partial r} - \frac{1}{r^2} H \right) J_1(\lambda r) dr = \int_0^{\infty} r(0) J_1(\lambda r) dr,$$

or

$$\begin{aligned} & \int_0^{\infty} r \frac{\partial^2 H}{\partial z^2} J_1(\lambda r) dr + \sigma \frac{\partial}{\partial z} \left(\frac{1}{\sigma} \right) \int_0^{\infty} r \frac{\partial H}{\partial z} J_1(\lambda r) dr \\ & + \int_0^{\infty} \left(r \frac{\partial^2 H}{\partial r^2} + \frac{\partial H}{\partial r} \right) J_1(\lambda r) dr - \int_0^{\infty} \frac{1}{r} H J_1(\lambda r) dr = 0, \end{aligned}$$

or

$$\begin{aligned} & \int_0^{\infty} r \frac{\partial^2 H}{\partial z^2} J_1(\lambda r) dr + \sigma \frac{\partial}{\partial z} \left(\frac{1}{\sigma} \right) \int_0^{\infty} r \frac{\partial H}{\partial z} J_1(\lambda r) dr \\ & + \int_0^{\infty} \frac{\partial}{\partial r} \left(r \frac{\partial H}{\partial r} \right) J_1(\lambda r) dr - \int_0^{\infty} \frac{1}{r} H J_1(\lambda r) dr = 0, \end{aligned}$$

or

$$\begin{aligned} & \int_0^{\infty} r \frac{\partial^2 H}{\partial z^2} J_1(\lambda r) dr + \sigma \frac{\partial}{\partial z} \left(\frac{1}{\sigma} \right) \int_0^{\infty} r \frac{\partial H}{\partial z} J_1(\lambda r) dr \\ & + \lim_{a \rightarrow 0^+} \int_a^1 \frac{\partial}{\partial r} \left(r \frac{\partial H}{\partial r} \right) J_1(\lambda r) dr + \lim_{b \rightarrow \infty} \int_1^b \frac{\partial}{\partial r} \left(r \frac{\partial H}{\partial r} \right) J_1(\lambda r) dr \\ & - \int_0^{\infty} \frac{1}{r} H J_1(\lambda r) dr = 0. \end{aligned}$$

Integrating by parts on the third and fourth terms of the above equation yields

$$\begin{aligned}
& \int_0^{\infty} r \frac{\partial^2 H}{\partial z^2} J_1(\lambda r) dr + \sigma \frac{\partial}{\partial z} \left(\frac{1}{\sigma} \right) \int_0^{\infty} r \frac{\partial H}{\partial z} J_1(\lambda r) dr \\
& + \lim_{a \rightarrow 0^+} \left(r \frac{\partial H}{\partial r} J_1(\lambda r) \right) \Big|_a^1 - \lim_{a \rightarrow 0^+} \int_a^1 r \frac{\partial H}{\partial r} \frac{d}{dr} J_1(\lambda r) dr \\
& + \lim_{b \rightarrow \infty} \left(r \frac{\partial H}{\partial r} J_1(\lambda r) \right) \Big|_1^b - \lim_{b \rightarrow \infty} \int_1^b r \frac{\partial H}{\partial r} \frac{d}{dr} J_1(\lambda r) dr \\
& - \int_0^{\infty} \frac{1}{r} H J_1(\lambda r) dr = 0,
\end{aligned}$$

or

$$\begin{aligned}
& \int_0^{\infty} r \frac{\partial^2 H}{\partial z^2} J_1(\lambda r) dr + \sigma \frac{\partial}{\partial z} \left(\frac{1}{\sigma} \right) \int_0^{\infty} r \frac{\partial H}{\partial z} J_1(\lambda r) dr \\
& - \lim_{a \rightarrow 0^+} \int_a^1 r \frac{\partial H}{\partial r} \frac{d}{dr} J_1(\lambda r) dr - \lim_{b \rightarrow \infty} \int_1^b r \frac{\partial H}{\partial r} \frac{d}{dr} J_1(\lambda r) dr \\
& - \int_0^{\infty} \frac{1}{r} H J_1(\lambda r) dr = 0.
\end{aligned}$$

Integrating by parts again on the third and fourth terms of the above equation, we obtain

$$\begin{aligned}
& \int_0^{\infty} r \frac{\partial^2 H}{\partial z^2} J_1(\lambda r) dr + \sigma \frac{\partial}{\partial z} \left(\frac{1}{\sigma} \right) \int_0^{\infty} r \frac{\partial H}{\partial z} J_1(\lambda r) dr \\
& - \lim_{a \rightarrow 0^+} \left(r H \frac{\partial}{\partial r} J_1(\lambda r) \right) \Big|_a^1 + \lim_{a \rightarrow 0^+} \int_a^1 H \frac{d}{dr} \left(r \frac{d}{dr} J_1(\lambda r) \right) dr \\
& - \lim_{b \rightarrow \infty} \left(r H \frac{\partial}{\partial r} J_1(\lambda r) \right) \Big|_1^b + \lim_{b \rightarrow \infty} \int_1^b H \frac{d}{dr} \left(r \frac{d}{dr} J_1(\lambda r) \right) dr \\
& - \int_0^{\infty} \frac{1}{r} H J_1(\lambda r) dr = 0,
\end{aligned}$$

or

$$\begin{aligned} & \int_0^{\infty} r \frac{\partial^2 H}{\partial z^2} J_1(\lambda r) dr + \sigma \frac{\partial}{\partial z} \left(\frac{1}{\sigma} \right) \int_0^{\infty} r \frac{\partial H}{\partial z} J_1(\lambda r) dr \\ & + \lim_{a \rightarrow 0^+} \int_a^1 H \frac{d}{dr} \left(r \frac{d}{dr} J_1(\lambda r) \right) dr + \lim_{b \rightarrow \infty} \int_1^b H \frac{d}{dr} \left(r \frac{d}{dr} J_1(\lambda r) \right) dr \\ & - \int_0^{\infty} \frac{1}{r} H J_1(\lambda r) dr = 0, \end{aligned}$$

or

$$\begin{aligned} & \int_0^{\infty} r \frac{\partial^2 H}{\partial z^2} J_1(\lambda r) dr + \sigma \frac{\partial}{\partial z} \left(\frac{1}{\sigma} \right) \int_0^{\infty} r \frac{\partial H}{\partial z} J_1(\lambda r) dr \\ & + \int_0^{\infty} H \frac{d}{dr} \left(r \frac{d}{dr} J_1(\lambda r) \right) dr - \int_0^{\infty} \frac{1}{r} H J_1(\lambda r) dr = 0, \end{aligned}$$

or

$$\begin{aligned} & \int_0^{\infty} r \frac{\partial^2 H}{\partial z^2} J_1(\lambda r) dr + \sigma \frac{\partial}{\partial z} \left(\frac{1}{\sigma} \right) \int_0^{\infty} r \frac{\partial H}{\partial z} J_1(\lambda r) dr \\ & + \int_0^{\infty} H \frac{d}{dr} \left(r \frac{d^2}{dr^2} J_1(\lambda r) + \frac{d}{dr} J_1(\lambda r) \right) dr - \int_0^{\infty} \frac{1}{r} H J_1(\lambda r) dr = 0, \end{aligned}$$

or

$$\begin{aligned} & \int_0^{\infty} r \frac{\partial^2 H}{\partial z^2} J_1(\lambda r) dr + \sigma \frac{\partial}{\partial z} \left(\frac{1}{\sigma} \right) \int_0^{\infty} r \frac{\partial H}{\partial z} J_1(\lambda r) dr \\ & + \int_0^{\infty} H \frac{d}{dr} \left(\lambda^2 r J_1''(\lambda r) + \lambda J_1'(\lambda r) \right) dr - \int_0^{\infty} \frac{1}{r} H J_1(\lambda r) dr = 0, \end{aligned}$$

or

$$\begin{aligned} & \int_0^{\infty} r \frac{\partial^2 H}{\partial z^2} J_1(\lambda r) dr + \sigma \frac{\partial}{\partial z} \left(\frac{1}{\sigma} \right) \int_0^{\infty} r \frac{\partial H}{\partial z} J_1(\lambda r) dr \\ & + \int_0^{\infty} r H \left(\lambda^2 J_1''(\lambda r) + \frac{\lambda}{r} J_1'(\lambda r) - \frac{1}{r^2} J_1(\lambda r) \right) dr = 0. \end{aligned}$$

Since J_1 is the solution of Bessel's differential equation, we now have

$$\lambda^2 J_1''(\lambda r) + \frac{\lambda}{r} J_1'(\lambda r) - \frac{1}{r^2} J_1(\lambda r) = -\lambda^2 J_1(\lambda r).$$

This yields

$$\int_0^{\infty} r \frac{\partial^2 H}{\partial z^2} J_1(\lambda r) dr + \sigma \frac{\partial}{\partial z} \left(\frac{1}{\sigma} \right) \int_0^{\infty} r \frac{\partial H}{\partial z} J_1(\lambda r) dr - \lambda^2 \int_0^{\infty} r H J_1(\lambda r) dr = 0.$$

Hence, the Hankel transform of equation (4.5) result in

$$\frac{\partial^2 \tilde{H}}{\partial z^2} + \sigma \frac{\partial}{\partial z} \left(\frac{1}{\sigma} \right) \frac{\partial \tilde{H}}{\partial z} - \lambda^2 \tilde{H} = 0. \quad (4.8)$$

Since the electrode is in the overburden which the end of the electrode is positioned at $z = h$, so that a magnetic field will be separated into two parts. The magnetic field is come from the ground layer that can be described by the general solution of equation (4.8) and the magnetic field arising from probe sources H_0 , which is only one element. It can be explained by the Ampere's law [31, 34], as

$$H(r, z) = \frac{I}{2\pi r},$$

where I is the current at the probe on the ground surface. From equation (4.6), we have

$$\tilde{H}_0(\lambda, z) = \int_0^{\infty} r \left(\frac{I}{2\pi r} \right) J_1(\lambda r) dr = \frac{I}{2\pi \lambda}.$$

Therefore, the magnetic field in each layer can be obtained by taking the inverse Hankel transform to the solution of equation (4.8), which satisfies the following boundary conditions [5, 7]:

1. The vertical component of the current density must be zero at the ground surface ($z = 0$),

$$\sigma_1(z) E_1^z(r, z)|_{z=0} = 0, \quad (4.9)$$

where E_1^z is the vertical component of the electric field in overburden.

2. The azimuthal component of the magnetic field needs to be continuous on each of the boundary planes in the earth,

$$\lim_{z \rightarrow h^-} \tilde{H}_1(\lambda, z) = \lim_{z \rightarrow h^+} \tilde{H}_2(\lambda, z). \quad (4.10)$$

where H_1 and H_2 are magnetic fields in the first and second layer, respectively.

3. The radial component of the electric field, denoted by E^r , needs to be continuous on each of the boundary planes in the earth,

$$\lim_{z \rightarrow h^-} \tilde{E}_1^r(\lambda, z) = \lim_{z \rightarrow h^+} \tilde{E}_2^r(\lambda, z). \quad (4.11)$$

where E_1^r and E_2^r are the radial component of electric fields in the first and second layer, respectively. To determine the radial and vertical components of the electric

field related to the azimuthal component of the magnetic field, we expand equation (4.2) and obtain

$$E = \left(\frac{1}{\sigma r} \frac{\partial H_z}{\partial \phi} - \frac{1}{\sigma} \frac{\partial H_\phi}{\partial z} \right) e_r + \left(\frac{1}{\sigma} \frac{\partial H_r}{\partial z} - \frac{1}{\sigma} \frac{\partial H_z}{\partial r} \right) e_\phi + \left(\frac{1}{\sigma r} \frac{\partial}{\partial r} (r H_\phi) - \frac{1}{\sigma r} \frac{\partial H_r}{\partial \phi} \right) e_z.$$

Since the problem is axisymmetric and \vec{H} has only the azimuthal component in cylindrical coordinates, for simplicity as equation (4.4), we use H to represent the azimuthal component H_ϕ in the above derivations. This yields

$$E^r = -\frac{1}{\sigma} \frac{\partial H}{\partial z}, \quad E^z = \frac{1}{\sigma r} \frac{\partial}{\partial r} (r H).$$

By equation (4.6), we have

$$\tilde{E}_r(\lambda, z) = \int_0^\infty r \left(-\frac{1}{\sigma(z)} \frac{\partial}{\partial z} H(r, z) \right) J_1(\lambda r) dr = -\frac{1}{\sigma(z)} \frac{\partial}{\partial z} \tilde{H}(\lambda, z).$$

4.3 A Geometric 2-Layered Earth Model

In our geometric model, two-layered earth model is considered which the interface between the layers is a plane parallel to the ground surface. A point source of direct current I is located into the overburden which the end of the electrode is positioned at $z = h$. For the first layer, the conductivity of overburden is denoted by $\sigma_1(z) = \sigma_0 e^{-b(z-l)^2/2}$, $0 \leq z \leq h$, where σ_0 , b and l are positive constants and l is used to locate the peak of the bulge, h is the thickness of overburden. The second layer, the conductivity of host medium, $z > h$, is constant and is given by $\sigma_2(z) = \sigma_0$.

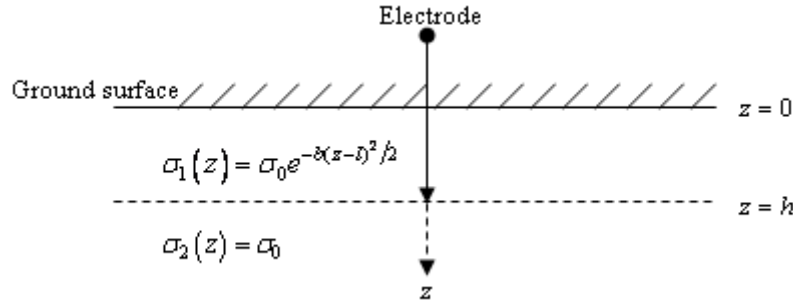


Figure 4.1: Geometric model for 2-layered earth

4.4 Solution of Magnetic Field for a 2-Layered Earth Model

An overburden has a variation of conductivity $\sigma_1(z)$ with thickness h over a conductive host medium having constant conductivity $\sigma_2(z)$. Hence the

equation for the magnetic field in overburden and host medium can be simplified by substituting $\sigma_1(z)$ and $\sigma_2(z)$ into the equation (4.8), thus, we obtain

$$\frac{\partial^2 \tilde{H}_1}{\partial z^2} + b(z-l) \frac{\partial \tilde{H}_1}{\partial z} - \lambda^2 \tilde{H}_1 = 0, \quad (4.12)$$

and

$$\frac{\partial^2 \tilde{H}_2}{\partial z^2} - \lambda^2 \tilde{H}_2 = 0. \quad (4.13)$$

The power series method and auxiliary equation are used to find the magnetic field formulation in an overburden, denoted by \tilde{H}_1 , and conductive host medium, denoted by \tilde{H}_2 , respectively. Therefore, the solutions of the equations (4.12) and (4.13) are written by [4, 26]

$$\tilde{H}_1(\lambda, z) = \frac{I}{2\pi\lambda} \left(1 + \frac{\lambda^2 z^2}{2} \right) + A_1 \left(1 + \frac{\lambda^2 z^2}{2} \right) + A_2 \left(z + \frac{bz^2}{2} \right), \quad (4.14)$$

and

$$\tilde{H}_2(\lambda, z) = A_3 e^{-\lambda(z-h)} + A_4 e^{\lambda(z-h)},$$

respectively, where A_1, A_2, A_3 and A_4 are arbitrary constants, which can be determined by using the boundary conditions. The condition at $z \rightarrow \infty$, the magnetic field tends to zero, that leads \tilde{H}_2 to

$$\tilde{H}_2(\lambda, z) = A_3 e^{-\lambda(z-h)}. \quad (4.15)$$

For the first boundary condition in equation (4.9), we obtain

$$\sigma_1(z) \left(\frac{1}{r\sigma_1(z)} \frac{\partial}{\partial r} (rH_1(r, z)) \right) = 0.$$

Since $\sigma_1(z)$ and r are not zero, then

$$\frac{\partial}{\partial r} (rH_1(r, z)) = 0,$$

or

$$rH_1(r, z) = \int \frac{\partial}{\partial r} (rH_1(r, z)) dr = \int (0) dr = 0.$$

Since $r > 0$, thus $H_1(r, z) = 0$ and $\tilde{H}_1(\lambda, z) = \int_0^\infty rH_1(r, z) J_1(\lambda r) dr$.

Hence,

$$\frac{I}{2\pi\lambda} \left(1 + \frac{\lambda^2 z^2}{2} \right) + A_1 \left(1 + \frac{\lambda^2 z^2}{2} \right) + A_2 \left(z + \frac{bz^2}{2} \right) = \int_0^\infty r(0) J_1(\lambda r) dr = 0.$$

Since no electric current across at the air-earth interface, $I = 0$ then

$$\left[A_1 \left(1 + \frac{\lambda^2 z^2}{2} \right) + A_2 \left(z + \frac{bz^2}{2} \right) \right]_{z=0} = 0. \text{ Thus, } A_1 = 0.$$

By the second boundary condition, we obtain

$$\lim_{z \rightarrow h^-} \left[\frac{I}{2\pi\lambda} \left(1 + \frac{\lambda^2 z^2}{2} \right) + A_2 \left(z + \frac{bz^2}{2} \right) \right] = \lim_{z \rightarrow h^+} A_3 e^{-\lambda(z-h)}.$$

Thus,

$$A_3 = \frac{I}{2\pi\lambda} \left(1 + \frac{\lambda^2 h^2}{2} \right) + A_2 \left(h + \frac{blh^2}{2} \right). \quad (4.16)$$

Applying the third boundary condition, we have

$$\lim_{z \rightarrow h^-} \left[-\frac{1}{\sigma_1(z)} \frac{\partial}{\partial z} \tilde{H}_1(\lambda, z) \right] = \lim_{z \rightarrow h^+} \left[-\frac{1}{\sigma_2(z)} \frac{\partial}{\partial z} \tilde{H}_2(\lambda, z) \right],$$

or

$$\begin{aligned} \lim_{z \rightarrow h^-} \left[-\frac{1}{\sigma_0 e^{-b(z-l)^2/2}} \frac{\partial}{\partial z} \left(\frac{I}{2\pi\lambda} \left(1 + \frac{\lambda^2 z^2}{2} \right) + A_2 \left(z + \frac{blz^2}{2} \right) \right) \right] \\ = \lim_{z \rightarrow h^+} \left[-\frac{1}{\sigma_0} \frac{\partial}{\partial z} (A_3 e^{-\lambda(z-h)}) \right]. \end{aligned}$$

Hence,

$$A_3 = -\frac{1}{\lambda e^{-b(h-l)^2/2}} \left(\frac{I\lambda h}{2\pi} + A_2 (1 + blh) \right). \quad (4.17)$$

From equation (4.16) into the equation (4.17), we obtain

$$\frac{I}{2\pi\lambda} \left(1 + \frac{\lambda^2 h^2}{2} \right) + A_2 \left(h + \frac{blh^2}{2} \right) = -\frac{1}{\lambda e^{-b(h-l)^2/2}} \left(\frac{I\lambda h}{2\pi} + A_2 (1 + blh) \right).$$

Therefore,

$$A_2 = -\frac{I}{2\pi} \left(\frac{(2 + \lambda^2 h^2) \alpha_1 + 2\lambda h}{2h\lambda\alpha_1 + blh^2\lambda\alpha_1 + 2(1 + blh)} \right), \quad (4.18)$$

where $\alpha_1 = e^{-b(h-l)^2/2}$.

Since $A_3 = -\frac{1}{\lambda\alpha_1} \left(\frac{I\lambda h}{2\pi} + A_2 (1 + blh) \right)$, then with the use of equation (4.18), we obtain

$$A_3 = \frac{I}{2\pi\lambda\alpha_1} \left[\frac{((2 + \lambda^2 h^2) \alpha_1 + 2\lambda h) (1 + blh)}{2\lambda h\alpha_1 + bl\lambda h^2\alpha_1 + 2(1 + blh)} - \lambda h \right]. \quad (4.19)$$

Hence, with the use of inverse Hankel transforms, the magnetic field in overburden and conductive host medium are shown, respectively, as

$$\begin{aligned} H_1(r, z) \\ = \int_0^\infty \frac{I}{2\pi} \left[1 + \frac{\lambda^2 z^2}{2} - \lambda \left(\frac{(2 + \lambda^2 h^2) \alpha_1 + 2\lambda h}{2h\lambda\alpha_1 + blh^2\lambda\alpha_1 + 2(1 + blh)} \right) \left(z + \frac{blz^2}{2} \right) \right] J_1(\lambda r) d\lambda, \end{aligned} \quad (4.20)$$

and

$$H_2(r, z) = \int_0^\infty \frac{I}{2\pi\alpha_1} \left[\frac{((2 + \lambda^2 h^2) \alpha_1 + 2\lambda h) (1 + blh)}{2\lambda h\alpha_1 + bl\lambda h^2\alpha_1 + 2(1 + blh)} - \lambda h \right] e^{-\lambda(z-h)} J_1(\lambda r) d\lambda. \quad (4.21)$$

4.5 Numerical Experiments

In our numerical experiments, the magnetic field due to a direct current source on the ground surface of the model is calculated. Chave's algorithm [3] is used for numerical calculating the inverse Hankel transform of the magnetic field solutions. The current 1-Ampere is injected to the ground by the probe length of 1m and 3m perpendicular to the ground surface, $\sigma_0 = 2\text{S/m}$ and $b = 0.005\text{m}^{-2}$. The results of magnetic field response are performed as the graphs in Figures 4.2, 4.3, 4.4 and 4.5. The graphs are shown the behavior of the magnetic field against source-receiver spacing (r) while the values of h , l and z are adjusted.

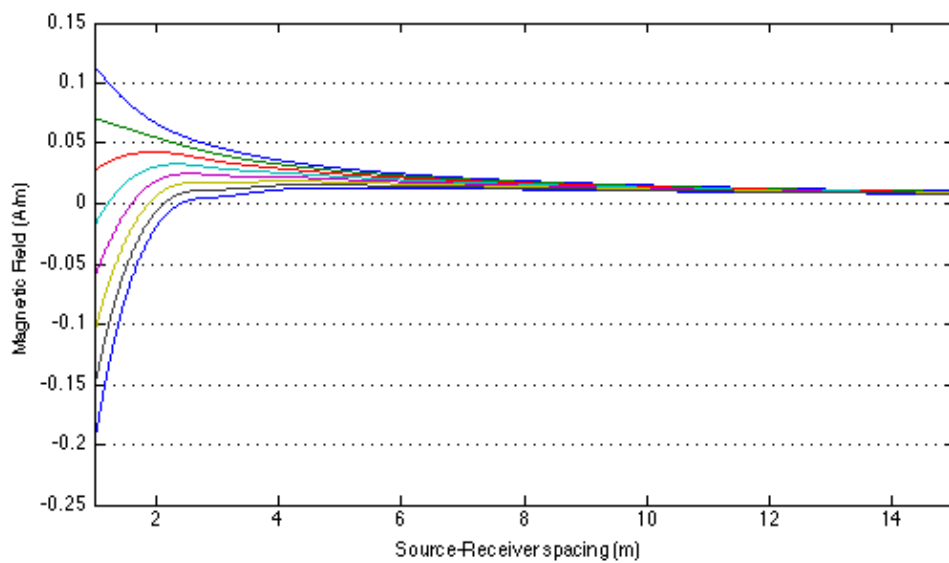


Figure 4.2: The behavior of magnetic field against r at different depth $z = 0.5, 1, 1.5, \dots, 3.5, 4\text{m}$; $h = 5\text{m}$; $l = 3\text{m}$.

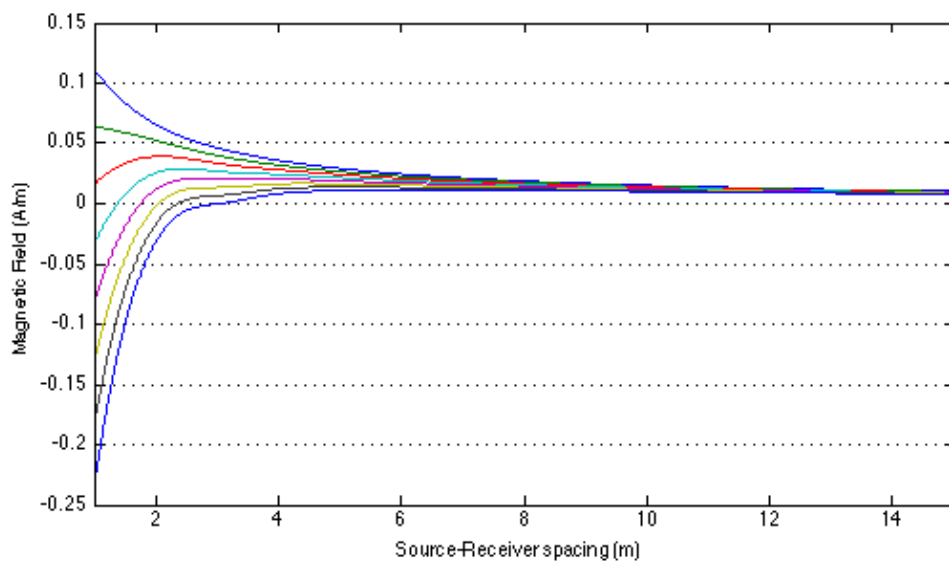


Figure 4.3: The behavior of magnetic field against r at different depth $z = 0.5, 1, 1.5, \dots, 3.5, 4\text{m}$; $h = 3\text{m}$; $l = 5\text{m}$.

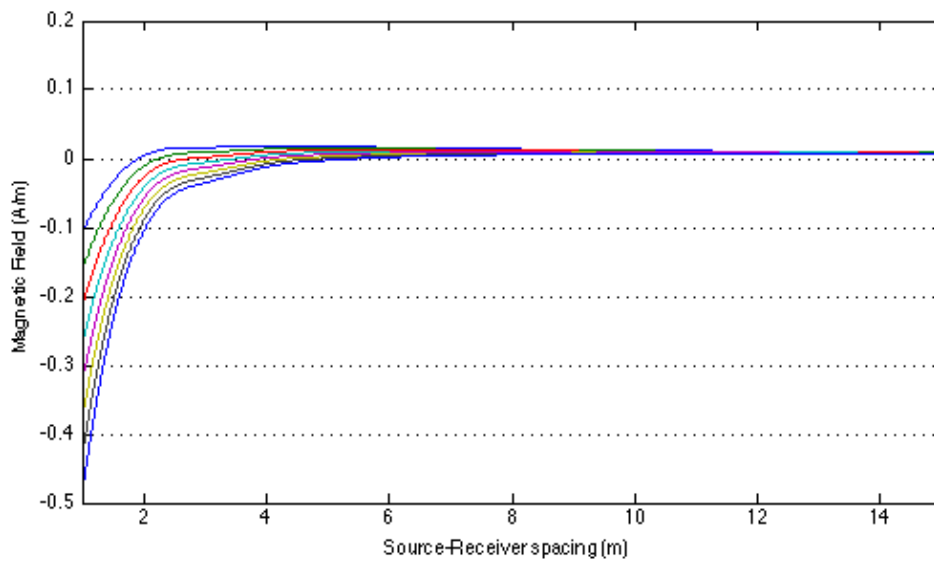


Figure 4.4: The behavior of magnetic field against r at different depth $z = 2.5, 3, 3.5, \dots, 5.5, 6\text{m}$; $h = 2\text{m}$; $l = 1\text{m}$.

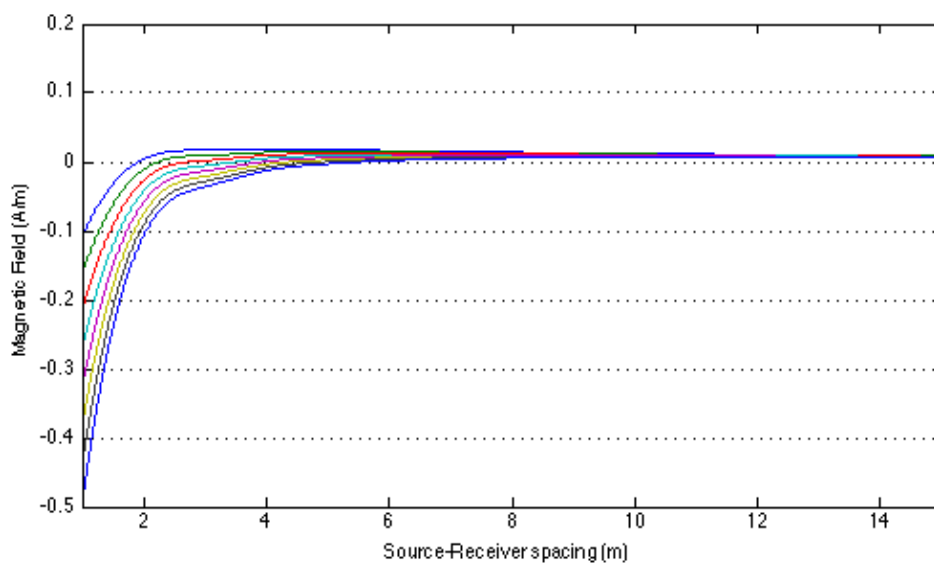


Figure 4.5: The behavior of magnetic field against r at different depth $z = 2.5, 3, 3.5, \dots, 5.5, 6\text{m}$; $h = 2\text{m}$; $l = 3\text{m}$.

4.6 Inversion Process

In our inverse model examples, we simulate array data of magnetic field from our forward model of practical interest. The two-layered earth model of ground structures is used to investigate the conductivity profile. Chave's algorithm is used for numerically calculating the inverse Hankel transform of magnetic field solutions [3]. The special function is computed by using the Numerical Recipes source codes [33]. The electric current of 1 ampere is used in our computations.

The Newton-Raphson method in optimization is applied to find a conductivity parameter of the ground.

4.6.1 Sample Test

We firstly consider the magnetic field data obtained from the model of simple case. The test model is the heterogeneous conductive half-space. The test ground model has two layers. The overburden of the model has an exponentially varying conductivity denoted by $\sigma_{over}(z) = \sigma_0 e^{-b(z-l)^2/2}$ with thickness h , whereas the host has a constant conductivity denoted by $\sigma_{host}(z) = \sigma_0$ with infinite depth. The values of the model parameters are given in Table 4.1. The parameter l is a vertical location of the peak of the bulge for the model structure, which assumed to be our sample test. This implies that the example model has only one unknown parameter, namely, b . The iterative procedure using the Newton-Raphson method [33] is applied to estimate the model parameter b of conductivity variation. We start the iterative process to find the value of the conductivity parameter with an initial guess $b = 0.05 \text{ m}^{-2}$. The optimal result is close to the true value with misfit less than $10^{-12} \text{ A} \cdot \text{m}^{-1}$ after using 3 iterations (see Table 4.2).

Table 4.1: Model parameters used in our sample tests.

Parameter			
z (m)	h (m)	l (m)	b (m^{-2})
5	5	2	0.005

Table 4.2: Successive iterations for finding a conductivity parameter of the model in our sample tests.

Iteration	Parameter b (m^{-2})	Misfit ($\text{A} \cdot \text{m}^{-1}$)
0	$5.0000000000000000 \times 10^{-2}$	$4.1128371832222289 \times 10^{-2}$
1	$1.199810840189358 \times 10^{-4}$	$4.522401944826133 \times 10^{-3}$
2	$4.946807268417725 \times 10^{-3}$	$4.604121343772035 \times 10^{-7}$
3	$4.999993634207877 \times 10^{-3}$	$9.856162440966542 \times 10^{-14}$

4.6.2 Simulated Real Data

We now consider the real data of magnetic radiation obtained from the simulation model. The magnetic fields are generated by the forward problem of the test model in our sample test. Random errors up to 3% are superimposed on the magnetic fields to simulate the set of real data. The iterative procedure using the Newton-Raphson method is also applied to estimate the model parameter of conductivity variation.

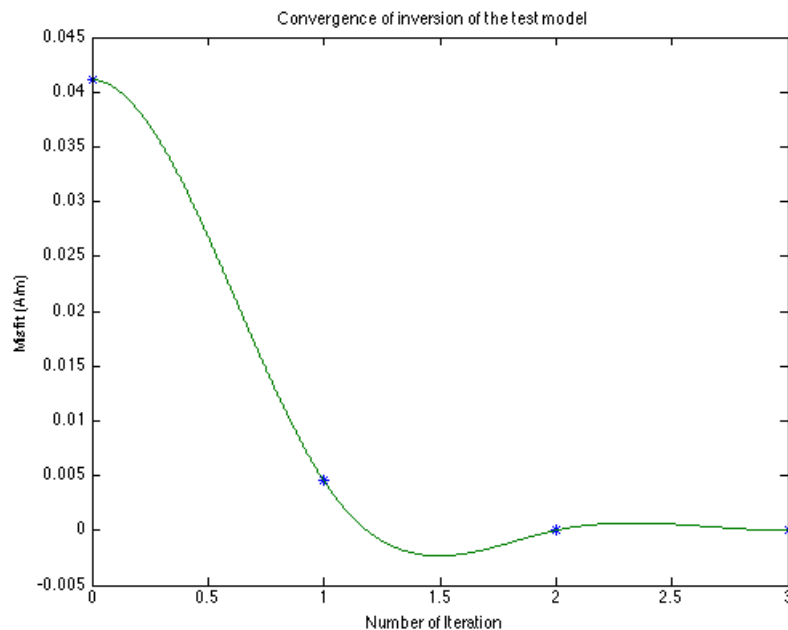


Figure 4.6: Curve of misfit versus number of iterations for the model in our sample test.

4.7 Discussions

Analytical solution of the steady state magnetic field due to a direct current source are derived by using the expression (4.20). The expression (4.20) is applicable to specific case in which two layers have exponentially varying conductivities. The effects of magnetic fields obtained from the DC method is plotted. The magnetic field of an earth having the electrical conductivity $\sigma_1(z) = \sigma_0 e^{-b(z-l)^2/2}$ for the depth $0 \leq z \leq h$, and $\sigma_2(z) = \sigma_0$ for the depth $z > h$ are considered. We fix the value of h , the magnetic field curves are quite different as z and l are varied between $h \geq l$ and $h \leq l$. The integral expressions are derived and computed the values of the magnetic field which is used to determine the behavior of the magnetic field against source-receiver spacing. The curves of the magnetic field against source-receiver spacing are plotted and shown the advantage in the ground exploration. The magnetic field intensities drop very fast when the value of z close to the value of h . At large depth(z), the magnitude of magnetic fields tends to be small value as we expect. As the thickness of overburden is increased, the shape of graph is similar to the conductivity profile of the ground. This is the advantage of magnetic field that can be performed some relationship to the conductivity profile of the ground.

An inverse problem via the use of an optimization technique is introduced for finding a conductivity parameter of the ground. The iterative procedure using the Newton-Raphson method is applied to estimate the model parameter of conductivity variation. The optimal result of our sample test converge very fast

to the true value with misfit less than $10^{-12} \text{A} \cdot \text{m}^{-1}$ after using only 3 iterations. These illustrate the advantage in using Newton-Raphson method which gives the convergence much faster than using another method of inversion (e.g., Oldenburg [12], Vozoff and Jupp [21]). The inversion method leads to the robustness of our model and procedure.

4.8 Summary and Conclusions

Magnetometric method used for investigation of a two-layered earth structure is presented in this study. The method proposed here is based on the measurement of low-level, low-frequency static magnetic fields associated with noninductive current flow between two current electrodes on the earth's surface. We derive analytical solutions of the steady state magnetic field due to a direct current source on two-layered earth structure having exponentially varying conductivity. The Hankel transform is introduced to our problem and analytical result is obtained. Our solutions are achieved by solving a boundary value problem in the wave number domain and then transforming the solution back to the spatial domain. The power series technique is used to solving the problem. The effects of magnetic fields obtained from the DC method is plotted and show the behavior in response to many different depths while some parameter are approximately given. The inversion process, using the Newton-Raphson method, is conducted to estimate a conductivity parameter of the ground. The method leads to very good result and has high speed of convergence.



Chapter 5

Conclusions and Future Works

5.1 Conclusions of the Thesis

Of all the electrical prospecting methods, direct current resistivity sounding is the simplest way to understand in principle. This thesis has been concerned about the problem of determining resistivity kernel function for a horizontally stratified layered earth. An inverse problem in resistivity interpretation has also been described and discussed in this study.

In the first part of this thesis, Chapter 2, we present a mathematical model of the scalar potential numerically at various positions by assuming that the earth structure contains only one layer having exponential conductivity. There are probes of direct current voltage and a receiver on the ground surface which picks up the signal on the ground surface at different electrode spacing. The electrode spacing starts from 10 to 100 meters. We use Finite Element Method (FEM) by applying Galerkin's Method of Weighted Residuals to solve the partial differential equation. Maple program is used to calculate and plot graphs of the value of the scalar potential at different depths and different electrode spacing from the probe.

In the second part (Chapter 3) of this study, we derive the analytical solution of normalized apparent resistivity from DC source located on a two-layered earth model which having exponentially varying conductivity. The Hankel transforms and power series method are used to solve the partial differential equation to find the potential functions. The expression for the Wenner configuration is introduced to formulate the normalized apparent resistivity. Numerical solutions are computed to show the behavior of the curves by using Chave's algorithm while some parameters are given. The curves of computation results of normalized apparent resistivity are plotted against electrode spacing. The inversion process, using the Newton-Raphson method, is conducted to estimate the conductivity variation parameter.

The last part of the thesis, Chapter 4, we present an electrical method used for investigation of two-layered earth structure. The method proposed here is base

on the measurement of low-level, low-frequency static magnetic fields associated with noninductive current flow between two current electrodes on the earth's surface. Analytical solutions of the steady state magnetic field response from DC source located on a two-layered are derived in this study. The earth structure having exponentially varying conductivity is considered. The Hankel transform is considered to our problem and analytical result is obtained. Our solutions are expressed in the form of integral expressions. Numerical solutions are computed to show the behavior of the magnetic field while some parameter are given approximately. An inverse problem via the use of the Newton-Raphson optimization technique is introduced for finding a conductivity parameter of the ground.

5.2 Future Works

Even though the work presented in this thesis provides interesting ideas about the solutions to the forward and inverse problems in geoelectrical resistivity sounding, the issues that we dealt with suggest numerous avenues for possible extensions and future works. In the area of electrical resistivity methods described in this thesis, the following outline is a list of interesting future directions that require further investigation:

- In Chapters 3 and 4, analytical solution could be developed in the general case for the problem of a multilayered earth with layers having exponentially varying conductivities which can be derived by using the boundary conditions described in these chapters.
- The inverse problem of Chapter 2 should be proposed.
- The difference conductivity model should be considered.

References

- [1] A. Binley, DC Electrical Methods, *Treatise on geophysics* 2nd. ed. **11**(2015), p. 233-259.
- [2] I. Ali and S. Kalla, A generalized Hankel transform and its use for solving certain partial differential equation, *J. Austral. Math. Soc. Ser.B* **41** (1999), 105-117.
- [3] A.D. Chave, Numerical integration of related Hankel transforms by quadrature and continued fraction expansion, *Geophysics* **48** (1983), 1671-1686.
- [4] A. Jeffrey, Handbook of Mathematical Formulas and Integrals, Academic Press, (1995).
- [5] B. Banerjee, B.J. Sengupta and B.P. Pal, Apparent resistivity of a multilayered earth with a layer having exponential conductivity, *Geophysical Prospecting* **28** (1980), 435-452.
- [6] B. Wiwatanapataphee, *Finite Element Method*, Mahidol University Department of Mathematics.
- [7] C.H. Stoyer and J.R. Wait, Resistivity probing of an “*exponential*” earth with a homogeneous overburden, *Geoexploration* **15** (1977), 11-18.
- [8] C. Johnson, *Numerical solutions of partial differential equations by the finite element method*, Cambridge Univ. Press, New York, 1987.
- [9] D. Hutton, *Fundamentals of finite element analysis*, McGraw-Hill, Companies, 2004.
- [10] D. Braess, *Finite Elements : Theory, fast solvers, and applications in solid mechanics*, second edition, Cambridge University Press, United Kingdom, 2001.
- [11] D. Pardo, L. Demkowicz, C. Torres-Verdin and L. Tabarovsky, International Journal for Numerical Method in Engineering, *Int. J. Numer. Meth.Engng* V.65(8)(2006), 1269-1309.
- [12] D. W. Oldenburg, The interpretation of direct current resistivity measurements, *Geophysics* **43**(3)(1978), 610-625.

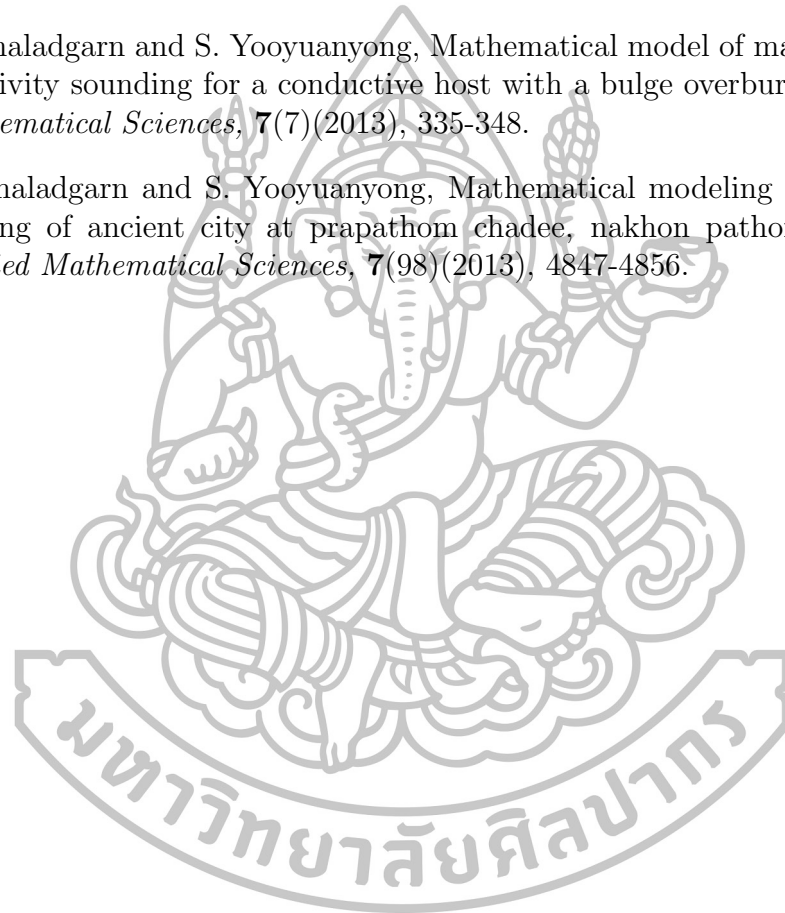
- [13] F.S. Grant and G.F. West, *Interpretation Theory in Applied Geophysics*, McGraw-Hill, New York, N.Y.,1965, pp.584.
- [14] H. O. Seigel, The magnetic induced polarization (MIP) method, *Geophysics* **39**(3)(1974), 321-339.
- [15] H. O. Seigel and A. W. Howland-Rose, Magnetic induced-polarization method, in J. B. Fink, B. K. Sternberg, E. O. McAlister, W. G. Wieduwilt and S. H. Ward, eds., *Induced Polarization: Applications and Case Histories*, Investigations in Geophysics No. 4, Soc. Expl. Geophys., Tulsa, 1990, pp.23-56.
- [16] H.S. Kim and K. Lee, Response of a multilayered earth with layers having exponentially varying resistivities, *Geophysics* **61**(1)(1996), 180-191.
- [17] I.N. Sneddon, *Special Functions of Mathematical Physics and Chemistry*, Interscience Publishers, Inc., New York, (1961).
- [18] J. Chen and D. W. Oldenburg, Magnetic and electrical fields of direct currents in a layered earth, *Expl. Geophys* **35**(2)(2004), 157-163.
- [19] J. J. Jakosky, Method and apparatus for determining underground structure, *U.S. Patent No. 1906271*, 1933.
- [20] J. J. Jakosky, *Exploration Geophysics*, 2nd ed., Trija Pub. Co., Los Angeles, 1950.
- [21] K. Vozoff and D. L. B. Jupp, Joint inversion of geophysical data, *Geophys. J. R. astr. Soc.* **42**(3)(1975), 977-991.
- [22] M. N. Nabighian, G. L. Oppliger, R. N. Edwards, B. B. H. Lo and S. J. Cheesman, Cross-hole magnetometric resistivity (MMR), *Geophysics* **49**(8)(1984), 1313-1326.
- [23] M. N. Nabighian, *Electromagnetic Methods in Applied Geophysics*, Volume 2, Society of Exploration Geophysicists, 1991.
- [24] P. F. Siew and S. Yooyuanyong, Some Mathematical Inverse Problems from Geophysics, *Optimization techniques and applications*, V.1, Australia, 1998, pp.510-517.
- [25] P. Ketchanwit, *Time domain electromagnetic response in heterogeneous media*, M.Sc.Thesis, Silpakorn University, 2001.
- [26] P. Yehuda and R. Jacob, *An Introduction to Partial Differential Equations*, Cambridge University Press, 2005.
- [27] R. N. Edwards, A downhole MMR technique for electrical sounding beneath a conductive surface layer, *Geophysics* **53**(4)(1988), 528-536.

- [28] R. N. Edwards and E. C. Howell, A field test of the magnetometric resistivity (MMR) method, *Geophysics* **41**(6)(1976), 1170-1203.
- [29] S. Yooyuanyong, Ground Water Exploration, *Proceeding of AMC 2002*, (2002), 145-166.
- [30] S. Yooyuanyong and W. Sripanya, Mathematical Modelling of Magnetometric Resistivity Sounding Earth Structures, *Thai J. Math* **3**(2)(2005), 249-258.
- [31] S. Yooyuanyong and W. Sripanya, Magnetic field of direct current in heterogeneous ground, *Songklanakarin J. Sci. Technol* **29**(2) (2007), 565-573.
- [32] T. Chaladgarn and S. Yooyuanyong, Mathematical Modeling of Resistivity Probing of Ancient City at Propathom Chadee, Nakhon Pathom, Thailand, *Applied Mathematical Sciences* **V.7**(98)(2013), 4847-4856.
- [33] W. H. Press, S. A. Teukolsky, W. T. Vetterling and B. P. Flannery, *Numerical Recipes in Fortran 77: The Art of Scientific Computing*, Fortran Numerical Recipes Vol. 1, 2nd ed., Cambridge Univ. Press, 1992.
- [34] W. Sripanya, Magnetic Field of Direct Current in Heterogeneous Media, Master Sciencist Thesis. Silpakorn University, 2005.
- [35] W. Sripanya, Mathematical Solutions of Electric Potential and Magnetic Field Response from Heterogeneous Media, Doctoral Sciencist Thesis. Silpakorn University, 2011.
- [36] W.M. Telford, L.P. Geldart and R.E. Sheriff, *Applied Geophysics* Second Edition, Cambridge University Press, 1996.



Publications of the Thesis

- T. Chaladgarn and S. Yooyuanyong, Mathematical modeling of resistivity probing of 1-dimensional underground water with a bulge overburden, *Oral presentation of the Silpakorn University International Conference on Academic Research and Creative Arts : Integration of Art and Science*, 2012.
- T. Chaladgarn and S. Yooyuanyong, Mathematical model of magnetometric resistivity sounding for a conductive host with a bulge overburden, *Applied Mathematical Sciences*, **7**(7)(2013), 335-348.
- T. Chaladgarn and S. Yooyuanyong, Mathematical modeling of resistivity probing of ancient city at prapathom chadee, nakhon pathom, thailand, *Applied Mathematical Sciences*, **7**(98)(2013), 4847-4856.



Biography

Name	Teerasak Chaladgarn
Address	5/1145 Moo 10, Bangtalad, Pakkred, Nonthaburi, 11120
Date of Birth	09 June 1979
Institution Attended	
2002	Bachelor of Education in Mathematics, Srinakharinwirot University
2005	Master of Education in Mathematics, Srinakharinwirot University
2015	Doctor of Philosophy in Mathematics, Silpakorn University

